STUDIES ON SENSITIVITY OF NANOSIZED ENERGETIC MATERIALS

By
SANJAY VISHWASRAO INGALE

PHYS01201304025

Bhabha Atomic Research Centre, Mumbai

A thesis submitted to the

Board of Studies in Physical Sciences

In partial fulfillment of requirements

for the Degree of

DOCTOR OF PHILOSOPHY

of

HOMI BHABHA NATIONAL INSTITUTE

December, 2019

Homi Bhabha National Institute

Recommendations of the Viva Voce Committee

As members of the Viva Voce Committee, we certify that we have read the dissertation prepared by **Sanjay Vishwasrao Ingale** entitled **"Studies on Sensitivity of Nanosized Energetic Materials"** and recommend that it may be accepted as fulfilling the thesis requirement for the award of Degree of Doctor of Philosophy.

Chairman –	_(T C KAUSHIK)_
Guide / Convener –	22/09/2020 Dr. P. B. WAGH
Co-guide -	S. N. ACHARY, S. N. Achary 22-09-2020
Examiner -	DKSinha. (Dr R K sinha) 22/9/20

Name & Signature with date

Member 1-	22/09/2020 Prof. B. N. Jagatap

Final approval and acceptance of this thesis is contingent upon the candidate's submission of the final copies of the thesis to HBNI.

We hereby certify that we have read this thesis prepared under our direction and recommend that it may be accepted as fulfilling the thesis requirement.
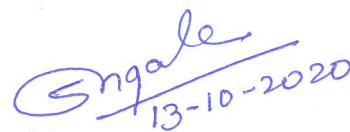
Date: 22/09/2020

Place: Trombay Mumbai

S. N. Achary
(Dr .S. N. Achary)
Co-guide

(Dr. P. B. Wagh)
Guide

(ii)

CERTIFICATION ON ACADEMIC INTEGRITY

1. I _**Sanjay Vishwasrao Ingale**_ HBNI Enrolment No. _**PHYS01201304025**_hereby undertake that, the Thesis titled _**"Studies on Sensitivity of Nanosized Energetic Materials"**_ is prepared by me and that the document reports the original work carried out by me and is free of plagiarism.

2. I am aware and undertake that if plagiarism is detected in my thesis at any stage in future, suitable penalty will be imposed as per the applicable guidelines of the Institute/ UGC.

13-10-2020

Signature of the Student
(with date)

Endorsed by Thesis Supervisor

13/10/2020

Signature (with date)

Name: Dr. P. B Wagh
Designation: SO/G
Department/ Centre: Applied Physics Division
Name of the CI/ OCC: Bhabha Atomic Research Centre

STATEMENT BY AUTHOR

This dissertation has been submitted in partial fulfillment of requirements for an advanced degree at Homi Bhabha National Institute (HBNI) and is deposited in the Library to be made available to borrowers under rules of the HBNI.

Brief quotations from this dissertation are allowable without special permission, provided that accurate acknowledgement of source is made. Requests for permission for extended quotation from or reproduction of this manuscript in whole or in part may be granted by the Competent Authority of HBNI when in his or her judgment the proposed use of the material is in the interests of scholarship. In all other instances, however, permission must be obtained from the author.

Sanjay V. Ingale

DECLARATION

I, hereby declare that the investigation presented in the thesis has been carried out by me. The work is original and has not been submitted earlier as a whole or in part for a degree / diploma at this or any other Institution / University.

Sanjay V. Ingale

List of Publications arising from the thesis

Journal

1. Studies on Effect of Particle Size on Thermal Sensitivity and Decomposition of Hexogen; **S. V. Ingale**, P. B. Wagh, Amit Rav, T. C. Kaushik, *Science and Technology of Energetic Materials*, **80** (2019) 222-228

2. Studies on Impact Sensitivity of Nanosized Trinitrotoulene (TNT) Confined in Silica Processed by Sol-Gel Method, **S. V. Ingale**, P. B. Wagh, P. U. Sastry, C. B. Basak, Satish C. Gupta, *Defence Technology*, **12** (2016) 46-51

3. Resorcinol-Formaldehyde Ammonium Nitrate Energetic Nanocomposites Processed by Sol-Gel Method, **S V Ingale**, P B Wagh, N H Raje, A Ghosh, T C Kaushik, S. C. Gupta; *International Journal of Multidisciplinary and Current Research*, **3** (2015) 961-965

4. Preparation of Nano-Structured RDX in a Silica Xerogel Matrix, **S. V. Ingale**, P.U. Sastry, P. B. Wagh, A. K. Tripathi, R. Tewari, R. D. Wasnik, B. Bhattacharya, S. C. Gupta, *Propellants Explosives Pyrotechnics*, **38** (2013) 515-519.

Conferences

1. Sensitivity Studies of Nano Structured TNT processed by Sol-Gel Method; **S. V. Ingale**, P. B. Wagh, C. B. Basak, S. C. Gupta, 9th Int. High energy Materials Conference and Exhibit (HEMCE -2014), Thiruvananthpuram, India, (Feb. 13-15, 2014).

2. Phlegmatization of RDX by Viton Using Water Dispersion Method and its Characterization; P. B. Wagh, **S. V. Ingale**, Ratanesh Kumar, T. C. Kaushik, S. C. Gupta; 10th Int. High energy Materials Conference and Exhibit (HEMCE -2016), Hyderabad, India (Feb. 11- 13, 2016).

Sanjay V. Ingale

DEDICATIONS

Dedicated to All My Teachers Who Not Only Taught Bookish Knowledge But Taught Me Values in Life Which Helped Me to Become A Better Human Being

ACKNOWLEDGEMENTS

TABLE OF CONTENTS

CONTENTS	Page No.

SUMMARY

In chemical energetic materials, sudden release of energy causing an explosion is an important feature which has been utilized in making their use for specialized applications. However, unless release of the stored chemical energy is controlled, the material is unsafe and therefore has limitations in processing and use. Therefore, in development of these materials, a major objective is to have desired control on its energy release rate and sensitivity to initiation. Particle size in these materials can be one important parameter to control their properties. Several researchers have attempted to investigate and characterize the effects, but no clear trend has emerged out or agreed upon. The focus of the present research work is to study the effect of particle size on properties of energetic materials like TNT, RDX, PETN and composite of Resorcinol and Ammonium nitrate to infer whether decrease in sensitivity and improvement in performance can be achieved by reducing their particle size. Effect of introducing voids in controlled manner on ignition mechanism in these materials and their sensitivity has also been studied.

TNT, RDX and PETN have been prepared with particles size in wide range from 350 micrometer down to 50 nanometers using solvent/non solvent precipitation, spray drying and sol-gel processing and studied effect of particle size on energetic properties of these materials. Sol gel process has been utilized for preparation of nano sized energetic materials with induced defects like porosity and studied effect of controlled defects on sensitivity and performance of these materials. Fourier Transform Infra-Red (FTIR) spectroscopy and X-ray Diffraction (XRD) studies confirmed that chemical and crystal structures of prepared materials are same as those of raw materials. Thermo gravimetric and differential scanning calorimetric (TG-

DSC) studies used for qualitative and quantitative confirmation of energetic materials in samples. Electron microscopy and small angle X-ray scattering measurement techniques were used to analyze the microstructure while particle sizes were measured using SEM and TEM micrographs.

The studies on processed energetic materials carried out using fall hammer impact apparatus showed that sensitivity to impact initiation decreased by about 15 % in RDX and by 40 % in TNT with reduction in particle size. Impact sensitivity in RDX materials has been found to increase by about 5 to 7 % with inclusion of porosity even though the particle size is reduced. In the composites of silica with TNT, RDX and PETN having different energetic material loading and varying pore volume, it is also demonstrated that microstructure of the sol-gel processed material can be tailored and effectively used for controlling their sensitivity and energy release rate. The impact sensitivity in TNT materials could be tuned in the range of 25 % to 65 % by varying the process parameters of sol-gel method.

The kinematics parameters calculated from thermal analyses to understand decomposition mechanism in energetic materials showed an increase in activation energy with decrease in particle size. In materials processed by sol-gel method, silica environment around energetic particles and reduced particle size has led to increase in activation energy. However, kinetic parameters suggest improvement in energy release rate due to high surface energy associated with smaller size particles. More number of molecules undergoing decomposition simultaneously due to high proportion of molecules on the surface and that contributes to faster decomposition in materials with reduced particle size. In sol-gel processed materials also, the energy release rate is enhanced as compared to that of raw materials. This suggests that high

defect density leads to increased number of ignition centers with increase in collision frequency that leads to faster ignition to detonation transition. The improvement in energy release rate as predicted by thermal analysis is further substantiated by detonation velocity (VoD) measurements. The detonation velocity in energetic materials with reduced particle was found to be increased by about 15 % as compared that for raw material.

The effect of particle size is prominently demonstrated in resorcinol- and ammonium nitrate (AN) composites containing more than 85 % AN with stoichiometric oxygen balance. The nanostructure composites processed by sol-gel method with reduced particle size showed increase in energy release rate as compared to that from physical mixture of resorcinol and ammonium nitrate. These composites are safer than traditional energetic materials like RDX and PETN due to less sensitivity and hence can be useful in various civilian applications.

From the systematic studies carried out on different nanosized energetic materials, it is inferred that decrease in ignition sensitivity and improvement in detonation velocity can be achieved with reduction in particle size in energetic materials. The microstructure of these materials can also be tailored by using sol-gel process for effectively controlling their sensitivity and energy release rate. This study has helped to understand the ignition process in energetic materials.

LIST OF FIGURES

LIST OF TABLES

CHAPTER 1

INTRODUCTION

Chemical energetic materials have always been subject of curiosity for mankind. However, common people's awareness of these materials is limited to firecrackers in festival seasons and media news related to terrorist activities. Both these things do not present correct picture of potential use of energetic materials. These materials have fascinated humans but more than that they have horrified them due to their destructive capacity. The capability of energetic materials, especially their energy density and high power has also been utilized in the development of modern society. Energetic materials are widely used in civil applications like road blasting, metal welding, for warheads in military applications and in basic research as a tool for generating high pressure. The energetic materials are like a character in fairy tale which can fulfill our any wishes when it is in our control, but it is equally harmful when it becomes uncontrolled. The development of energetic materials has caused numerous casualties and the accidental destruction of facilities. However, the benefits of controlling an explosive effect of these materials are so valuable and useful that the efforts to characterize and understand these materials and experiments to explore their potential never seized but are continuing.

Energetic materials are associated with explosion which generates a damagingly high-pressure pulse into the surroundings. It could also be accompanied with fragments of casing or surrounding structures. Explosions can be sub-divided into three types depending on their energy source namely nuclear, physical and chemical explosions. Nuclear explosions are caused by a runaway chain reaction in

fissile material which releases large quantities of neutrons, different types of radiation and a large amount of heat energy. Physical explosions occur when large quantity of physical potential energy is released very rapidly. This explosion may occur without an energetic material, that is, without any material which contains intrinsically the energy needful to produce the explosion. A steam boiler is example of physical explosion. It may explode because of the heat energy put into the water. But the energy is not intrinsic to water, and water is not an explosive. Chemical explosions are caused by chemical energetic materials. In chemical explosions, sudden release of large quantities of stored chemical energy generates very high temperature gases and high pressures. In this work, we have studied these chemical energetic materials.

Chemical energetic materials have large amount of stored energy and burst with sudden release of this energy generally associated with high temperature and high-pressure gases. These materials commonly require some stimulus, like an impact or a spark to trigger them to release their energy. When suitably initiated, they release this energy violently producing explosion. This sudden release of energy makes these materials different from other fuels like coal, and makes them suitable for use in specialized applications. The first ever known chemical energetic material is gunpowder. It is mixture of Coal, Nitrate salt and Sulfur. This is still used in firecrackers and in propellants. The major development in field of energetic materials, after gun powder, began with invention of nitroglycerine and its use in stabilized compositions like dynamite and blasting gelatin. After World War I, use of some powerful energetic materials like Trinitrotoluene (TNT), Cyclotrimethylenetrinitramine (RDX), and Penta Erythritol Tetra Nitrate (PETN) was started, mostly in military applications. The recent technological progress demands

more powerful and more stable energetic materials which led to development and use of materials like Tri-Amino Tri-Nitro Benzene (TATB), Hexanitrostilbene (HNS), C4, Cyclotetramethylenetetranitramine (HMX) in modern applications.

A combination of a fuel and an oxidizer is required in an energetic material. When fuel and oxidizer react, it produces energy by a process called oxidation. For release of maximum amount of energy, a balance between fuel and oxidizer is necessary. This is represented by a quantity known as oxygen balance.

In a simple oxidation reaction mentioned below, 1 mole of methane burns with 2 moles of oxygen to form 1 mole of carbon dioxide and 2 moles of water.

$$CH_4 + 2\,O_2 \rightarrow CO_2 + 2\,H_2O$$
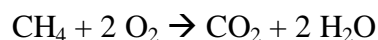
The heat of reaction is 218.2 kcal per mole of methane [1]. Since 1 mole of methane weighs 16.042 grams and 1 mole of oxygen weighs 32.0 grams, the heat of reaction per unit weight is as calculated as follows:

$$212.8 \text{ kcal} / (16.042 \text{ g} + 2 \times 32.0 \text{ g}) = 2.659 \text{ kcal/g}$$

This energy release per unit weight of material is termed as energy density and is one of the important features of energetic materials. In oxidation, coal releases approximately eight times more energy than that of one commonly used high energy material TNT [2]. However, TNT releases its energy far more quickly, approximately 10^6 times faster than coal and causes much severe effect. For energy release, fuel and oxidizer can be physically mixed to allow them to react. Alternatively, these two can be present in the same molecule, as is the case with most of efficient energetic materials used in military applications. The intimacy of fuel (mostly carbon and hydrogen atoms) and oxidizers (oxygen atoms) is the main reason for violent energy release through rapid decomposition process causing explosion in these materials.

The velocity with which the reaction propagates in the mass of the energetic materials is referred as velocity of detonation. Along with energy density, velocity is an important element influencing energy yield of these materials. Depending on the energy release rate, these materials are classified as low explosives and high explosives. Energetic materials in which the chemical reaction front moves faster through the material than the speed of sound are known as High Explosives (HE). Low explosives are materials where the rate of decomposition proceeds through the mass is less than the speed of sound. Under normal conditions, low explosives undergo deflagration at rates that vary from a few centimeters per second to approximately 400 meters per second [3]. A low explosive is usually a mixture of a combustible substance and an oxidant that decomposes rapidly (deflagration); however, they burn more slowly than high explosives. Low explosives or propellants burn but do not explode and function by producing gas. Black powder is a common example of low explosives. High explosives detonate under the influence of shock with reaction propagating at a rate ranging from 3 to 9 km/s [4]. They exert a mechanical effect upon whatever is near them, when they explode, whether they are confined or not. Examples of high explosives are dynamite, trinitrotoluene, tetryl, picric acid, etc. They are normally employed in mining, demolition, and military applications.

Most chemical energetic materials are composed of carbon, hydrogen, oxygen and nitrogen, and are referred as CHNO explosives. In these materials, nitrate molecules typically provide required oxygen to burn the carbon and hydrogen fuel. The oxidizers need not be from a source separate from fuel. In energetic materials, the different oxidizer subgroups like $-NO_2$, $-NHNO_2$ and $-ONO_2$ are the major source of

oxygen. Energetic materials based on these oxidizer subgroups in the molecule are classified into nitro, nitramine and nitrate esters, respectively. It is interesting to note that same nitro groups in these materials which make them effective energy source, also make them susceptible to release energy with small trigger energy due to its metastable nature. TNT is nitro compound in which nitro group is attached to carbon. RDX is representative of nitramine class in which nitro group is attached to nitrogen atom. PETN is from nitrate ester group in which nitro group is attached to oxygen atom. These chemical groups also play an important role in governing the stability of such materials.

Energetic materials exist in meta-stable state i.e. these materials may not undergo rapid chemical decomposition until a definite energy (activation energy) has been added to get the process initiated. This is termed as ignition or initiation. Various means used for initiation in energetic materials are heat, electrostatic impulses, friction, shock waves, or any combination of these energy sources. The ease with which an energetic material can be initiated is known as its sensitivity. Among energetic properties of these materials, sensitivity to initiation is very critical because the materials should be insensitive enough from safety view that minimizes the hazard during handling but at the same time, it should be reliable for functioning when desired. According to sensitivity to initiation, energetic materials are categorized into primary and secondary explosives. Energetic materials under primary category are extremely sensitive to stimuli like impact, friction, heat, static electricity, electromagnetic radiation, etc. The materials like Mercury Fulminate, Lead Azide and Lead Styphnate that can be initiated with relatively small amount of energy and easily detonate belong to primary category. Consequently, they are very unsafe to

handle, and considerable precautions are required when handling them. These are often used in detonators to ignite bigger charges of secondary energetic materials which are relatively less sensitive. A secondary type energetic material such as RDX or TNT requires more energy for initiation as compared to that of primary type materials. However, once they detonate, a powerful shock is generated. Because of their less sensitivity, secondary energetic materials are usable in a variety of applications and are safer to handle and store.

Considering many forms and structures in which hydrocarbons can be arranged and large number of subgroups that can be attached to them, it should be possible to have large varieties of energetic materials. However, a very few energetic materials viz. TNT, RDX, HMX, PETN, HNS are commonly used in military and scientific applications. The number is limited by several factors like thermal stability, chemical compatibility, physical form, handling sensitivity and energetic output properties [5]. Thus, the choice of energetic materials being used is limited and therefore it becomes desirable to modify the properties of available materials to control their performance. In order to develop safer materials to reduce the chance of inadvertent explosion events, it is necessary to understand how these energetic materials work. The most important feature of any energetic material is its stability. Unless the release of the stored chemical energy can be controlled, the material is unsafe to handle and has limitations in its use. Today, good quantum of research in this field is aimed at addressing safety of energetic materials. From these studies, it is observed that energetic properties of material depend upon microstructure, particle size and its distribution, surface area, internal voids and inclusions and processing methods of energetic materials. Among these, one of the parameters that can be

effectively used to modify the properties of the energetic materials is particle size. Several researchers have attempted to study the effect of the particle size on sensitivity to initiation in energetic materials, but no clear trends have emerged or agreed upon. Interestingly, the results are seen to be contradictory as both the increasing and decreasing trends in sensitivity to initiation have been observed as the particle size of these materials is reduced from coarser to fine [6-10]. The reason for this could be one fact that these studies have been conducted on materials with different processing history and having different range of particle size distribution. Different measures of initiation like using heat or impact energy were used to measure sensitivity properties, or different parameters considered as measure of ignition may also give different results. Therefore the available literature results are inadequate and open for further research. Thus, it is still of great interest to investigate the effect of particle size on the sensitivity of energetic materials to initiation.

Composites using mixture of fuel and oxidizer is another class of energetic materials used in many applications. Gun powder, a mixture of charcoal, potassium or barium nitrate and sulfur is the oldest known composite of this class. Their composition with different proportion of fuel and oxidizer may provide energy over wide range to suit various applications. The thermite mixtures consisting of metal oxides like iron oxide and metallic aluminum as fuel are also studied [11] but, these mixtures have less power being gasless compositions. Solid rocket propellants also use composites containing organic polymers as fuels and ammonium perchlorate as oxidizer [12]. The intimacy of fuel and oxidizer components through control of their particle size and their homogeneous distribution is the key for successful energetic composites. Organic gel has potential to be explored as fuel in energetic composites.

Three of commonly used energetic materials like TNT, RDX and PETN are chosen in present study. Some of the important properties of these materials are summarized as below:

TNT:

Trinitrotoluene (TNT) which is more specifically named as 2-methyl-1, 3, 5-trinitrobenzene is a chemical with molecular formula $C_6H_2 (NO_2)_3CH_3$.
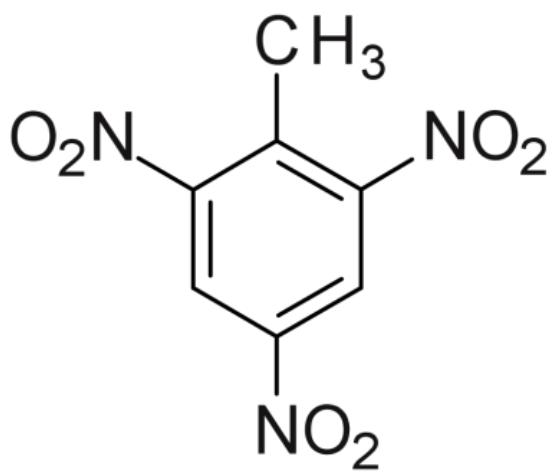
Fig. 1.1 Structural formula of TNT

It is a relatively insensitive energetic material with convenient handling and processing properties. This is one of the earliest known and most widely used energetic materials for military, industrial, and mining applications. TNT melts at 80 °C, far below the temperature at which it will spontaneously detonate (240 ^{o}C). It allows to use it in casting operation and to safely combine with other energetic materials. For detonation, TNT must be initiated by a pressure wave from another more sensitive energetic material, called as booster. The heat of detonation for TNT is 4.184 mega joules per kilogram (MJ/kg) [13]. In detonation, only the oxygen available in TNT molecule is used for oxidation of carbon. Energy density of TNT is used as a reference point for many other materials including nuclear weapons. Its heat of

combustion is 14.5 MJ/kg [14]. In combustion, all carbon atoms react with either molecular or atmospheric oxygen to release more energy as compared to that of detonation. Some properties of TNT are listed in Table 1.1.

Table 1.1 Some important properties of TNT

Chemical formula	$C_7H_5N_3O_6$
Molecular weight	227.13 g/mol
TMD	1.65 g/cm^3
Melting point	80 ^{o}C
Detonation Temperature	240 ^{o}C
Detonation velocity	6900 m/s at 1.65 g/cc
Heat of Detonation	4184 kJ/kg

RDX:

RDX is the most popular energetic material. Chemical name for RDX is Hexogen or more specifically Cyclo-1,3,5-trimethylene-2,4,6, - trinitramine. Molecular formula for RDX is $C_3H_6N_6O_6$. The chemical structure of RDX is as below:
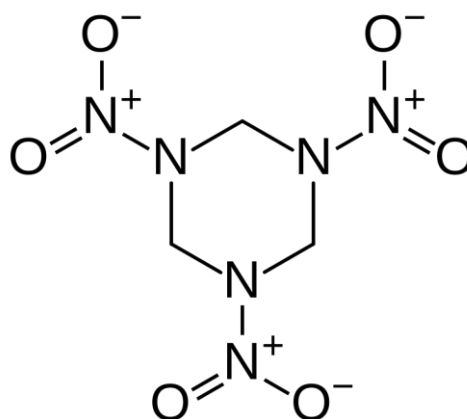
Fig. 1.2 Chemical structure of RDX.

It has high brisance that is high pulverizing power due to its high detonation velocity. It was considered a candidate for replacing TNT after the 1st World War and industrial scale production of RDX started during the Second World War. During development stage, it was referred as Research and Development Explosive and termed as RDX. It belongs to the family of high energy density nitramine energetic materials which also includes cyclotetramethylenetetranitramine (HMX) and hexanitro-hexaazaisowurtzitane (CL-20). However, processing of RDX is less troublesome than HMX or CL-20 as both HMX and CL-20 have four stable polymorphs of which only one is desired [15]. RDX is soluble in solvents like acetone, cyclohexanone, acetonitrile, and DMF. It is sparingly soluble in water, alcohols, and hydrocarbons. Commercially available RDX ranges in crystal size of hundreds of microns. Larger grained RDX is typically produced by recrystallization from solvents such as cyclohexanone. Finer grained RDX is produced by precipitation. Some properties of RDX are listed in Table 1.2.

Table 1.2 Some important properties of RDX

Chemical formula	$C_3H_6N_6O_6$
Molecular weight	222.1 g/mol
TMD	1.82 g/cm^3
Melting point	204 ^{o}C
Detonation Temperature	210 ^{o}C
Detonation velocity	8750 m/s at1.76 g/cc
Heat of Detonation	6322 kJ/kg

PETN:

Pentaerythritol tetranitrate (PETN) has IUPAC name as 1, 3-Propanediol, 2, 2-[bis-(nitroxy) methyl]–dinitrate. Molecular formula of PETN is $C-(CH_2ONO_2)_4$. Fig.1.3 shows structural formula of PETN.
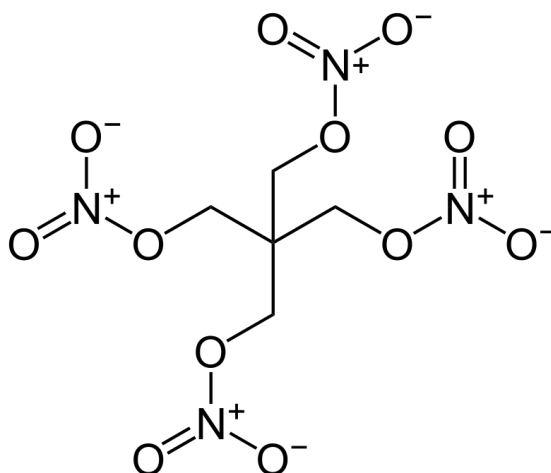
Fig. 1.3 Structural formula of PETN

It is a white crystalline aliphatic nitrate ester with melting point 141 ºC. It is the most sensitive among secondary energetic materials and its sensitivity is attributed to the nitrate ester group [16]. Some properties of PETN are listed in Table 1.3.

Table 1.3 Some important properties of PETN

Chemical formula	$C_5H_8N_4O_{12}$
Molecular weight	316.1 g/mol
TMD	1.77 g/cm^3
Melting Temperature	141 ^{o}C
Detonation Temperature	150 ^{o}C
Detonation velocity	8400 m/s at1.7 g/cc
Heat of Detonation	5810 kJ/kg

It is used as booster explosive, in detonating fuses, demolition charges and initiation devices. Its high sensitivity to mechanical and frictional stimulations poses hazard in its handling. It is soluble in acetone and nearly insoluble in water. This property of PETN can be used for reducing its particle size by precipitation method.

Focus of the present research work is to study the effect of particle size on sensitivity properties of these commonly used energetic materials like TNT, RDX and PETN to know whether ignition sensitivity and performance can be controlled by reducing particle size. Also organic-inorganic composite using Resorcinol as fuel and Ammonium nitrate as oxidizer has been prepared using sol gel method. Being processed by sol-gel method, the oxidizer with nanosized particles is dispersed in three-dimensional porous network of fuel and provides homogeneous distribution. Energetic properties of these nano composites have also been studied.

REFERENCES:

[1]   The Thema1 Decomposition of Methane, C. J. Chen and M. H. Bac, *Canadian J of Chemistry*, **54** (1976), 3175-3184.

[2]   Blast Waves and How They Interact With Structures, I G Cullis, *J R Army Med Corps* **147** (2001)16-26

[3]   Research topics in explosives - a look at explosives behaviors, J L Maienschein , *Journal of Physics: Conference Series,,***500** (2014) 052027

[4]   Distribution and Fate of Military Explosives and Propellants in Soil: A Review, John Pichtel, *Applied and Environmental Soil Science*, **2012** (2012) Article ID 617236, 33 pages

[5]   P. W. Cooper, Use forms of explosives in *Explosives Engineering.* Wiley-VCH. (1996).

[6]   Effect of Particle Size on Shock Initiation of PETN, RDX and Tetryl, Calvin L Scott, *Fifth Symp. (Int.) on Detonation*, Office of Naval Research, Pasadena, Calif USA, (1970) pp. 259-266

[7]   Grain-Size Effects on Shock Sensitivity of HNS, R. Setchell, *Combust. Flame*, **56,** 3 (1984) 343-345

[8]   Shock Initiation Sensitivity of HNS, A. C. Schwarz, *Seventh Symp. (Int.) on Detonation*, NSWC MP 82-334, Washington, D.C.: U.S. Gov. Print. Office, (1981) pp. 1024-1028

[9]   D. B. Hayes, in Shock Waves, Explosions, and Detonations (J. Bowen, N. Manson, A. Oppenheim, and R. Soloukhin, Eds.) *Prog. Astro. Aero*, **87** (1983) 445-467

[10] Shock Initiation of TATB Formulations, C. A. Honodel, J. R. Humphrey, R. C. Weingart, R. S. Lee, and P. Kramer, *Seventh Symp. (Int) on Detonation*, NSWC MP 82-334, Washington, D.C.: U.S. Gov. Print. Office, (1981), pp. 425-434

[11] Reflected Shock Ignition and Combustion of Aluminum and Nanocomposite Thermite Powders, T. Bazyn, N. Glumac, H. Krier, T. S. Ward, M. Schoenitz, E. L. Dreizin, *Combustion Sci. and Technol.*, **179** (2007) 457-47

[12] Ammonium Perchlorate-based Composite Solid Propellant Formulations with Plateau Burning Rate Trends, S. Banerjee, S. R. Chakravarthy, *Combustion, Explosion, and Shock Waves*, **43** (2007) 435–441

[13] M. A. Cook, *The Science of High Explosives*, R. E. Krieger Publ., New York, (1971)

[14] R. Meyer, *Explosives*, Second Edition, Verlag Chemie, (1981)

[15] Understanding Metastable Phase Transformation During Crystallization of RDX, HMX and CL-20: Experimental and DFT Studies, M. Ghosh, S. Banerjee, Md A. S. Khan, N. Sikder and A. K. Sikder, *Phys. Chem. Chem. Phys*., **18** (2016) 23554-23571

[16] Tailoring the Sensitivity of Initiating Explosives, V. W. Manner, D. N. Preston, C. J. Snyder, D. M. Dattelbaum and B. C. Tappan, *AIP Conference Proceedings*, **1793** (2017) 040036

CHAPTER 2

LITERATURE SURVEY

A major objective in development of energetic material is to have desired control on its sensitivity to initiation and energy release rate. An ideal energetic material is expected to release high amount of energy and should be relatively insensitive to accidental initiation. However, usually there is a delicate balance between the two i. e. the energetic materials that release more energy are more sensitive to initiation [1]. It is therefore a challenge to enhance the performance of an energetic material without sensitizing it to inadvertent detonation. Research in this field is aimed to reduce the sensitivity and increase the performance of an energetic material with focus on modification of the chemical and physical structure of such materials.

Particle size, as a key parameter, has been studied widely to modify properties of energetic materials [2]. However, results obtained in various studies made to analyze the effect of particle size on decomposition of energetic materials are diverse in nature. Some researchers have reported that sensitivity of energetic materials to impact initiation decreases with decrease in particle size [3] whereas some have reported that sensitivity of the energetic materials was found to increase with decrease in particle size [4]. Fathollahi et al. [5] studied thermal decomposition of RDX nano particles prepared by wet ball milling technique and reported that activation energy of micron size RDX is 1.5 times higher than that for nano RDX which suggests that nano RDX is more sensitive than coarse RDX. Huang et al. [6] reported that nano size FOX-7 material prepared by spray freeze drying technique has higher decomposition

temperature than micron size material indicating that nano explosives is less sensitive than the coarse one. This observation has been attributed by them to the smaller internal stress in nanoparticles. This study also suggests that while evaluating effect of particle size on sensitivity of energetic materials, it needs to consider the difference in particle size distribution due to different processing methods. Hence, the method of processing of these materials for reducing particle size becomes important. Some typical findings are summarized here to have overall picture.

2.1 Effect of processing techniques on particle size of energetic materials:

Several researchers have used different processing techniques to reduce particle size of energetic material and to achieve narrow size distribution [7]. These techniques include wet milling, crystallization out of solutions, crystallization using supercritical fluids, spray drying sol-gel technique, etc.

In milling, solid particles are broken down with mechanical forces. As these forces may cause hazard during processing, this technique is restricted to wet milling process in case of energetic materials. Estabrook and Somoza [8] succeeded to achieve particle size less than 20 μm using wet grinding method. Teipel and Mikonsaari [9] used a rotor-stator milling device with ring gear disperser to reduce size of RDX and CL20 explosives. They succeeded to reduce particle size of these materials from about 500 μm to less than 10 μm with size distribution of processed material ranging from 2 to 30 μm. Song and Li [10] used raw RDX with mean particle size of 41.8 μm with a size distribution ranging from 300 nm to 300 μm. They reduced its particle size to a mean value of 2.86 μm using wet riddling method.

Another technique used for reducing particle size is spray drying, which involves dissolution of the energetic material in suitable solvent and then spraying

droplets of the solution into a heated chamber. The solvent from the droplets is evaporated resulting in crystallization of energetic materials particles. The spray drying technique requires high temperature to evaporate the solvent and hence is not suitable for materials which may decompose at relatively lower temperatures. Qiu et al. [11] prepared RDX and CL20 microparticles using spray of a dilute solution of an energetic material and acetone. The average diameter for particles of energetic material was about 15 μm with most particles in the range of 5 – 30 μm. Wang and coworkers [12] produced HMX/estane nanocomposites using a similar technique. Morphology of these nano-composites was found to be micro-spherical (1 to 8 μm diameter) and composed of many tiny particles of 30 to 150 nm in size. Qiu and coworkers [13] demonstrated preparation of sub-micron size HMX by spray drying method using acetone as solvent. Average granule size of prepared materials was ~1 μm with majority of particles in range of 0.4 to 1.6 μm. Castro-Rosario and coworkers [14] prepared RDX nano particles from an aerosol jet of RDX solution in acetonitrile. They obtained particles with the largest and smallest diameters slightly over 1 μm and 160 nm, respectively.

The method of crystallization out of solutions is another simple and safe technique to reduce particle size. In this method, the solubility of a substance in a solvent can be reduced by rapidly lowering the temperature of the solution [15] or by adding a non-solvent [16]. In a given solution, as solubility reduces, a super saturation state is created, which leads to the nucleation of small crystallites that are separated by filtration. Though this method is simple, it is difficult to control particle size [17] and to obtain sub-micron sized particles. Cave et al. [18] have prepared TNT material with mean particle size of 28 μm and size distribution ranging from 3.5 μm to 65 μm using

this method. Kim and coworkers [19] prepared Nitrotriazolone (NTO) particles in mixture of water and N-methyl 2-Pyrrolidone (NMP) using crystallization method. Spherical particles of NTO with average diameter ranging from 30 to 300 μm were crystallized by adjusting the composition of co-solvent, temperature and the agitation rate. They studied the control on particle size by varying the composition and agitator speed and their results have been displayed in Fig. 2.1 [19].
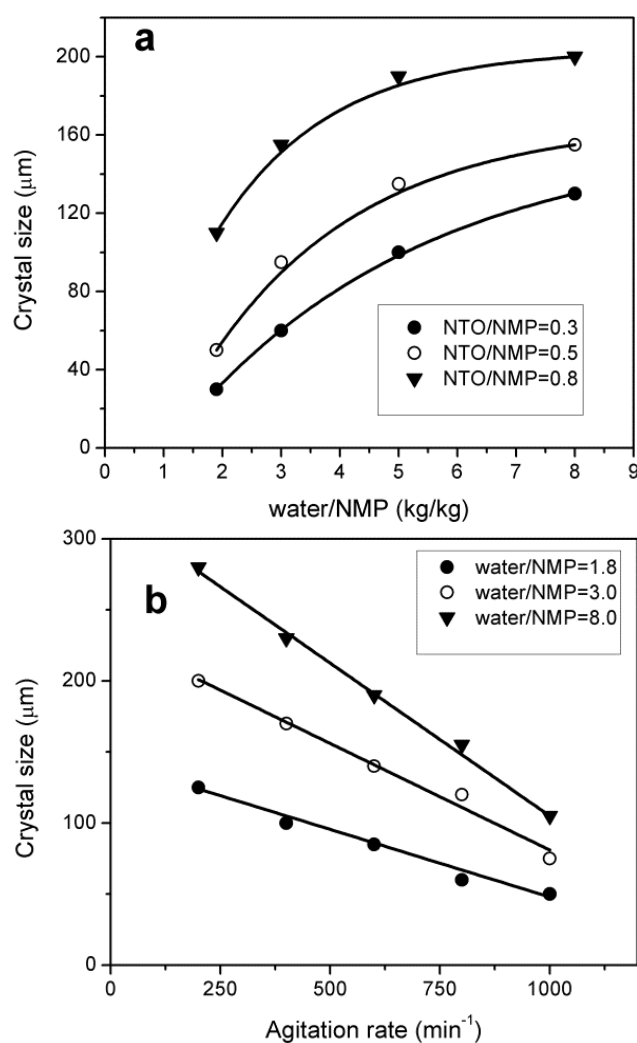
Fig. 2.1 Effect of a) solvent ratio; b) agitation rate on particle size of NTO [19]

Vijayalakshmi et al. [20] used similar method and achieved particle size distribution of NTO ranging from 10 to 200 μm with controlling operation variables like cooling rate, agitator configuration, speed, etc. Li and coworkers [21] prepared

HMX material with particle sizes ranging from 2.98 μm to 16.1 μm by changing solvent and non-solvent combination, stirring rate, temperature difference between solvent and non-solvent. Moore and coworkers [22] have prepared submicron sized HMX by pouring a solution of HMX in acetone into a cold nonsolvent hexane while stirring at high speed. They prepared HMX material having average particle width of ~300 nm and length of ~1-2 μm. Bayat and coworkers [23] prepared submicron HMX by spraying HMX solution made in acetone into water. The size of HMX obtained was ranging from 14.98 μm to 481 nm depending on anti-solvent temperature, compressed air flow rate and nozzle diameter. Yang and his group [24] prepared nano TATB using concentrated sulfuric acid as solvent and water as non-solvent. They prepared TATB particles with a size of about 60 nm. They reported that due to small diameter and high surface energy, TATB particles tended to agglomerate.

Vandana and coworkers [25] utilized ultrasonic treatment along with solution crystallization and produced HNS particles of mean diameter of 5 μm with broad size range up to 26 μm. Sivabalan et al. [26] dissolved CL20 in ethyl acetate and added heptanes to this solution as an anti-solvent in presence of ultrasound. The particle size of CL-20 material thus obtained is around 5 ± 1μm with a narrow particle size distribution. Bayat et al [27] used similar technique and prepared ultrafine HMX with average particle size of 50-90 nm.

One of the recent and sophisticated techniques used for producing nano-sized energetic materials in pure form is supercritical fluid extraction known as Rapid Expansion of Supercritical Solvent (RESS) method. In this method, a solution of energetic material is made in suitable fluid, mostly liquid CO_2 at its supercritical state (temperature ~ 31.1°C and pressure ~ 7.4 MPa) and then suddenly the solution is

sprayed through a heated nozzle. The rapid expansion of the solution through the nozzle causes super saturation at local level and thereby precipitation of energetic material [28]. This method requires sophisticated instrumentation including low temperature and high-pressure set-up. Mean particle size obtained for TNT using this method is 10 μm and the size distribution is the range of 3.5 μm to 28 μm [29]. Lee's group [30] examined the influence of extraction temperature (293 – 333 K), extraction pressure (8 - 20 MPa) and size of orifice nozzle (50, 100, 200 and 250 μm) on the size and morphology of the RDX particles obtained by RESS process. The prepared RDX particles were submicron-sized with spherical morphologies. The mean particle size of RDX was found ranging from 2.48 to 0.36 μm. Krasnoperov's group [31] produced RDX nanocrystals by RESS method. They performed experiments by expansion of supercritical carbon dioxide solution through sapphire nozzles (ID: 100 and 150 μm) at varying pressures of 15.0 to 29.5 MPa. They produced particles of mean size in range of 110- 220 nm.

RESS method with some modification is used as supercritical anti-solvent (SAS) method in which a supercritical fluid is used as anti-solvent to produce nanoparticles. Supercritical anti-solvent causes precipitation of energetic material dissolved in a liquid solvent. Lee's group [32] prepared micron size RDX materials using SAS process and studied the influence of different solvents viz. Dimethyl sulfoxide, dimethylformamide, acetone, acetonitrile, *n*-methyl 2-pyrrolidone (NMP), and cyclohexanone at temperature 50 °C and pressure (13.7 or 15 MPa). Mean particle size of the recrystallized RDX ranged from 2.6 to 17.7 μm. Using similar process, Pourmortazavi et al [33] synthesized HMX nanoparticles of about 56 nm under optimum conditions such as 3.5 mol/l HMX concentration, 3 ml/min solution flow

rate, cyclohexanone as solvent, and 70 ml/min flow rate of CO_2 as anti-solvent. Essel et al. [34] reported preparation of RDX nano particles of about 30 nm median size by expansion of saturated supercritical carbon dioxide/RDX solution into water.

Another method to produce energetic materials with particle size in the range of nanometers is sol – gel method. In sol - gel method, the energetic material is dissolved in solvent and to this solution gel forming precursors like tetramethoxysilane and water are added which form nano size primary particles suspended in solution, called as sol. The primary particles cross link to form a three-dimensional network, referred to as gel that contain energetic material in the gel pores. Evaporation of liquid from gel results in xerogel which consists of porous network of solid silica containing nano sized energetic materials in the pores of silica network. This method was utilized by Tillotson et al. [35] to prepare the composite of energetic materials with silica for reducing the particle size of RDX and PETN materials with compositions having 45 % of energetic materials and 55 % silica. They examined impact sensitivity of the resulting xerogel but no details on particle size data of energetic materials in the xerogel have been mentioned. Fude-Nie et al. [36] used sol-gel method to prepare nanoparticles of HMX/ammonium perchlorate (AP) using Resorcinol-formaldehyde gel. The mean size of HMX crystals is less than 100 nm. Luo and coworkers [37] prepared $AP/RDX/SiO_2$ nanocomposites by sol-gel method using freeze drying process. The mean grain size of AP is about 60 to 100 nm whereas that of RDX is 100 to 200 nm.

Weeks and coworkers [38] have shown that spin coating and Dip pen nanolithography can also be used for preparing energetic materials such as PETN and HMX on the nanoscale without heating of the energetic material. The thickness of the

PETN film thus prepared was ~250 nm and the roughness of the film was found to be ~25 nm. However, this technique is still less explored for energetic materials.

2.2 Decrease in sensitivity with decrease in particle size for energetic materials:

Many researchers have reported decrease in sensitivity of energetic materials with decrease in particle size. Armstrong et al [39] studied the impact sensitivity of energetic materials with particle size ranging from 0.01 mm to 1 mm and the results reported in this study are shown in Fig. 2.2. They showed that impact sensitivity decreases with decrease in particle size and proposed that large crystals give larger hot spot sizes and lower critical temperature that affect initiation of energetic materials.
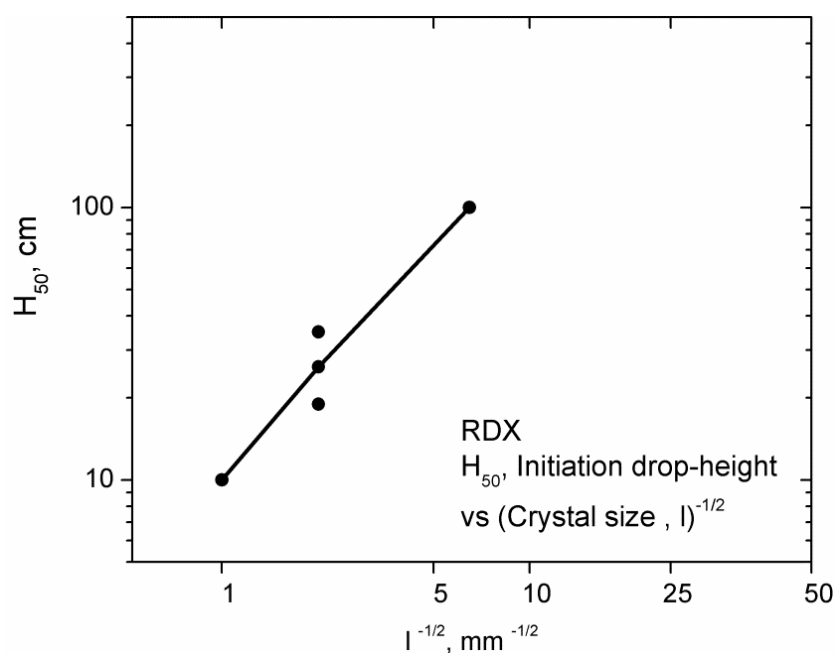
Fig. 2.2 Particle size dependence on initiation of RDX in drop-weight impact [39]

Gifford and coworkers [40] performed drop-weight experiments on PETN and RDX available in conventional grain size (10 - 500 μm) and with fine particle size (<1 μm). They determined the relative sensitivity of these materials and reported that trapped gas appeared to be the main reason for ignition. As fine powders have smaller

interstices between grains, the samples with fine particle size were less sensitive to drop-weight impact than the conventional grain size material.

Sivabalan [26] studied the sensitivity of CL20 materials with particle size in the range of 4-7 μm with an average particle size of 5 μm. They found that impact sensitivity of CL 20 decreased with decrease in particle size.

Spear et al [41] determined figure of insensitivity (F of I) on two lots of RDX powders, one with the larger size (250 μm) particles and other with smaller size (3.9 μm) particles. Of the two, the 3.9 μm ball milled RDX exhibits lower sensitiveness. Their explanation is that as particle size decrease, the permeability decreases and it reduces the area of surface exposed to reaction products leading to reduced shock sensitivity. Moreover, smaller grain size materials have smaller voids and hence smaller hot spots, thus energy loss in thermal conduction will be higher.

Antoine et al [42] studied the sensitivity of RDX particles ranging from 1 to 10 μm prepared by solvent/ non-solvent technique and of particles in the range of ~ 400 nm to several micrometers prepared by evaporative crystallization process. Their experiments showed that impact sensitivity of explosives decreased when used smaller particle size RDX instead of bigger size RDX in PBX formulations.

Li and group [43] investigated response of HMX powders with different particle sizes ranging from 0.6 to 56 μm to impact initiation. They proposed that a fractal characteristic, quantized by size fractal dimension (D), is the dominating factor in sensitivity of HMX rather than particle size. HMX samples with higher D value exhibit lower impact sensitivity. They proposed that with increase in the proportion of fine particles, thermal conductivity of HMX particles improves because of increase in specific surface area. The size of numerous tiny holes scattered among the compressed

particles becomes smaller which gives a higher critical temperature T_c and hence it is hard to form hot spots under impact action.

Li and coworkers [21] prepared HMX powders with particle sizes ranging from 0.6 μm to 21 μm and studied their impact sensitivity. Their results are shown in Fig. 2.3. They found that smaller HMX particles are less sensitive to impact force. They attributed this to the influence of crystal defects or voids inside HMX particles. They suggested that smaller HMX particles have uniform texture and a few crystal deficiencies which reduce sensitivity of HMX. Furthermore, plenty of tiny air holes among the spherical particles can cushion a blow from the impact action resulting in lower impact sensitivity.
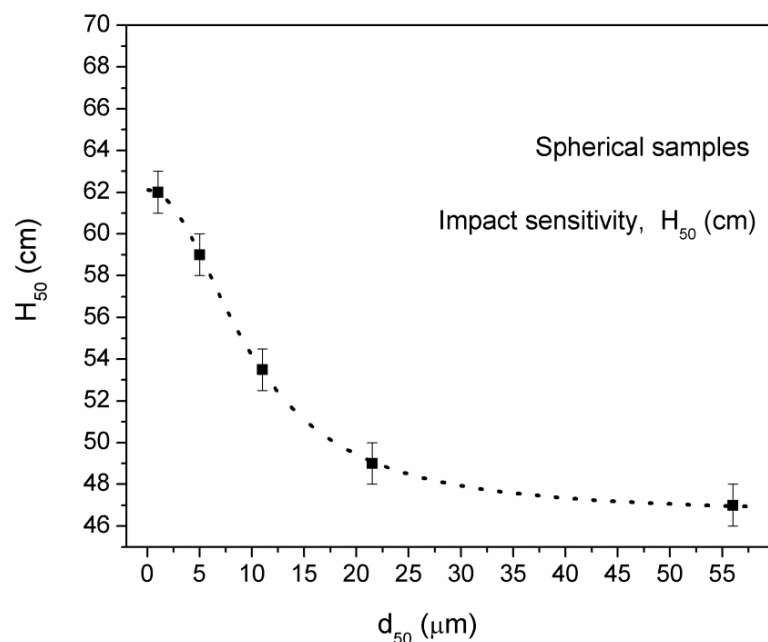
Fig. 2.3 Impact sensitivity of HMX as a function of particle size [21].

Qiu et al. [11] reported that for RDX particles within size range of 0.1 to 1 μm prepared by spray drying technique, sensitivity decreased with reduced crystal size. The low sensitivity was attributed to small crystal size as well as small void size

(~250 nm). They proposed that lowering of void size desensitizes energetic materials to mechanical stimuli by mitigating the formation of critical hotspots.

Stephnov and coworkers [31] measured impact sensitivity of nanosized RDX in loose powder and pellet form. The sensitivity in terms of height at which initiation probability is 50 % (H_{50}) for the 150 nm RDX powder was over 100 cm whereas for 150 nm RDX pellet H_{50} was 42 cm. The H_{50} for 350 nm RDX in loose form was 73.5 cm and for pellets it was 35.5 cm. The H_{50} for 4.8-micron RDX loose powder was 32.2 cm. Stephnov proposed that with smaller particle size, average inter-crystalline void size is smaller than for larger RDX crystals. Consequently, having a larger number but of smaller size voids leads to reduced initiation sensitivity.

Dabin and coworkers [44] prepared reticular structured HMX of about 50 nm using re-precipitation method. The impact test results showed that this smaller size HMX is less sensitive to impact. Song et al [10] produced RDX micro particles using solvent-non solvent re-crystallization method. They observed that for these samples H_{50} increases as the particle size decreases indicating that particles with smaller size are more resistive to impact force. The average value of H_{50} for narrow distribution samples ($H_{50} = 52$ cm) is slightly higher than that of broad distribution particles ($H_{50} = 46.49$ cm) suggesting that the former is less sensitive to impact. They proposed that during impact, the smaller RDX particles dissipate heat faster and therefore "hot spot" is hard to form and to enable detonation.

Tillotson et al [35] produced nanosized RDX and PETN by sol-gel process using solution crystallization and powder addition method. Fig. 2.4 shows the drop-hammer sensitivity test results of Tillotson et al [35]. These results indicate that

pellets made from powders prepared by sol-gel process have significantly lower sensitivities than the pellets made of raw explosive powders.
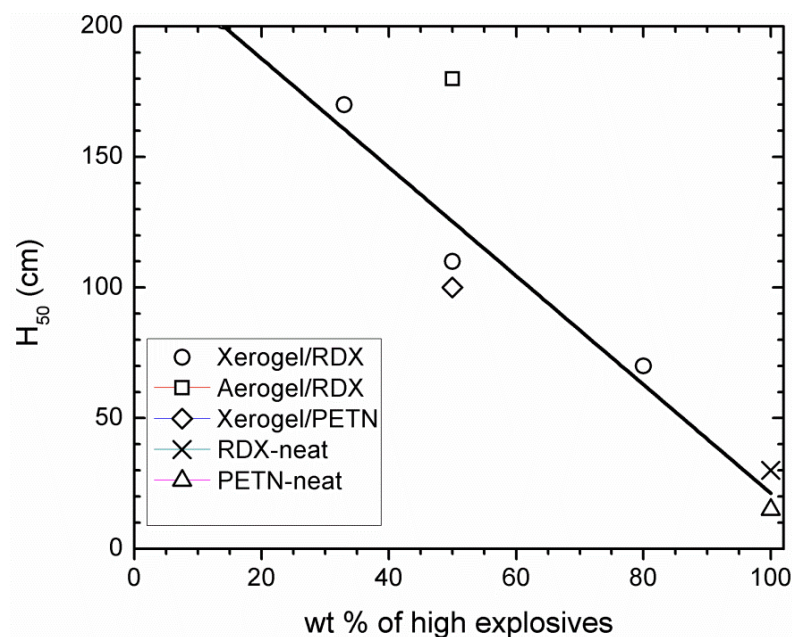
Fig. 2.4 Impact sensitivity of sol-gel derived energetic materials and corresponding neat energetic materials [35]

It is reported that the aerogels containing 50 wt. % energetic materials and 50 wt. % silica failed to detonate. They proposed that the presence of gel structure decreases the impact sensitivity due to intimate mixing of energetic material and inert matrix. They also proposed that porous gel structure influences the sensitivity by providing a protective insulating barrier around the energetic molecules. This structure may absorb and transport the heat generated on impact, away from the energetic molecules, thereby alleviating the possibility of runaway reactions and detonation.

Borne et al [45] explained ignition of energetic material due to impact, based on pores inside the energetic particles (intra-granular pores) and the pores in the bulk (extra-granular pores). They proposed that with the decrease in particle size, the amount of intra-granular pores decrease that reduces the shock sensitivity. Some of

the intra-granular pores are usual solvent inclusions resulting from the crystallization process. These intra-granular pores can affect the sensitivity of energetic materials. The particles internal defect population is confirmed as a very important feature to control the sensitivity of energetic materials.

2.3 Increase in sensitivity due to reduced size of explosives:

There are also several reports claiming on increase in sensitivity of energetic materials with reduction in particle size. Campbell and group [46] carried out experiments on TNT pellets pressed from coarse particles (200-250 μm) and fine grained material (20-50 μm). Their results showed that pellets made from fine grained TNT were more sensitive than those made from coarse material.

Pant et al. [47] prepared ultrafine RDX by its non-aqueous precipitation from acetone using hexane. It gave rod-shaped crystals with diameter < 1 μm. Oval shaped (< 5 μm) crystals were also precipitated with aqueous anti solvent. They reported that precipitated material was more sensitive to impact however, recommended for detailed study to explain these experimental observations.

Stephnov and co-workers [48] prepared RDX powders with mean crystal sizes of 200 and 500 nm by RESS method and studied impact sensitivity of these materials for powder samples as well as pressed pellets. They found that sensitivity of RDX decreased with decrease in particle size up to 500 nm and RDX with particle size of 500 nm being the least sensitive as shown in Fig. 2.5.
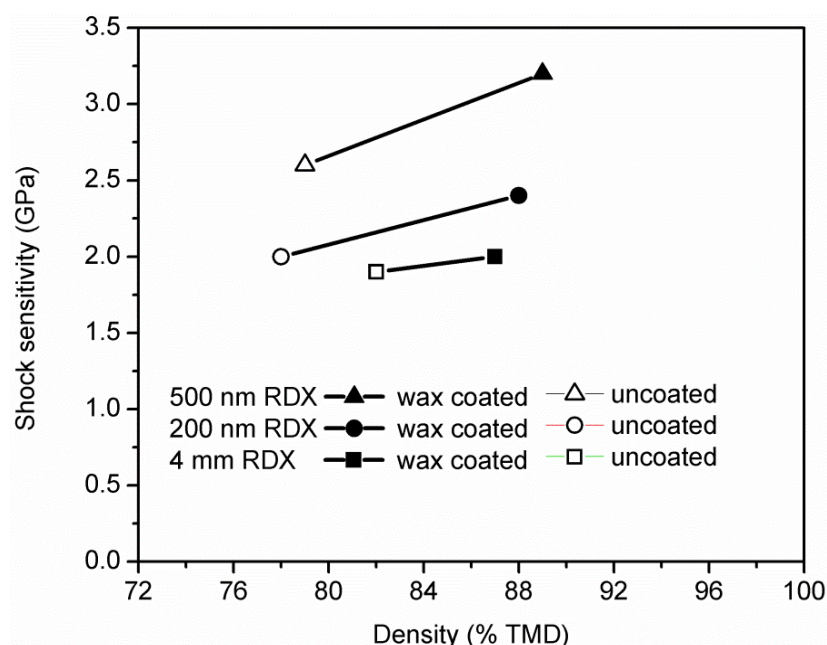
Fig. 2.5 Shock sensitivities of uncoated and wax coated samples of 200 nm, 500 nm, 4 μm RDX [48].

However, they found that the sensitivity trend reverses when RDX particle size is further reduced and sensitivity exhibited by 200 nm RDX is higher compared to the 500 nm RDX. They suggested that below a certain crystal size re-sensitization may occur. Generally, crystalline energetic materials are expected to initiate via formation of critical hot spots due to void collapse. This mechanism appears to be applicable in describing the trend observed for sizes down to 500 nm. However, the reversal of the sensitivity trend for 200 nm RDX indicates that the more favorable initiation mechanism for these samples, similar to that observed with homogeneous explosives, occurring via thermal explosion. The enhanced reactivity due to the higher specific surface area may explain the increased impact sensitivity of the 200 nm RDX.

Effect of particle size has also been studied in composite energetic materials. Thermite mixtures of metallic fuel and metallic oxidizer are being used in delays or

certain specialized applications. Effect of reducing particle size on sensitivity in thermite mixtures consisting of dispersed phase of metal oxides like iron oxide and Aluminum as metallic fuel has been studied in literature [49]. These mixtures have less power due to gasless compositions. The other energetic composites in which effect of reduced particle size has been studied are with organic gels as fuels and oxidizers as dispersed phase. A few attempts have been made in this area using organic components like resorcinol or phenol gel network as fuels whereas inorganic materials like ammonium nitrate, ammonium perchlorate and magnesium chlorates as oxidizers [50-51]. However, these compositions are not found much powerful because of difficulties in loading high oxidizer content to highly oxygen deficient organic gel [50]. The efficient organic-inorganic nano composites should have nearly stoichiometric oxygen balance for high energy output to explore use of nano sized particles.

From the literature survey, it has been observed that particle size plays an important role in sensitivity and ignition mechanism of the energetic materials. However, systematic study in wide range of particle size of these materials is needed to propose a clear trend of particle size effect on properties of energetic materials. Since these energetic materials are not as such available with the desired particle size, suitable processes capable of producing these materials with wide range of particle size need to be developed for studying their energetic properties. The effect of introducing controlled defects like porosity on ignition mechanism of energetic materials which has not been significantly explored while evaluating the sensitivity properties also need to be studied.

REFERENCES:

[1]   Trends in Shock Initiation of Heterogeneous Explosives, P M Howe, *Eleventh Symposium (international) on Detonation*, Ed. J M Short and J. E. Kennedy, Office of Naval Research, Arilngton VA, (1998) pp.670-677.

[2]   Preparation and Characterization of Insensitive Nano RDX, J. Liu, L. Wang, Q. Li, J. Zeng, S. Zhou, W. Jiang, F. Li, *Chin J. Explos. Propellants*, **6** (2012), 46-50

[3]   Particular Aspects of The Explosive Particle Size Effect on Shock Sensitivity of Cast PBX Formulations, H. Moulard, *In* Proceedings of 9th *Symposium (Int) on Detonation*, Portland, USA (1989) pp. 18-24.

[4]   Study on Influence of Particle Size on the Mechanical Sensitivity Of HMX, S Chen, Y R Zhang, Y H Zhang, *Chinese Sichuan Ordn. J.* **5** (2006) 27-28.

[5]   Kinetic Investigation on Thermal Decomposition of hexahydro -1, 3, 5- trinitro - 1,3,5-triazine (RDX) Nanoparticles*,* M. Fathollahi, B. Mohammadi, J. Mohammadi, *Fuel,* **104** (2013) 95–100

[6]   Construction and Properties of Structure and Size-controlled micro/nano Energetic Materials, B Huang, M Cao, F Nie, H Huang, C Hu. *Def Technol.* **9** (2013) 59–79.

[7]   Production of Particles of Explosives, Ulrich Teipel, *Propellants, Explos. Pyrotech.*, **24** (1999)134-139

[8]   Wet Grinding of Crystalline Energetic Materials, L C Estabrook, C Somoza, *US patent* 5197677 (1993)

[9]   Size Reduction of Particulate Energetic Material*,* U Teipel, I Mikonsaari, *Propellants, Explos. Pyrotech.*. **27** (2002) 168-174

[10] Dependence of Particle Size and Size Distribution on Mechanical Sensitivity and Thermal Stability of Hexahydro-1,3,5-trinitro-1,3,5-triazine , X Song, F Li,. *Def. Sci. J.* **59** (2009) 37-42

[11] RDX-based Nanocomposite Microparticles for Significantly Reduced Shock Sensitivity*,* H Qiu, V Stepanov, AR Di Stasio, T Chou, WY Lee, *J. Hazard. Mater.* **185** (2011)489-493

[12] Preparation and Characterization of HMX/Estane Nanocomposites, X. Shi, J. Wang, X. Li, C. An, *Central European J. Energ. Mater.* **11** (2014) 433-442.

[13] Single-step Production and Formulation of HMX Nanocrystals*,* H. Qiu, V Stepanov, T Chou, A. Surapaneni, AR DiS tasio, WY Lee, *Powder Technol.* **226** (2012) 235-238.

[14] Synthesis and Characterization of High-Energy Nanoparticles, L. Mercado, PM Torres, LM Gomez, N Mina, SP Hernandez, R Lareau, RT Chamberlain, ME Castro-Rosario, *J. Phys. Chem. B*.**108** (2004) 12314-12317.

[15] Yalkowsky, Samuel H. *Solubility and Solubilzation in Aqueous Media,* 1st Edition. An American Chemical Society Publication, (1999)

[16] Study on Preparation of Fine PETN for Initiating Devices, Shallu Gupta, Simran Kaur, D K Pal, T Raychaudhuri, *First National Symposium & Exhibition on Trends in Explosive Technology*, TBRL, Chandigarh, India (2008)

[17] Application of Supercritical Carbon Dioxide in Energetic Materials Processes: A Review, S. M. Pourmortazavi, and S. S. Hajimirsadeghi, *Ind. Eng. Chem. Res.* **44** (2005) 6523-6533.

[18] Preparation of Explosives of Fixed Particle Size and Shape, G. A. Cave, N. J. Krotinger, and J. D. Jiccaleb, *Ind. and Eng. Chem.* **41** (1949) 1286-1290.

[19] Growth Kinetics in Seeded Cooling Crystallization of 3-nitro-1,2,4-triazol-5-one in water-N-methylpyrrolidone, K J Kim, K M Kim, *Powder Technol.* **122** (2002) 46-53

[20] Particle Size Management Studies on Spherical 3-Nitro-1,2,4-triazol-5-one, V Ramavat, R. Sarangapani, SR Patil, MG Gore, KA Sikder, *Part. Part. Syst. Charact.***28** (2012) 57-63

[21] Dependence of Particle Morphology and Size on the Mechanical Sensitivity and Thermal Stability of octahydro-1,3,5,7-tetranitro-1,3,5,7-tetrazocine, X Song, Y Wang, C An, C; X Guo, F. Li, *J. Hazard. Mater.* **159** (2008) 222-229

[22] Submicron-Sized Gamma-HMX: Preparation and Initial Characterization, K Y Lee, D S Moore, B W Asay, A. Llobet, *J. Energ. Mater.* **25** (2007)161-171

[23] Y. Bayat, M. Eghdamtalab, V. Zeynali, Control of the Particle Size of Submicron HMX Explosive by Spraying in Non-Solvent. *J. Energ. Mater.* **28** (2010) 273-284

[24] Preparation and Characterization of Nano-TATB Explosive, G. Yang, F. Nie, H. Huang, L. Zhao, W. Pang, *Propellants, Explos. Pyrotech.* **31** (2006) 390-394

[25] Evaluation of Ultrasonic Treatment for the Size Reduction of HNS and HMX in Comparison to Solvent-antisolvent Crystallization, J. Kaur, VP Arya, G Kaur, T Raychaudhuri, P. Lata, *Propellants Explos. Pyrotech.* **37** (2012,) 662-669

[26] Study on ultrasound assisted precipitation of CL-20 and its effect on morphology and sensitivity, R Sivabalan, G M Gore, U R Nair, A Saikia, S Venugopalan, B R Gandhe, *J. Hazard. Mater.***A139** (2007)199-203

[27] Ultrasonic Assisted Preparation of Nano HMX, Y. Bayat, S R Shirizinia, R Marandi, *Int. J. Nanosci. Nanotechnol.* **6** (2010) 210-215

[28] Nano-RDX Synthesis by RESS Process and Sensitivity Characterization, T M Wawiernia, A C Cortopassi, J T Essel, P J Ferrara, and K K Kuo, *8th International Symposium on Special Topics of Chemical Propulsion*, Cape Town, South Africa, (2009).

[29] Formation of Particles of Explosives with Supercritical Fluids, U. Teipel, U. Fçrter-Barth, P. Gerber, H H Krause, *Propellants Explos. Pyrotech.* **22** (1997)165-169

[30] Preparation of Submicron-sized RDX Particles by Rapid Expansion of Solution Using Compressed Liquid Dimethyl Ether, B M Lee, D S Kim, Y H Lee, B C Lee, H S Kim, H. Kim, Y W Lee, *J Supercritical Fluids.* **57** (2011) 251-258

[31] Production of Nanocrystalline RDX by Rapid Expansion of Supercritical Solutions, V Stepanov, L N Krasnoperov, I B Elkina, X Zhang, *Propellants Explos. Pyrotech.*, **30** (2005) 178-183

[32] Supercritical Antisolvent Micronization of Cyclotrimethylenetrinitramine: Influence of the Organic Solvent, B M Lee, J S Jeong, Y H Lee, B C Lee, H S Kim, H. Kim, Y W Lee, *Ind. Eng. Chem. Res.* **48** (2009) 11162-11167

[33] Statistical Optimization of Supercritical Carbon Dioxide Antisolvent Process for Preparation of HMX Nanoparticles, Y Bayat, S M Pourmortazavi, H. Iravani, H. Ahadi, *J Supercrit Fluids.* **72** (2012) 248-254

[34] Characterization of Nano-sized RDX Particles Produced Using RESS-AS Process, J T Essel, A C Cortopassi, K K Kuo, C G Leh, J H Adair, Formation and *Propellants Explos. Pyrotech.* **37** (2012) 699-706

[35] Sol–Gel Processing of Energetic Materials, T M Tillotson, L W Hrubesh, R L Simpson, R S Lee, R W Swansiger, L R Simpson, *J. Non-Cryst. Solids.* **225** (1998) 358-363

[36] Sol–Gel Synthesis of Nanocomposite Crystalline HMX/AP Coated by Resorcinol–Formaldehyde, F Nie, J. Zhang, Q. Guo, Z. Qiao, G. Zeng, *J. Phys. Chem. Solids.* **71**(2010)109-113

[37] Preparation and Properties of an AP/RDX/SiO2 Nanocomposite Energetic Material by the Sol-Gel Method, R. Chen, Y. Luo, J. Sun, G. Li, *Propellants Explos. Pyrotech.* **37**(2012) 422-426

[38] Patterning High Explosives at the Nanoscale, O A Nafday, R. Pitchimani, B L Weeks, J Haaheim, *Propellants Explos. Pyrotech.* **31** (2006)376-381.

[39] Crystal Size Dependences for Impact Initiation of Cyclotrimethylenetrinitramine Explosives, R W Armstrong, C S Coffey, V F DeVost, W L Elban, *J Appl. Phys.* **68** (1990) 979-984.

[40] High-Speed Photographic Study of the Drop-Weight Impact Response of Ultrafine and Conventional PETN and RDX, J E Balzer, J E Field, M J Gifford, W G Proud, S M Walley, *Combustion and Flame.* **130** (2002) 298-306.

[41] Mechanism of and Particle Size Effects on Shock Sensitivity of Heterogeneous Pressed Explosives: Preliminary Assessment of Binder less RDX in Fuze Trains, R J Spear, Victor Nanut, Defence Science and Technology Organization, Materials Research Laboratories Melbourne, *Report MRL-R-1077* (1988).

[42] Energetic Materials: Crystallization, Characterization and Insensitive Plastic Bonded Explosives, A. Vander Heijden, Y. Creyghton, E. Marino, R. Bouma, G

Scholtes, W. Duvalois, M. Roelands, *Propellants, Explos. Pyrotech.* **33** (2008) 25-32.

[43] Dependence of Mechanical Sensitivity on Fractal Characteristics of Octahydro-1,3,5,7-tetranitro-1,3,5,7-tetrazocine Particles, Y Wang, X Song, D Song, W Jiang, H Liu, F Li, *Propellants Explos. Pyrotech.* **36** (2011) 505-512.

[44] Preparation and Characterization of Reticular Nano-HMX, Y. Zhang, Dabin Liu, L. Chunxu, *Propellants, Explos. Pyrotech.* **30** (2005) 438-441.

[45] Reduced Sensitivity RDX in Pressed Formulations: Respective Effects of Intra-Granular Pores, Extra-Granular Pores and Pore Sizes, L. Borne, Julien Mory, Franck Schlesser, *Propellants, Explos. Pyrotech.* **33** (2008) 37-43.

[46] Shock initiation of Solid Explosives, A W Campbell, W C Davis, J B Ramsey, J R Travis, *The Physics of Fluids.* **4** (1961) 511-521.

[47] Preparation and Characterization of Ultrafine RDX, A. Pant, A K Nandi, S P Newale, V P Gajbhiye, H. Prashanth, R K Pandey, *Central European J. Energ. Mater.* **10** (2013) 393-407.

[48] Production and Sensitivity Evaluation of Nanocrystalline RDX-based Explosive Compositions, V. Stepanov, V. Anglade, W A B Hummers, A V Bezmelnit, L N Krasnoperov, *Propellants Explos. Pyrotech.* **36** (2011) 240-246.

[49] Reflected Shock Ignition and Combustion of Aluminum and Nanocomposite Thermite Powders, T. Bazyn, N. Glumac, H. Krier, T. S. Ward, M. Schoenitz, E. L. Dreizin, *Combustion Sci. Technol.* **179** (2007) 457-476

[50] Preparation and Characterization of Energetic Nanocomposites of Organic Gel – Inorganic Oxidizers, S. Cudziło and W. Kicioski, *Propellants Explos. Pyrotech.*, **34** (2009)155 – 160

[51] Sol–Gel Synthesis of Nanocomposite Crystalline HMX/AP Coated by Resorcinol–Formaldehyde, N. Fude, J. Zhang, Q. Guo, Z. Qiao, G. Zeng , *J of Phys. and Chem. of Solids*, **71** (2010) 109-113

CHAPTER 3

EXPERIMENTAL TECHNIQUES USED TO CHARACTERIZE PROCESSED

ENERGETIC MATERIALS

In present works, energetic materials with different particle size have been prepared using various processing methods. These processed energetic materials have been characterized using techniques like FTIR, XRD, TG-DSC, SAXS, FESEM, TEM and surface area analyzer to get information about the chemical and crystal structures, microstructure, morphologies and particle sizes of the materials studied. To study the energetic properties of these materials, widely accepted techniques like drop hammer impact test to measure impact sensitivity, TGDSC analysis to study thermal initiation and kinematics of decomposition reaction in energetic materials, gap test for shock sensitivity and self-shorting sensor pin techniques for detonation velocity measurement have been utilized. In the present chapter, brief description of the experimental setup which is in accordance with acceptable standard and used for measurements along with its working principle and main components of the equipment and parameters studied has been provided.

3.1   Powder X-ray Diffraction (XRD)

Powder X-ray diffraction is a versatile non-destructive and widely used analytical method to characterize materials in powder form. It provides information about crystal structure, impurities and grain size. A powder XRD equipment consists of X-ray tube equipped with filter. Cathode part of X-ray tube generates electrons which are made to accelerate from cathode to anode with high voltage. These electrons hit the target material and some of these electrons eject lower shell electrons from atoms of target material. In this process, X-rays are generated during electrons

from higher energy shell fall to lower energy shell, and the energy corresponding to difference between electron shells is emitted as X-rays. The principle of XRD is based on scattering of the X-rays by a well-defined array of atoms in a crystal. X-rays have wavelengths of the order of a few angstroms that match with typical inter-atomic distances in crystalline solids. Bragg's law proposes that the incident X-ray radiation would produce a diffraction peak if X-ray reflections from various planes interfered constructively. This geometric requirement is met by following equation 3.1:

$$2d \sin \theta = n\lambda \qquad \qquad \text{... (3.1)}$$

Where n is a positive integer and λ is the wavelength of incident X-ray beam and d is the inter planer spacing in a crystal.

Inter-planar spacing thus determined from XRD pattern is characteristics of a material, and hence can be used to identify the material under study. In most of the diffractometers, Cu-Kα is used as the X-ray source and a proportional counter (Argon filled) is used as the detector. In present work, XRD data for the processed energetic materials has been obtained on a Rigaku X-ray diffractometer operated with accelerating voltage of 30 KV and current 20 mA. Cu Kα (λ=1.542 Å) is used for recording the XRD patterns. The diffracted X-rays data were collected by scanning in step-scan mode from 2θ of 10 $^\circ$ to 80 $^\circ$ with scan step size of 0.02°.

3.2   Fourier transforms infrared (FTIR) spectroscopy

In a material, bonds between different atoms vibrate at various frequencies depending on the nature of atoms and the type of bonds. This feature is studied in IR spectroscopy. Traditionally, IR spectrometers have been used to analyze samples by means of transmitting the infrared radiation directly through the sample. Some of the infrared radiation is absorbed by the sample and some of it is passed through

(transmitted). The resulting spectrum represents the molecular absorption and transmission, creating a molecular fingerprint of the sample. An infrared spectrum represents a sample with absorption peaks which correspond to the frequencies of vibrations of bonds between the atoms making up the material. Therefore, infrared spectroscopy can result in a positive identification (qualitative analysis) of different kind of materials. FT-IR spectroscopy stands for Fourier Transform Infrared spectroscopy, the preferred method of infrared spectroscopy which is typically based on the Michelson Interferometer. The interferometer consists of a beam splitter, a fixed mirror, and a mirror that translates back and forth, very precisely. The X-axis of the interferogram represents the optical path difference. Each individual spectral component contributing to this signal is a single sinusoid with a frequency inversely proportional to its wavelength.

In sample analysis, attenuated total reflection (ATR) technique is getting popular in FTIR spectroscopy due to its versatility and non-requirement of special sample preparation. In ATR, the crystal is a parallel- sided plate, with very small crystals (typically about 2 mm across) with the upper surface exposed (Fig. 3.1). An infrared beam is directed onto an optically dense crystal with a high refractive index at a certain angle. Typically, ATR crystals have refractive index values between 2.38 and 4.01 at 2000 cm^{-1} [1], as majority of solids have much lower refractive indices. Diamond is by far the best ATR crystal material because of its robustness and durability. An attenuated total reflection of infrared beam occurs when the beam comes into contact with a sample (indicated in Figure 3.1) [2]. This internal reflectance creates an evanescent wave that extends beyond the surface of the crystal into the sample held in contact with the crystal. In regions of the infrared spectrum

where the sample absorbs energy, the evanescent wave is attenuated or altered. The attenuated energy from each evanescent wave is passed back to the IR beam, which then exits the opposite end of the crystal and is passed to the detector to generate an infrared absorption spectrum.
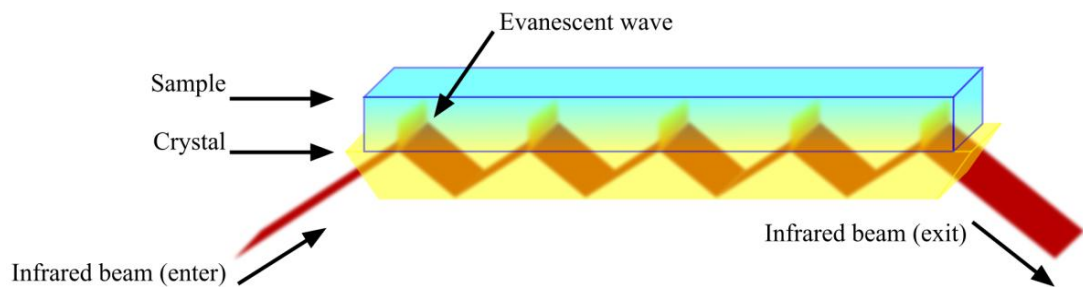
Fig. 3.1 ATR system (Source: http://sites.science.oregonstate.edu/ chemistry/courses/ch361464/ch362/IR_NMRuse/ATR.htm)

In present work, IR spectroscopy measurements on energetic materials have been carried out on Bruker make FTIR alpha spectrophotometer using ATR technique. For IR characterization, mostly powder samples of about 3 - 5 mg were scanned within the wave number range of 550 to 5000 cm^{-1} with resolution of 4 cm^{-1} using ZnSe detector. For recording FTIR spectra in transmission mode, pellets of test materials (2 % by weight) mixed with potassium bromide were used.

3.3 Scanning Electron Microscopy

Morphology of energetic materials has been studied with scanning electron microscopy. The scanning electron microscope (SEM) uses a focused beam of high-energy electrons to generate a variety of signals at the surface of solid specimens. Schematic diagram of scanning electron microscope is shown in Fig. 3.2.
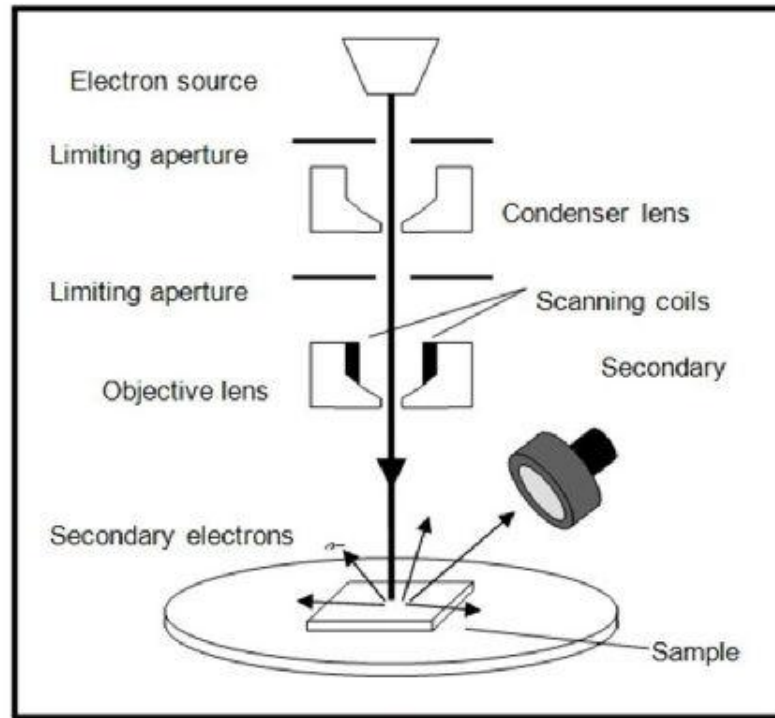
Fig. 3.2   Schematic diagram of scanning electron microscope (Source: Summer
Project 2015 at SNBNCBS, Ankan Mukhopadhyay, IIT, Guwahati)

In electron microscope, cathode generates an electron beam. These electrons
are accelerated through a column electromagnetic lens and focused onto objective and
also that swept across the surface of a sample. Accelerated electrons have significant
amount of kinetic energy which is dissipated in a variety of signals produced by
electron-sample interactions. These signals have secondary electrons (produce SEM
images) [3], backscattered electrons (BSE) and diffracted backscattered electrons.
Secondary electrons emitted from a thin layer of the sample surface and they are used
in imaging the morphology and topography on samples.

Field Emission Scanning Electron Microscope (FESEM) usually uses low
voltage because the FE Gun can produce high primary electron brightness even at low
accelerating potentials. This is a useful feature of FESEM for characterizing energetic

32

materials as these materials are sensitive to high electron energies which can damage the sample.

The microstructure of energetic materials in present work is studied with Carl Zeiss Auriga FESEM. For analysis, sample powder was suspended in methanol and suspension was dispersed on a copper plate. The samples were then gold coated to prevent charging of specimen. The accelerating voltage was in range of 3 to 20 kV.

3.4　Transmission Electron Microscope (TEM):

Transmission electron microscopy (TEM) is a tool for understanding the microstructure of materials. This allows for obtaining real-space images of materials with resolutions of the order of a few nanometers while simultaneously obtaining diffraction information from specific regions in the images. A simple ray diagram of a TEM containing two lenses recording images is shown in Figure 3.3 a [4].

(a)   (b)
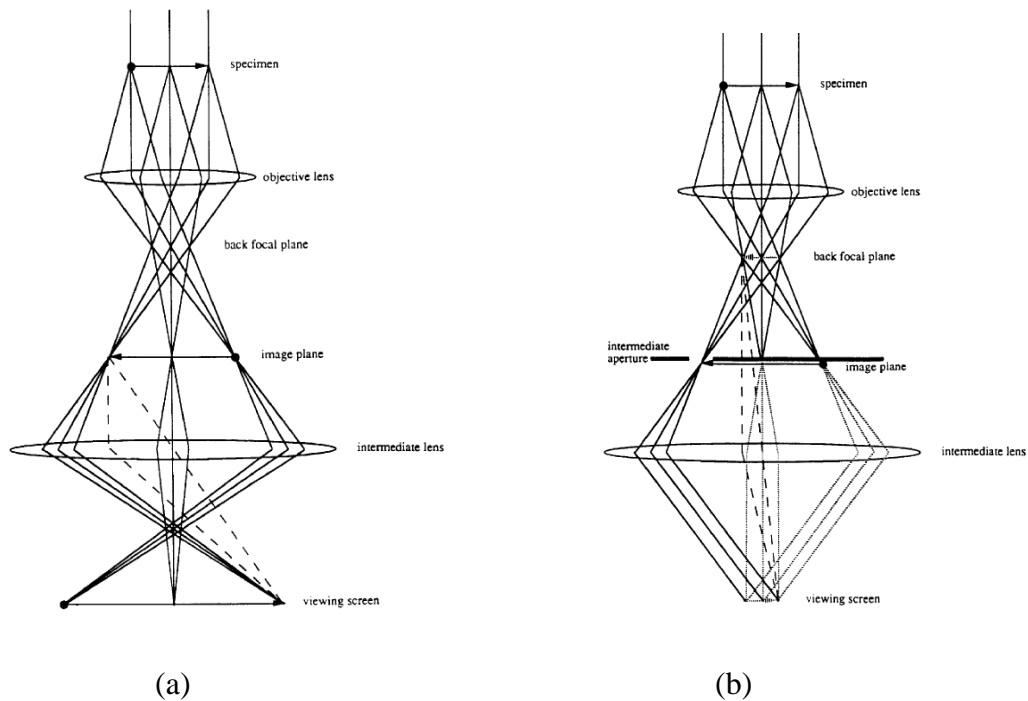
Fig. 3.3　Schematic ray diagrams for TEM. a) Image mode for TEM containing objective and intermediate lens and b) Selected area Diffraction (SAD) mode in TEM [4]

33

All transmitted and diffracted rays leaving the specimen are combined to form an image at the viewing screen, in a similar manner as in a conventional optical microscope. In this simple mode of imaging, the specimen generally shows little contrast because all the diffracted intensity reaches the viewing screen. Fig. 3.3 b shows a ray diagram for making diffraction patterns with the simplified two-lens transmission electron microscope. The transmitted beam and all the diffracted beams are imaged on the viewing screen. In this configuration, a second aperture, called an intermediate (or selected area) aperture, can be positioned in the image plane of the objective lens, and this provides a means of confining the diffraction pattern to a selected area of the specimen.

In the present work, a JEOL 2000FX transmission electron microscope operating at 160 kV has been used to record transmission electron micrograph. For TEM analysis, powder samples were suspended in methanol and ultrasonicated for 5 minutes. The resulting methanol–powder mixture was dispersed on a carbon coated copper grid of 200 mesh size. The methanol could evaporate leaving a uniform distribution of particles on the copper grid. The TEM images have been recorded on films which are subsequently scanned to obtain digital images. From the TEM micrographs, the particle size distributions are evaluated. TEM is also used to record diffraction pattern in selected area. The radius of the concentric rings from selected area electron diffraction (SAED) pattern was reduced to d- spacing using the formula given in equation 3.2:

$$Dd = \lambda L \qquad \qquad \dots (3.2)$$

where, wavelength of electron is $\lambda = 0.03$ A° for accelerating voltage of 160 kV; distance from target to screen- L = 1000 mm; D – radius of the diffraction pattern ring

3.5   Small Angle X-ray Scattering (SAXS):

Small-angle X-ray scattering have been found to be well suited for studying disordered systems, aggregates of particles, and gels [5]. Fractals [6] are one of the most important system studied using this technique. The intensity $I(Q)$ of the small-angle X-ray scattering from many disordered systems has been found to be proportional to a negative power of the quantity $Q = 4\pi \sin(\theta)/\lambda$ where θ is the scattering angle and, λ is the X-ray wavelength. Usually this dependence of $I(Q)$ on a negative power of Q is observed only when Q is large enough to satisfy the condition $\xi Q \gg 1$, where ξ is a length that characterizes the size of the structure producing the scattering. This kind of scattering is often called 'power-law' scattering and can be described by the equation [7]

$$I(Q) = I_0 (Q)^{-\alpha} \qquad \qquad \dots (3.3)$$

where α and I_0 are constants.

).
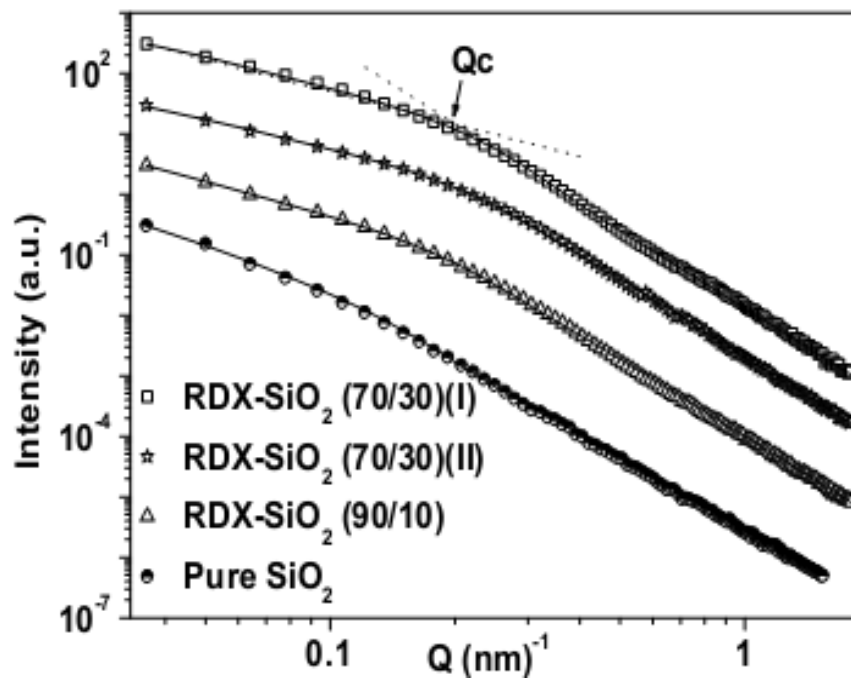
Fig. 3.4 Typical profiles of SAXS measurements [8]

Information of size and morphology are obtained from the magnitude of the exponent α of power-law scattering [9]. Typical SAXS profile is shown in Fig. 3.4. The scattering profiles plotted on log-log scale are straight lines over wider q-range with change of slope at low-q regions as marked in Fig. 3.4. The scattering at low-Q ($Q < Q_1$) region occurs from larger, sub-micron size particles and the inter-particle voids. Whereas the scattered intensity in the region $Q2 < Q < Q1$, arises due to surfaces of the smaller particles or pores within the aggregates. From the crossover point, the average size (D) of the basic particles within the aggregates is found. The linear behavior of profiles indicates that SAXS profile follow a power-law: $I(Q) \sim Q^{-\alpha}$. The value of α would be 4.0 for smooth surface of the scattering object following the Porod's law. Whereas a non-integer value for α indicates the fractal structure. For mass fractals with dimension D_m, $\alpha = D_m \leq 3$ whereas for surface fractals with dimension D_s, $\alpha = (6-D_s) > 3.0$ and $2 \leq D_s \leq 3$. Thus, the slope of the scattering curve on log-log scale indicates the type of the fractal. The slit corrected SAXS profiles of the samples of this study are fitted to the function

$$I\,(Q) = I\,(0)/\,[1+ (\xi Q)^{2}]^{-\alpha/2} \qquad \qquad \dots (3.4)$$

where $\alpha = 4$ for smooth surface of the pores and ξ is the correlation length [7]. For nearly spherical scattering object, ξ represents average radius (R). However, for the scattering profiles with the slope $\alpha \neq 4$, this function is modified [10] as:

$$I\,(Q) = I\,(0)/\,[1+ ((1+\alpha)/3)\,(RQ)^{2}]^{-\alpha/2} \qquad \qquad \dots (3.5)$$

In the present works, small angle x-ray scattering (SAXS) measurements have been carried out using a Rigaku small angle goniometer mounted on rotating anode x-ray generator. Scattered intensity I (Q) was recorded using a scintillation counter by

varying the scattering angle 2θ. Here Q is the scattering vector equal to $4\pi \sin(\theta)/\lambda$, λ is the wavelength of incident (Cu-K$_\alpha$) X-rays.

3.6   Thermo-gravimetric Differential Scanning Calorimetric (TG-DSC):

Thermo-gravimetric (TG) Analysis is used to measure the thermal stability of the compounds. This technique is used to characterize materials that exhibit weight loss or gain due to decomposition, oxidation, or dehydration. Schematic of a thermo-gravimetric analyzer is shown in Figure 3.5.
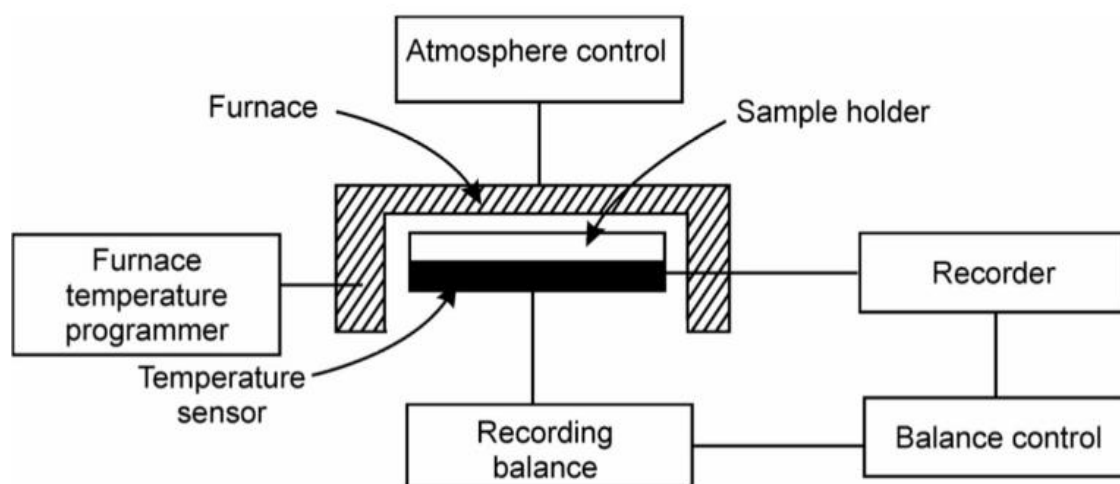
Fig. 3.5 Schematic illustration of thermo-gravimetric analyzer (source: https://www.slideshare.net/sureshselvaraj108/thermogravimetric-analysis)

In TG analysis, mass of a sample is measured with change in temperature in a controlled atmosphere. Measurements are used primarily to determine the composition of materials and to predict their thermal stability at temperatures up to 1000 °C [11]. Thermo-gravimetric analyzer consists of a high precision balance with a sample pan. The pan is placed in a small electrically heated furnace with a programmable temperature controller and a thermocouple to accurately measure the pan temperature.

The temperature is generally increased at constant rate. TG analyzer continuously measures mass of the sample while the temperature of a sample is changed over time.

In Differential Scanning Calorimetry (DSC), the difference in heat flow between the sample and reference is measured as a function of temperature. This difference in amount of heat is then plotted against time or against temperature (DSC curve). Generally, the sample holder temperature increases linearly as a function of time. Changes in the sample, either exothermic or endothermic, can be detected relative to the inert reference. Thus, a DSC curve provides data on the transformations that have occurred, such as melting, glass transitions, or exothermic decompositions. Schematic illustration of DSC instrument is shown in Figure 3.6.
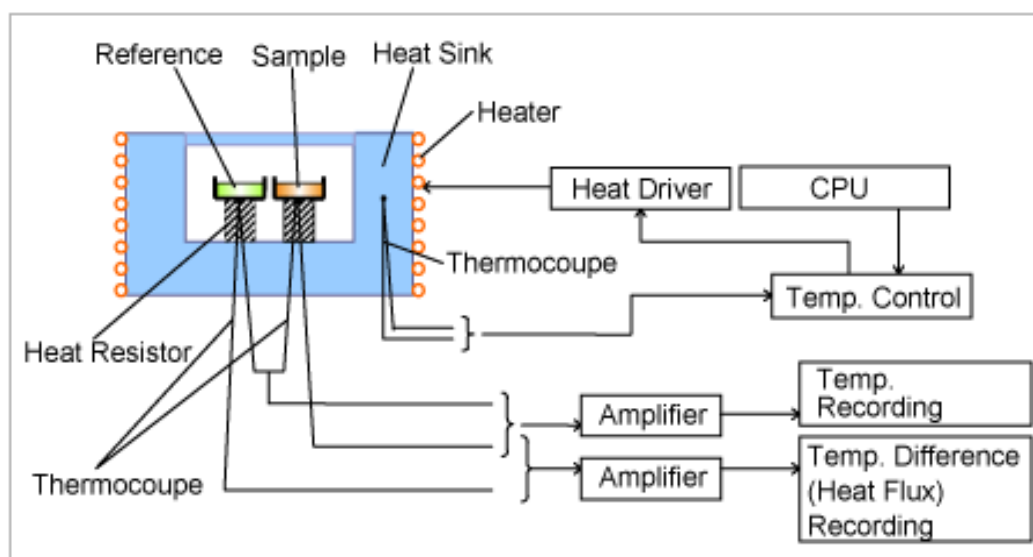
Fig. 3.6 Schematic illustration of differential scanning calorimeter (Source: http://Hitachi-Hightec.com)

It consists of two holders, one for sample and other for reference material. Both the sample and reference material are maintained at nearly same temperature at a time of the experiment. When the sample undergoes a physical transformation such as phase transitions, heat flows to it to maintain the sample and reference both at same

temperature [12]. Heat flow to the sample depends on whether the process is exothermic or endothermic. For example, as a solid sample melts to a liquid it will require more heat flowing to the sample to increase its temperature at the same rate as that of reference. This is due to the absorption of heat by the sample as it undergoes the endothermic phase transition from solid to liquid. Likewise, as the sample undergoes exothermic processes, less heat is required to raise the sample temperature.

Both TGA and DSC measurements can be performed with single equipment termed as simultaneous TG-DSC analyzer. By varying heating rate, information about decomposition temperature as well as activation energy and other kinetic parameters like reaction rate can be obtained which is useful to assess sensitivity of these materials to thermal initiation and their performance. In present work, TGDSC measurements on energetic materials have been carried out from room temperature to 500 ˚C using Mettler Toledo TGDSC analyzer. The weighed samples of about 1 mg were heated in alumina crucibles. Dry N_2 was used as carrier gas at flow rate of 20 mL/min. For DSC analysis, alumina sample holders were used as sample and reference carriers. An energetic material sample is subjected to a linearly increasing temperature and the heat flow, dH, is monitored continuously. For kinematic investigations, samples were heated at different heating rate of 5, 10 and 20 ^{o}C/min.

3.7   Surface Area Measurement:

The working principle of surface area analyzer is based on the theory proposed by Brunaur, Emmet and Teller, known as BET theory [13]. The dynamic method is used for measurement of surface area. In this method, gas mixture composed of nitrogen and helium continuously flows over the sample during the measurement. The sample is dipped in liquid nitrogen. At liquid nitrogen temperature (-198 °C) nitrogen

in this flow gets adsorbed on the surface and forms a mono layer on the surface of sample. This adsorbed N_2 is allowed to desorb by bringing the sample to room temperature. This desorbed nitrogen is proportional to the surface area and so measured to calculate surface area using following equation.

$$Surface\ area\ (S_s) = \left(\frac{4.38}{W}\right)\left(\frac{NS_c \times V_n}{NC_n}\right)\left(\frac{273}{(273+t)}\right)\left(\frac{1-P}{P_0}\right) \qquad \dots 3.6$$

Where, W = Weight of the sample in gms.

NC_S = Number of counts measured on instrument which are proportional to the quantity of desorbed nitrogen.

V_n = Amount of N_2 in c.c. injected for the purpose of calibration.

NC_n = Number of counts measured which are proportional to the injected N_2

t = Room temperature

P/P_0 = Partial pressure of adsorbed gas, e.g. it is 0.3 for 70 % He & 30 % N_2

Multiple readings are taken at different partial pressures and a straight line is drawn. From the sectional surface area of adsorbed gas molecule and Avogadro's number which gives number of molecules per 1 c.c. (6.023×10^{23} molecules/cm³ at NTP), the surface area covered by 1c.c. of gas is calculated.

The specific surface area and specific pore volume have been measured by nitrogen physisorption method using a Sorptomatic 1990 analyzer from CE Instruments. Prior to measurement, the samples were degassed and specific surface area was calculated from the amount of N_2 gas adsorbed at 77 K at various partial pressures (eleven points; $0.05 < p/p_0 < 0.3$). The pore volume measurements were carried out at a partial pressure of $P/P_0 = 0.99$ and the pore size distributions (PSD) were determined by Horvath- Kawazoe (H-K) method [14].

3.8 Impact Sensitivity Test:

Energetic materials are characterized by various techniques to determine their energetic properties like sensitivity to initiation and velocity of detonation, etc. Perhaps the simplest test that can be performed on small samples of energetic materials is the drop weight impact test. In this test, a distance through which a falling weight must drop upon the material to cause them to explode is determined. At different places different apparatus are used and in consequence the numerical results differ from laboratory to laboratory. The typical impact machine consists of an impactor and an anvil. Often between the impactor and the anvil, is a striker that transfers the impact force from the drop weight to the sample.
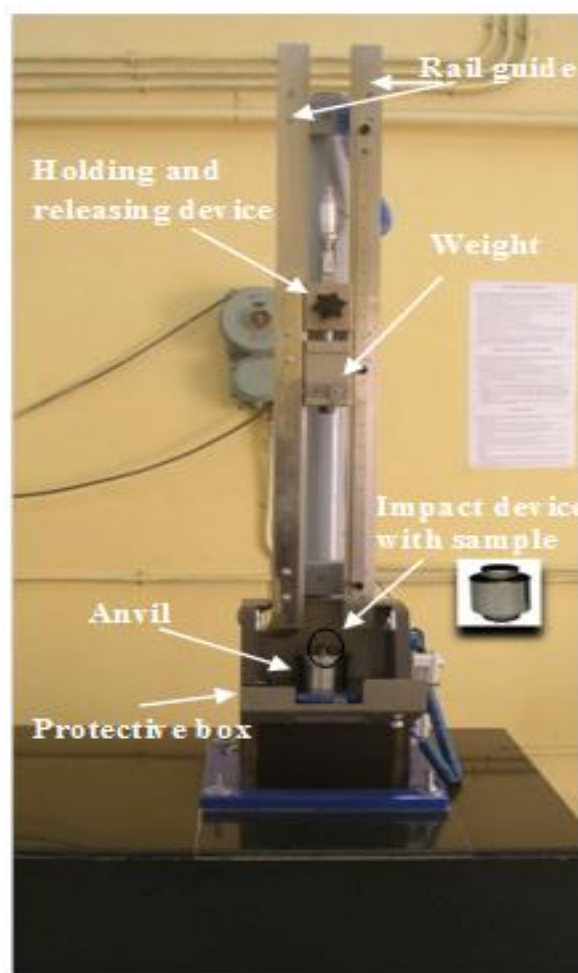
Fig. 3.7 Apparatus to study sensitivity to impact initiation (at our lab.)

The drop weight impact machine used in present work consists of a free-falling weight, tooling to hold energetic material sample and a supporting frame (Fig. 3.7). The sample to be tested is dried, usually under vacuum, and loaded into a sample holder. Depending on the bulk density, the sample weight varies from 30 to 40 mg. In our works, energetic materials have been used in powder as well as in 8 mm diameter pellet forms for test. The energetic material undergoing the test is placed in between two steel cylinders contained in a steel guide ring and the weight is dropped directly upon the cylinder. A standard test consists of 30 shots performed, following the Bruceton 'up-and-down' method [15] that is normally used in sensitivity testing. The interval between drop heights is 0.05 times the logarithm (base 10) of the preceding drop height. The logarithmic scale is used on the assumption that the height at which event occurs follows a lognormal distribution. The results are reported in terms of the height (H_{50}) at which an event is obtained 50 % of the time i.e. there is 50 % probability of initiation of the sample for dropping the particular mass from that height. A fresh sample is taken each time, and material which has not exploded from a single impact is discarded. The energy put into the machine by releasing the drop weight from a height H is calculated using equation 3.7:

$$E = MgH \qquad \qquad \dots (3.7)$$

Where, M – mass of drop weight, g- acceleration due to gravity and H- drop height

This energy is partitioned between the elastic energy stored in the machine, the plastic energy required to deform and heat the sample to ignition, plus the small but inevitable amount of energy lost in the machine during the impact [16].

42

3.9   Shock sensitivity:

For testing sensitivity of energetic materials to initiation with high velocity shock, gap test is used [17]. In shock sensitivity tests a standard donor charge of energetic material produces a shock pressure of uniform magnitude which is transmitted to the test material through an attenuating inert barrier or gap. Degree of shock attenuation is determined by the thickness of barrier material. By varying the thickness of the barrier between the donor and test (acceptor) energetic material, one can determine the barrier thickness required to inhibit detonation in the test material half the time (G_{50}). The gap thickness is measure of shock sensitivity of the material. Schematic of shock sensitivity test assembly is shown in Fig. 3.8.
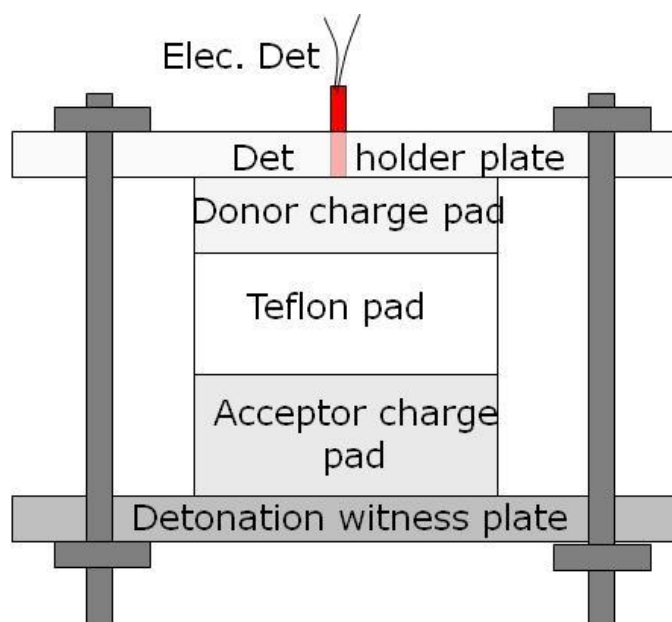
Fig. 3.8 Experimental configuration for shock sensitivity test

A variety of gap tests depending upon the barrier material and diameter of acceptor charge are used to measure the shock wave amplitude required to initiate detonation in energetic materials. In present work, shock sensitivity test was

performed with experimental configuration similar to that of used at Los Alamos Sandia Laboratory (LASL). The diameter of the cylindrical acceptor charge of test energetic material is 20 mm and thickness is 10 mm. Donor charge in all test experiments is of PETN with charge dimensions as 20 mm diameter and 5 mm thickness. The test procedure is to fire shots with the barrier thickness alternately increased and decreased until the spacer thickness that allows detonation in the acceptor charge is determined. The occurrence of detonation is determined based on the damage to the steel witness plate which receives blast resulting from the initiation of the test sample. A clear hole in the 5 mm thick steel witness plate was considered as indication of test material is detonated.

3.10   Detonation velocity measurement:

Performance of energetic material is an important aspect in its application. Performance of an energetic material is generally measured in terms of detonation pressure (P), commonly known as C-J pressure and velocity of detonation (D). Detonation pressure in energetic material is expressed in terms of particle velocity (u) and shock velocity (U) in the material as given below in equation 3.8 [18]:

$$P = \rho \, u \, U \qquad\qquad \dots (3.8)$$

Where, ρ is density of unreacted material.

Particle velocity is roughly half of shock velocity and shock velocity is roughly half of detonation velocity. Therefore, detonation pressure is roughly calculated from value of detonation velocity as below:

$$P = \rho \, D^2/4 \qquad \dots (3.9)$$

Therefore, detonation velocity can be considered as measure of performance of an energetic material. Detonation velocity is the rate of propagation of reaction in

energetic material. Detonation velocity in energetic material is measured using streak camera record, wedge technique or self-shorting sensor pins technique [19]. The self-shorting sensor pin technique is used in present work for measurement of detonation velocity. In this method, sensor pins are placed in energetic material charge at predetermined distance. Sensor pins get shorten when reaction passing through material charge reaches at pin position and generate a signal. From time scale between two pin signals and known distance between them, detonation velocity in the charge is measured. Schematic configuration of detonation velocity measurement test assembly is shown in Figure 3.9.
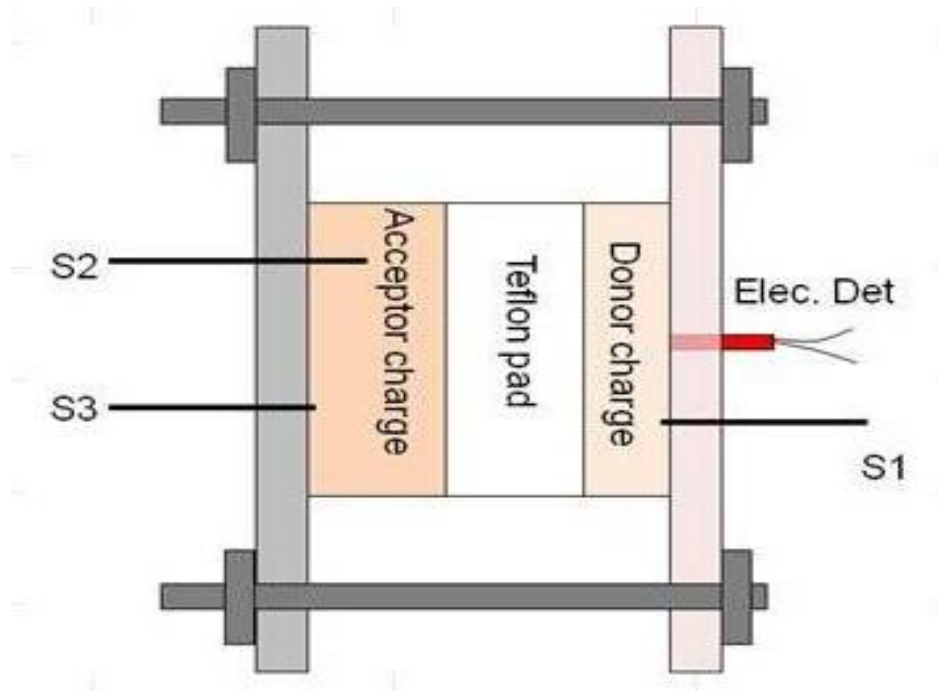
Fig. 3.9 Detonation velocity measurement test assembly

PETN pellets with 5 mm thick and 20 mm diameter have been used as donor charge and 10 mm thick and 20 mm diameter pellets of test energetic materials have

been used as an acceptor charge with Teflon disk between donor and acceptor charge. Donor charge was initiated using electrical detonator.

In summary, brief descriptions of techniques like FTIR, XRD, TG-DSC, SAXS, FESEM, TEM and surface area measurement set up used for this study are given in this chapter. Also techniques and principles involved in measurements of energetic properties, mainly associated with sensitivity and performance related properties of energetic materials are explained.

REFERENCES:

 [1]   Anand Subramanian Luis Rodriguez-Saona, Fourier Transform Infrared (FTIR) Spectroscopy in *Infrared Spectroscopy for Food Quality Analysis and Control* (2009), pp.145-178

[2]   Gerrit Renner, Torsten C. Schmidt, Jürgen Schram, Characterization and Quantification of Microplastics by Infrared Spectroscopy in *Characterization and Analysis of Microplastics* (2017) pp 67-118.

[3]   Scanning Electron Microscopy, D. McMullan, *Scanning,* **17** (1995) 175–185

[4]   E. N. Kaufmann, *Characterization of Materials*, *Vol.* 1, A John Wiley and Sons Publication, New Jersy, (2003) p. 1070.

[5]   SAXS Investigations of the Fractal Character of Additive Silica Xertogels, F He, X He, M. Li, S. Zhang, *J. Ceram. Proc. Res.* **9** (2008) 389-392

[6]   Small Angle Scattering by Fractal Systems, J. Texeira, *J. Appl. Crystallogr.* **21** (1988) 781-785

[7]   Scattering by an Inhomogeneous Solid. II. The Correlation Function and Its Application, P. Debye, H R Anderson Jr, H Brumberger, *J Appl Phys.* **28** (1957) 679–683

[8]   Preparation of Nano-Structured RDX in a Silica Xerogel Matrix, S. V. Ingale, P. U. Sastry, P. B. Wagh, A. K. Tripathi, R. Tewari, V. B. Jayakrishnan, S. B. Phapale, P. T. Rao, R. D. Wasnik, B, Bhattacharya, S. C. Gupta, *Propellants Explos. Pyrotech.*, **38** (2013) 515-519

[9]   Synthesis and Characterization of Ammonium Molybdophosphate–Silica Nano-Composite (AMP–Sio2) as a Prospective Sorbent for the Separation of ^{137}Cs from Nuclear Waste, S. V. Ingale, Ramu Ram, P. U. Sastry, P. B. Wagh, Ratanesh Kumar, Ram Niranjan, S. B. Phapale, R. Tewari, A. Dash & Satish C. Gupta, *J Radioanal Nucl Chem,* **301** (2014) 409-415

[10]   Characterization of Anisotropic Poly(vinyl alcohol) Hydrogel by Small and Ultra- small Angle Neutron Scattering, S D Hudson, J L Hutter, M P Nieh, J Pencer, L E Million, W. Wan, *J Chem Phys.* **130** (2009) 34903

[11]   Thermogravimetric Analysis: A Review, A. W. Coats, J. P. Redfern, *Analyst*, **88** (1963) 906-924.

[12]   Differential Scanning Calorimetry Techniques: Applications in Biology and Nanoscience, P Gill, T T Moghadam, B Ranjbar, *J Biomol Tech.* **21**. (2010) 167–193.

[13]   G. Zhu, H. Ren, *Porous Organic Frameworks: Design, Synthesis and Their Advanced Applications*, Springer, (2014)

[14]   Corrected HorvÁth-Kawazoe Equations for Pore-size Distribution, S. U. Rege, R. T. Yang, *AIChE Journal* **46** (2000) 734-750

[15] A Method for Obtaining and Analyzing Sensitivity Data, W. J. Dixon, A. M. Mood, *J of the Americal Statistical Association* **43** (1948) 109-126

[16] Impact Testing of Explosives and Propellants, C. S. Coffey, V. F. De Vost, *Propellants, Explos. Pyrotech*. **20** (1995) 105-115

[17] Analysis on Shock Attenuation in Gap Test Configuration for Characterizing Energetic Materials, B Kim, J Park, J J. Yoh, *J. Appl. Phys.* **119**, (2016) 145902.

[18] Pressure and Particle Velocity Measurements in Solids Subjected to Dynamic Loading, P. A. Urtiew, L. M. Erickson, B. Hayes, N. L. Parke, *Combustion, Explosion and Shock Waves*, **22** (1986) 597–614

[19] W. M. Isbell, *Shock Waves: Measuring the Dynamic Response of Materials*, World Scientific, (2005).

CHAPTER 4

PREPARATION OF ENERGETIC MATERIALS USING SOLUTION CRYSTALLIZATION AND SPRAY DRYING METHOD AND THEIR CHARACTERIZATION

The particle size and its distribution in the energetic materials as well as the method of processing these materials is an important aspect while studying energetic properties of these materials. To have a comprehensive picture of the particle size effect on initiation sensitivity of energetic materials, a wide range of particle size needs to be studied. Since the energetic materials are not as such available with the desired particle size, development of a process capable of producing these materials with desired particle size is necessary. Some of the popular techniques used to reduce particle size of energetic materials are wet milling, crystallization out of solutions, crystallization using supercritical fluids or Rapid Expansion of Supercritical Solvent (RESS), spray drying and sol-gel technique [1].

4.1 Processing methods used to reduce particle size of energetic materials:

After reviewing various methods, solution crystallization method, spray drying method and sol-gel method has been chosen to process the TNT, RDX and PETN raw materials on basis of simplicity in processing, infrastructure required and safety as well as for control over particle size. Solution crystallization and Spray drying method used to reduce particle size of energetic materials have been discussed in this chapter whereas studies made on energetic materials processed by sol-gel method to analyze effect of controlled porosity are discussed in next chapter.

Solution crystallization method (using solvent/ non-solvent combination) is useful to produce energetic materials with particle size in the range of 5 to 50 micron. This method uses the fact that the solubility of a substance in a solvent can be reduced rapidly by adding a non-solvent [2]. In this method, energetic material is dissolved in a solvent in which it has good solubility. Then non-solvent, generally deionized water is added to this solution. In a given solution, as solubility reduces, a super saturation state is created which results in precipitation of these materials with reduced particle size. These precipitated materials are separated by filtration. The particle size and particle size distribution depends on the parameters like temperature, solvent and concentration.

In spray drying method [3], energetic material is dissolved in suitable solvent. Then the solution is sprayed into a heated chamber through a pressurized nozzle. Instrument used in processing energetic materials by spray drying method is shown in Fig. 4.1.
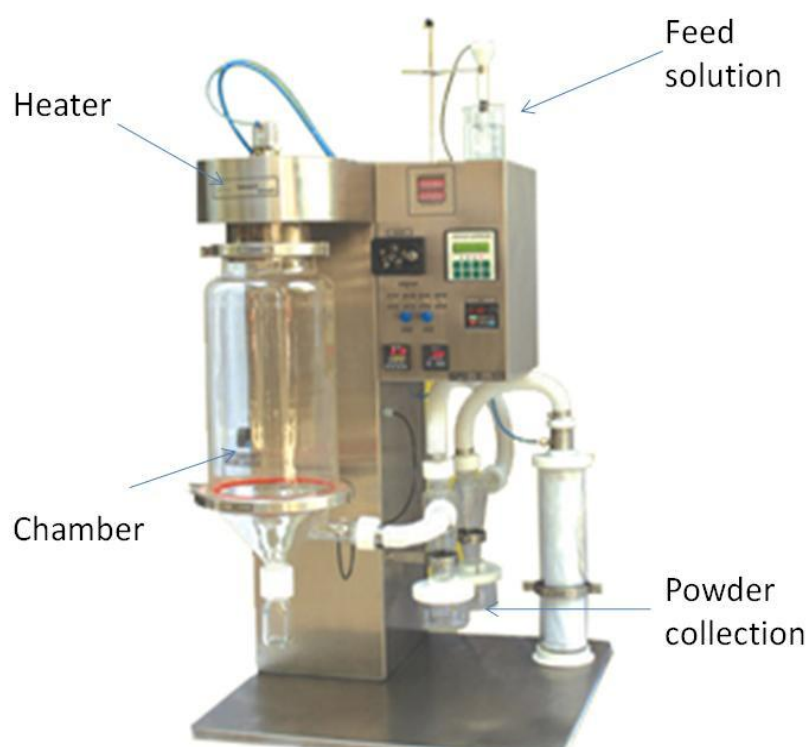
Fig. 4.1 Instrument for spray drying processing (at our lab)

On entering into the heated chamber, the solvent is evaporated by forming a super saturated solution that leads to crystallization of energetic materials into fine particles. The particle size of thus processed material is in the range of submicron to micron level. Particle size distribution depends upon concentration of energetic material in solution, pressure at the nozzle, nozzle diameter, etc.

4.2   Preparation of Energetic Materials with Reduced Particle Size

TNT, RDX and PETN were received from the supplier with particle size in range of 100 to 500 micrometers. These materials are designated as raw materials. These materials were further processed to reduce their particle size

4.2.1   Solvent/non-solvent crystallization:

For processing of TNT by solvent-non solvent crystallization method, TNT is dissolved in acetone. The solution is then added to distilled water which results in precipitation of TNT. For obtaining uniform particle size with narrow distribution, TNT: Acetone ratio and acetone: water ratios have been optimized to 1:5 and 1:10 by weight, respectively. The precipitated TNT is separated by filtration using sintered glass filter and dried in vacuum oven at ambient temperature. The resulted material processed by solvent/non-solvent crystallization has been designated as TNT (S/NS).

RDX and PETN have also been processed similarly to reduce their particle size. For RDX, the ratio of RDX/acetone is optimized to 1:15 ratio by weight whereas acetone to water ratio is optimized to 1:8 by weight. The precipitated RDX separated from water by filtration and then dried in oven. This sample has been designated as RDX (S/NS).

Raw PETN also is dissolved in acetone to form clear solution. PETN to acetone ratio maintained at 1:10 by weight. To precipitate PETN in acetone, water

was added. Acetone to water ratio was optimized to 1:8 by weight. PETN prepared by solvent/non-solvent crystallization processing is designated as PETN (S/NS).

4.2.2 Spray drying method:

In processing of TNT by spray drying method, TNT was dissolved in acetone. TNT to acetone ratio was optimized to 1:6 by weight. Droplets of this solution were sprayed in a heated chamber with feed rate at 1 ml /min. The temperature at inlet of the chamber was maintained at 60 ^{o}C. An ultrasonic nozzle was used for formation of micro droplets from TNT/acetone solution. The solvent from fine droplets evaporated, resulting in crystallization of ultrafine TNT particles. TNT prepared using spray drying method has been designated as TNT (SD).

RDX, while processing using spray drying method by dissolving in acetone, resulted in wide distribution of particle size. Therefore, dimethyl formaldehyde (DMF) which has more solubility for RDX [4] was used as solvent. RDX:DMF ratio is optimized to 1:6 by weight. Droplets of this solution were sprayed in a heated chamber with feed rate at 1 ml /min. The temperature at inlet of the chamber was maintained at 150 ^{o}C. The solvent from droplets evaporated, resulting in ultrafine RDX particles. The resulted material is designated as RDX (SD).

Auto ignition temperature for PETN being 140 °C, which is relatively less for processing by spray drying method. Hence, PETN has not been processed by this method.

4.3   Characterization of Processed Energetic Materials:

4.3.1   Fourier Transform Infra-Red (FTIR) Spectroscopy:

Energetic materials processed using different techniques have been characterized by FTIR spectroscopy to determine their chemical structure. IR

spectroscopy measurements have been carried out using attenuated total reflection (ATR) technique. For FTIR characterization, powder samples of about 3 - 5 mg were scanned within the wave number range of 550 to 5000 cm^{-1} using ZnSe detector. FTIR spectra of raw TNT, TNT (S/NS) and TNT (SD) are shown in Figure 4.2.
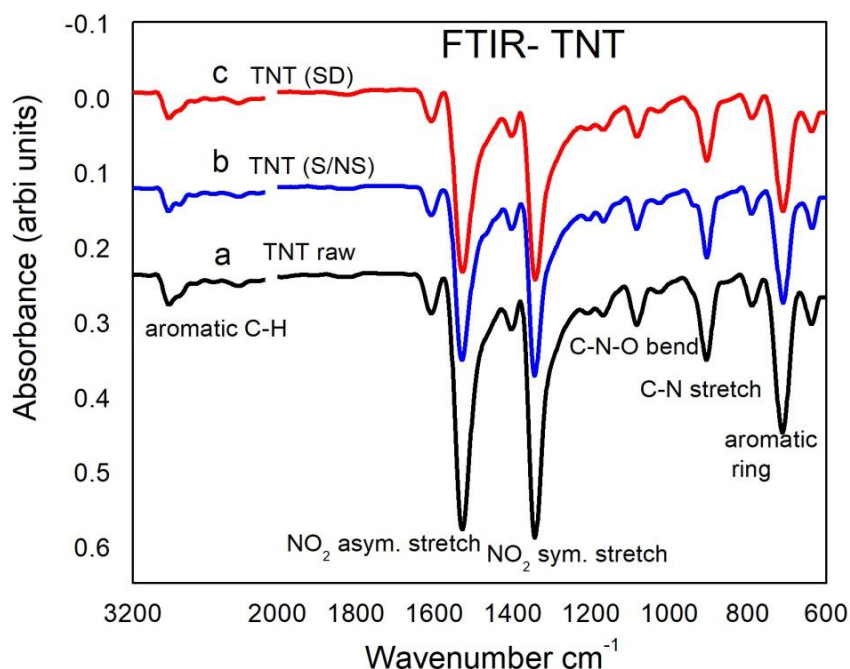
Fig. 4.2 FTIR spectra of a) raw TNT, b) TNT (S/NS) and c) TNT (SD)

FTIR spectra show that in all the samples, absorption bands observed at 900 cm^{-1} is assigned to C-N stretching and bands observed at 700 and 1085 cm^{-1} are assigned to C-N-O bending. Bands observed at 1350 and 1550 cm^{-1} are due to symmetrical stretching of para-nitro group (4-NO$_2$) and asymmetric stretching of ortho-nitro group (2,6 NO$_2$), respectively [5], and are typical signatures of TNT. Band observed at about 805 cm^{-1} is assigned to C-H deformation. Band observed at around 3050 cm^{-1} is due to aromatic C-H group. FTIR spectra show that there is no change or shift in absorption bands which indicates that chemical structure of TNT after processing is same to that of raw TNT.
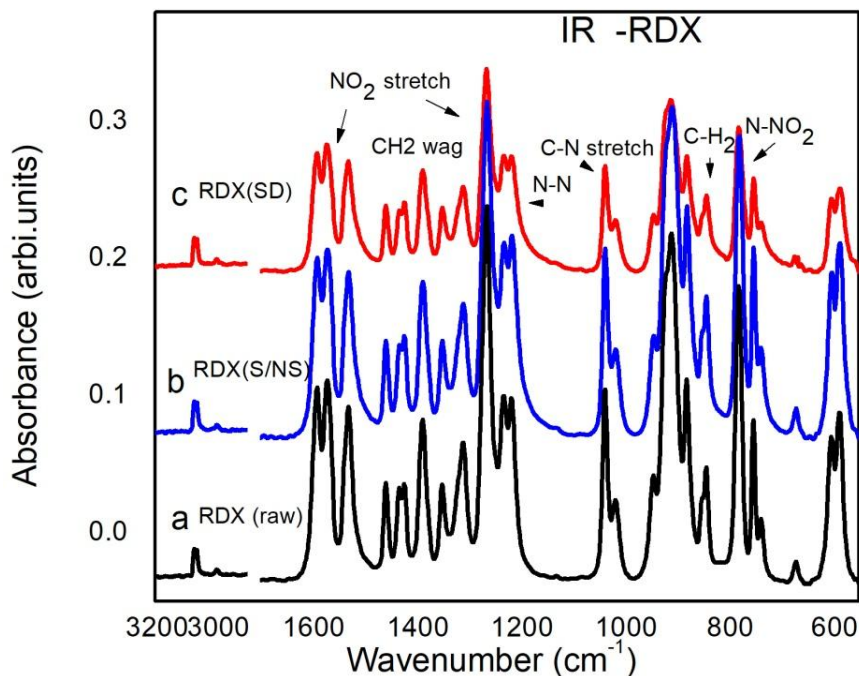
Fig. 4.3 FTIR spectra of a) raw RDX, b) RDX (S/NS) and c) RDX (SD)

Figure 4.3 shows the FTIR spectra of a) raw RDX, b) RDX (S/NS) and c) RDX (SD). It is evident that FTIR spectra of RDX processed using different methods are similar to that of raw material. In all these spectra, the band observed at 750 and 780 cm^{-1} assigned to non planer deformational stretching of N-NO$_2$. Peak at 850 cm^{-1} assigned to CH$_2$ rocking. The peaks at 1045 correspond to C-N stretching ring. The peaks at 1573, 1533, 1395 and 1330 cm^{-1} in the IR spectra correspond to stretching of NO$_2$ whereas the peak at 1456 cm^{-1} is assigned to CH$_2$ wagging. The bands observed at 1268 and 1596 cm^{-1} are attributed to symmetrical N-N vibration and anti-symmetrical NO$_2$ vibrations, respectively [6]. Peak at 3050 cm^{-1} correspond to C-H vibration. There is no change or shift in absorption bands which indicates that chemical structure of processed RDX is same to that of raw material.

The FTIR spectra for PETN materials are shown in Fig. 4.4. FTIR spectra of a) raw PETN and b) PETN (S/NS) show peaks at 2900 and 1400 cm^{-1} corresponding to C-H stretching vibrations from aliphatic compounds. The absorbance band at

52

1285 cm^{-1} corresponds to NO$_2$ symmetric stretching vibration of O-NO$_2$ band, characteristic of nitrate ester like PETN [7].
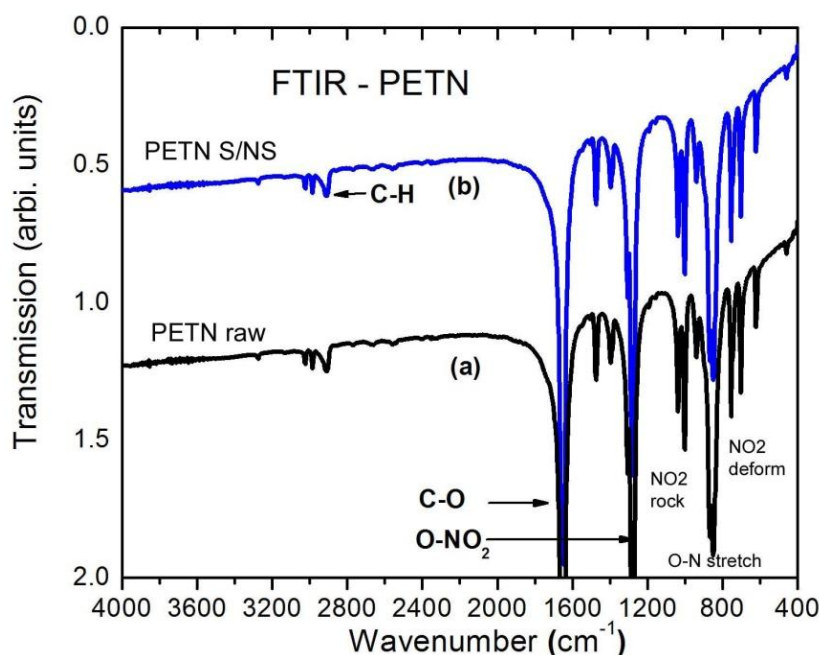
Fig. 4.4 FTIR spectra of a) raw PETN and b) PETN (S/NS)

The peak observed at 1700 cm^{-1} is due to CO from the formaldehyde structural group. Other important vibrational signatures appeared are at 703 cm^{-1} (-ON stretching, ±NO$_2$ rocking,), 753 cm^{-1} (-ONO$_2$ umbrella deformation), 869 cm^{-1} (-ON stretching), 1038 cm^{-1} and 1306 cm^{-1} (-NO$_2$ rocking) [8]. No change in absorption bands of both materials indicates same chemical structure for both raw and solvent/non solvent precipitated PETN.

FTIR characterization confirmed that processing of energetic materials to reduce particle size of these materials didn't change their chemical structures.

4.3.2 X-ray Diffraction (XRD):

XRD data has been recorded with Cu Kα (λ=1.542) X-rays to determine crystal structure of processed material.
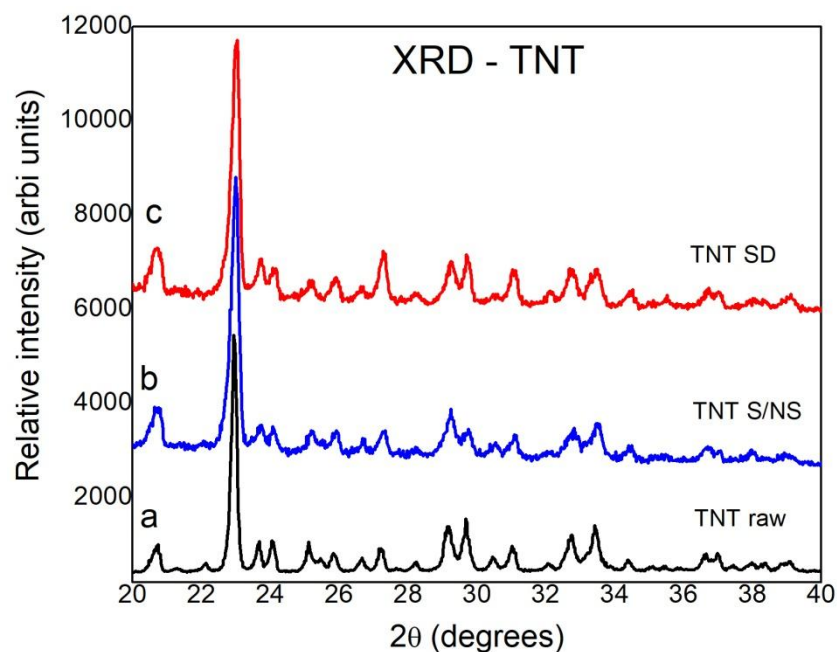
Fig. 4.5 XRD pattern for a) raw TNT b) TNT (S/NS) c) TNT (SD)

Fig. 4.5 shows the XRD patterns for raw TNT, TNT (S/NS) and TNT (SD). The diffraction peaks of crystalline phases are same for all samples. These peaks observed at 20.9, 23.1, 23.8, 25.3, 27.5, 29.2, 29.9, 31.3, 32.9 and 33.5 degree are assigned to monoclinic phase of TNT (PCPDF 28-1945) in light of available data for TNT [9].
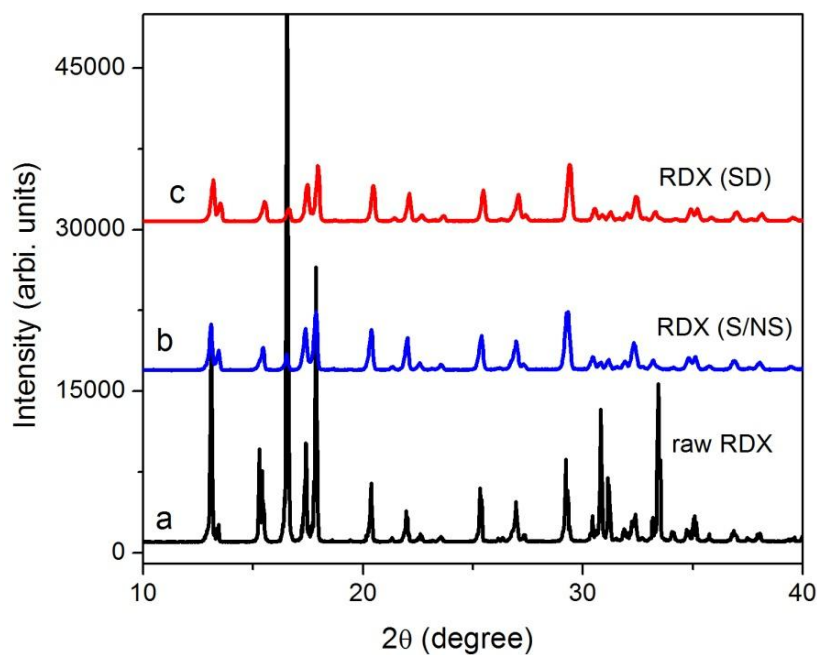
Fig. 4.6 XRD patterns for a) raw RDX b) RDX (S/NS), and c) RDX (SD)

54

XRD patterns recorded for raw RDX, RDX (S/NS) and RDX (SD) are shown in Fig. 4.6 in which the diffraction peaks are assigned to the orthorhombic crystal structure of RDX [10]. The peaks observed at 13.0, 15.4, 16.5, 17.3, 178, 20.3, 22.0, 25.3, 26.9, 29.3, 30.7, 32.3, 33.2 and 35.1 are in concurrence with PCPDF 46-1606. The variation of intensity in the XRD patterns can be due to the preferred orientation effect in the RDX (S/NS), and c) RDX (SD) samples.

In Fig. 4.7, diffraction patterns recorded for raw PETN and PETN processed by solvent/non-solvent recrystallization method are similar which indicates crystal structure of PETN(S/NS) is same as that of raw material. XRD peaks observed at 13.3, 16.2, 18.9, 21.1, 23.1, 25.0, 26.8, 29.8, 30.1, 33, 34.4, 38.1 degrees in both samples are assigned to PETN (PCPDF 44-1623).
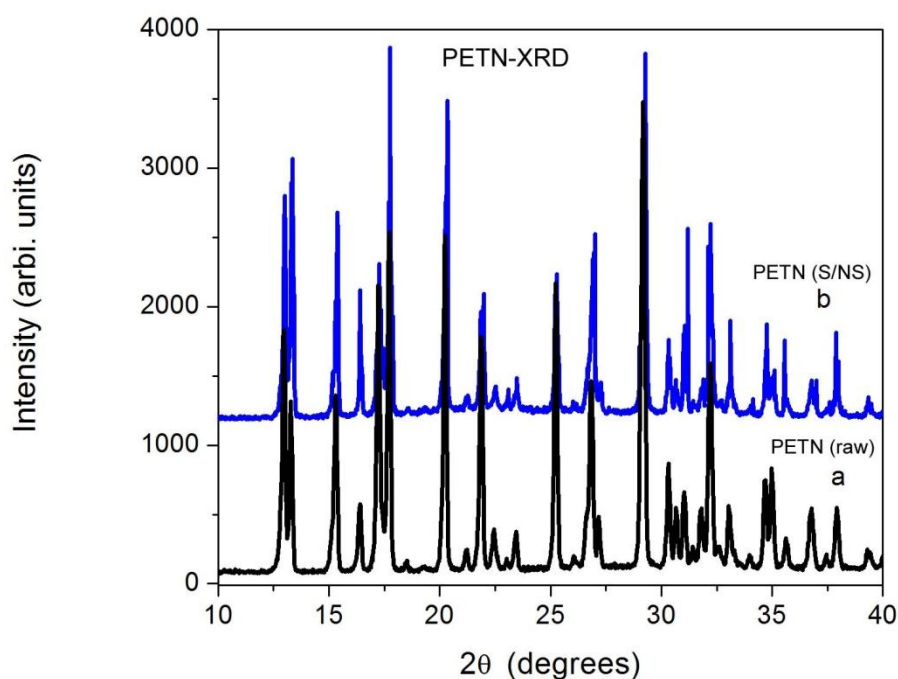
Fig. 4.7 XRD patterns for a) raw PETN and b) PETN ((S/NS)

It confirms that crystal structure of raw energetic materials and that of material processed using different methods are same. Thus it is concluded that the processed samples are same as the raw materials except there is a reduction in size.

4.3.3 Morphology:

The morphology of energetic materials was studied using Field Emission Scanning Electron Microscope (FESEM). The particle sizes are measured from the micrographs to obtain size distribution of processed material. Particle sizes of raw material found to be reduced by solution crystallization and spray drying processes.
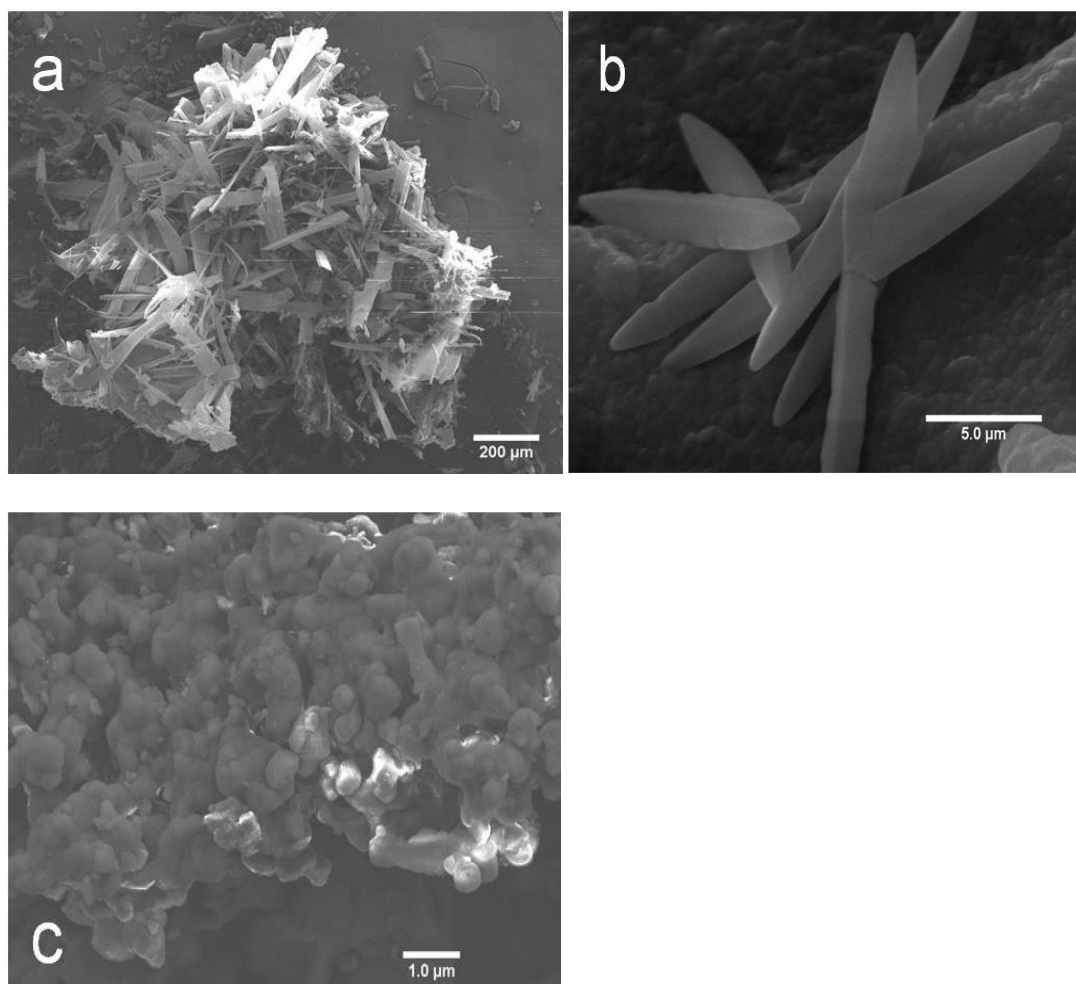
Fig.4.8 FESEM picture of a) raw TNT and TNT processed by b) solution crystallization and c) spray drying method.

It can be seen in Fig. 4.8 (a) that the raw TNT has bigger particles with highly irregular shapes and complex geometry. Particle size of raw TNT is in the range of 200 to 400 µm having average particle size of 350 µm with standard deviation of

50 µm. FESEM image of TNT processed by solution crystallization method (Fig. 4.8 b) shows regular rod type geometry. Also the grain size of TNT processed by solution crystallization is much reduced compare to the raw TNT. Particle size of this material is controlled between 5 to 10 µm by optimizing ratio of solvent and non solvent used in processing. The average particle size is of 7 µm with standard deviation of 1.7 µm. As shown in Fig. 4.8 c, particles of TNT processed by spray drying method are more regular and uniform with nearly spherical shape. Particle sizes are in range of 300 to 700 nm while the average particle size is 500 nm.
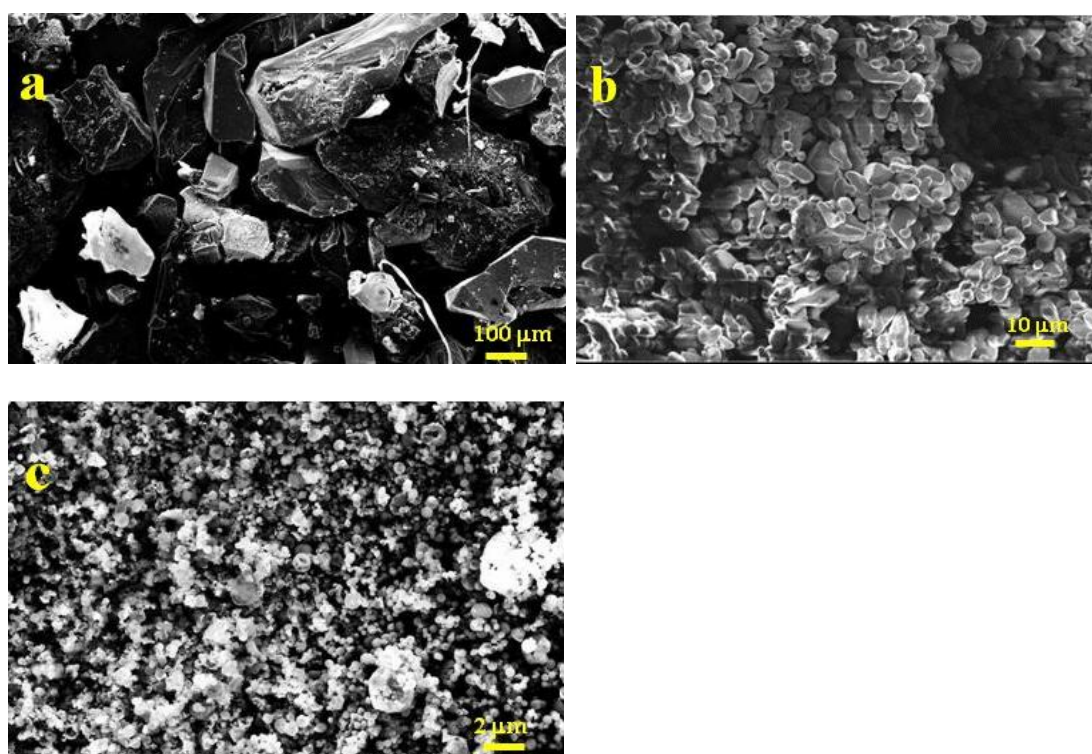
Fig. 4.9 FESEM of a) raw RDX and RDX processed by b) solvent precipitation RDX(S/NS) and c) spray drying RDX (SD)

FESEM images of raw RDX and RDX processed by solvent/non solvent crystallization and spray drying method are shown in Fig. 4.9. It can be seen in Fig. 4.9 a, that the raw RDX particles are relatively bigger in size and irregular in shape

with sharp edges or horns. The particle size of raw RDX is found to be in the range of 126 ± 45 µm. Morphology of RDX material processed by solvent precipitation method is shown in Fig. 4.9 b. The particle size of processed material is much smaller as compared to raw RDX and is in the range of 4.37 ± 2 µm. The particles are uniform with a few rod shaped particles where the sharp edges are reduced. Fig. 4.9 c displays the micrograph of RDX processed by spray drying method in which it can be seen that particles are nearly spherical in shape and uniform in size. These ultra-fine particles are in the range of 194 nm with size distribution of ± 63 nm.

FESEM images of raw PETN and PETN (S/NS) are shown in Fig. 4.10.
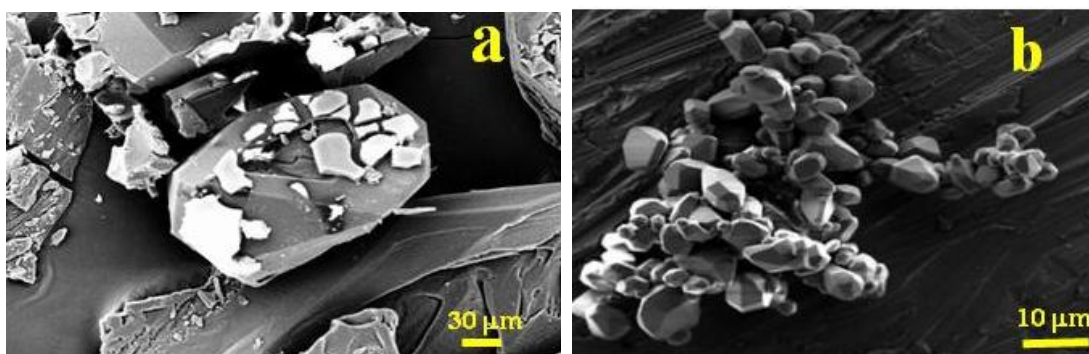
Fig. 4.10 FESEM images of a) raw PETN and b) PETN (S/NS)

Raw PETN particles are bigger in size and are having irregular shapes whereas PETN recrystallized from acetone –water mixture has particles with regular crystalline geometry. Particle size of raw PETN is about 300 ± 52 µm whereas PETN (S/NS) has particles with size in range of 4 to 7 µm.

FESEM characterization show that energetic materials prepared by solvent/non solvent crystallization and spray drying method have much smaller particles compared to raw material and are in range of micron and nanometer size, respectively. These reduced size particles have much regular shape with smooth surface.

For convenience, the particle size obtained for TNT, RDX and PETN by processing these materials using different methods is summarized in Table 4.1.

Table 4.1 Particle size of energetic materials prepare by different techniques

Processing technique	Mean Particle size		
	TNT	RDX	PETN
Raw (R)	350 ± 50 µm	126 ± 45 µm	300 ± 52 µm
Solution Crystallization (S/NS)	7 ± 1.7 µm	4.37 ± 2 µm	5 ± 1.5 µm
Spray drying (SD)	500 ± 109 nm	194 ± 63 nm	-

4.3.4 Thermo-gravimetric-Differential Scanning Calorimeter (TGDSC) analysis:

All energetic materials are meta-stable chemicals and decompose exothermally at a temperature. Thermal initiation of energetic materials is one of very important aspect as initiation by any external stimuli result in thermal decomposition of energetic materials [11]. In present work, we chose a comprehensive approach to understand thermal decomposition mechanism in energetic materials. Along with the apparent results from TG-DSC curves, kinetic parameters have been derived to explain the ignition and initiation to detonation transition in energetic material. For thermal analysis, TGDSC measurements on raw energetic materials and materials processed by solution crystallization and spray drying method were carried out within temperature range from room temperature to 500 ˚C. Weighed samples of about 1 mg were heated at different heating rate of 5, 10 and 20 ^{o}C/min. in inert (N_2) gas atmosphere. Fig. 4.11 shows the TGDSC curves for raw RDX, RDX processed by solvent precipitation (S/NS) and spray drying method, RDX (SD) recorded while heating at a rate of 5, 10 and 20 ^{o}C /min.
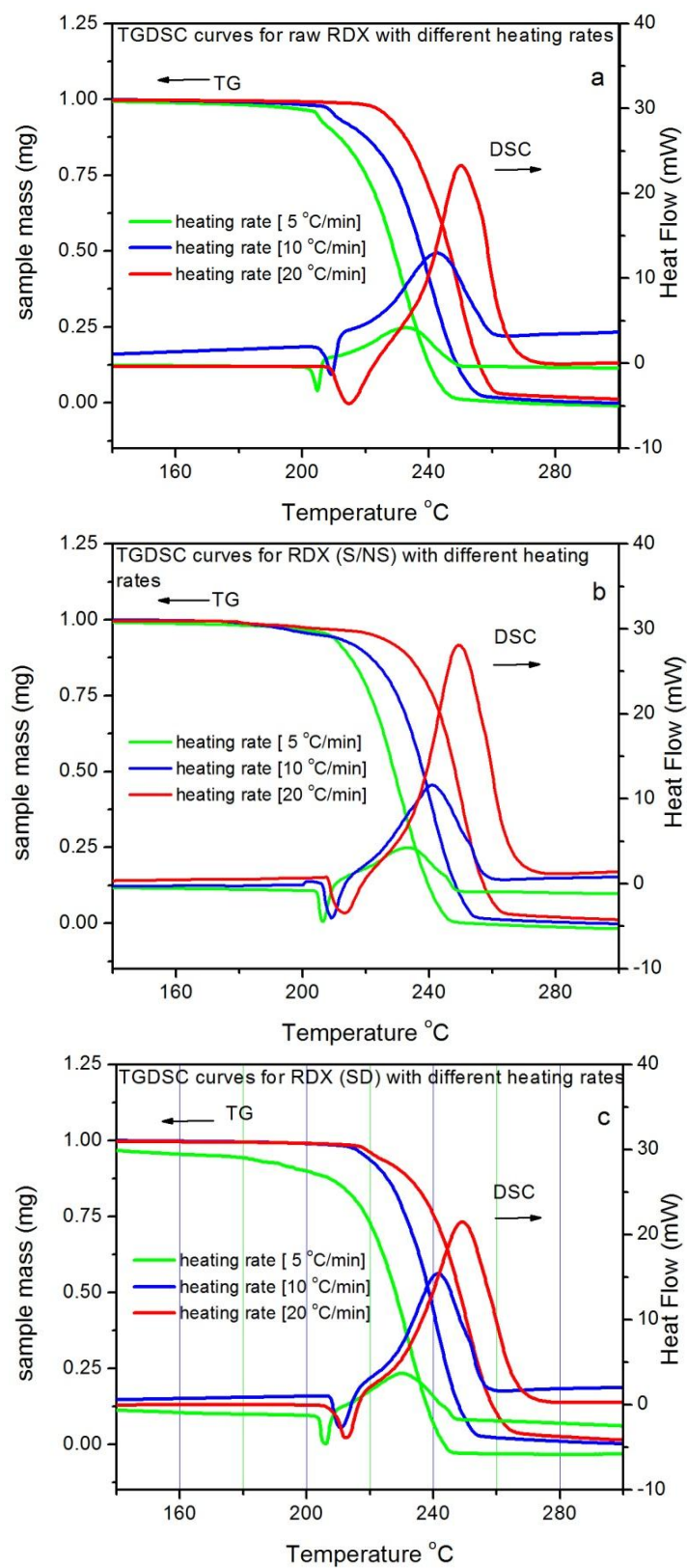
Fig. 4.11 TGDSC curves for a) raw RDX and RDX processed by b) solvent precipitation and c) spray drying

In Fig. 4.11, the weight loss observed in TG curves for all samples at around 220 to 260 ^{o}C is associated with thermal decomposition of RDX. These TG curves show mass loss of about 99 % attributed to complete RDX content in these samples.

In DSC curves, the endothermic peak at about 205 ^{o}C is associated with the melting of RDX and this is followed by an exothermic peak attributed to its decomposition [12]. In all these samples, the endothermic and exothermic peaks are found to be shifted to higher temperature with increase in heating rate. The exothermic peak temperatures in the DSC curves are given in Table 4.2. The energy associated with exothermic peak during decomposition is also more and the width of exothermic peak becomes narrower at higher heating rate. When heating rate is high, sample is heated to higher temperature at a relatively shorter time. At higher heating rate, reaction rate could be faster that may cause overlapping of thermo kinetic events resulting in high heat of reaction. The kinetic of decomposition process is function of temperature and time, therefore, peak temperature shifted to higher value with increase in heat of reaction.

Table 4.2 Exothermic peak temperature (Tp) and Onset Temperature (To) for RDX materials at different heating rate

Heating rate β [°C/min.]	Exothermic peak temperature (Tp) and Onset Temperature (To) for RDX in ^{o}C, [particle size of RDX is given in brackets]					
	RDX raw [126 µm]		RDX (S/NS) [4.37 µm]		RDX (SD) [194 nm]	
	Tp	To	Tp	To	Tp	To
5	233	212	232.6	212	231.2	215
10	242.5	215	241.2	217.5	241.0	220
20	251.1	220	250.4	223	249.1	225

As seen from Table 4.2, exothermic peak temperature shifted to lower value in DCS curves for RDX (S/NS) and RDX (SD). This can be attributed to the fact that materials with ultrafine particles have high surface area which favours faster decomposition and attain peak of energy release at lower temperature. Many researchers have reported that the shift in peak temperature to lower value indicates the increase in sensitivity of energetic materials with reduced particle size. However, as seen from Fig. 4.11, the onset of exothermic peak in these materials is observed at relatively higher temperature than the raw RDX due to increase in rate of change in heat flow is observed. In some reports, the transition from thermal decomposition to thermal explosion is assumed to begin at the onset temperature. It suggests that the sensitivity decreases with reduction of particle size. This appears to be the reason for difference in interpretation of sensitivity of energetic materials to thermal initiation reported in literature. Therefore, we tried to separate the ignition phenomenon and ignition to explosion transition on the basis of kinetic parameters. The higher values of onset temperature in materials with reduced particle size may be related to higher activation energy whereas the shift in exothermic peak temperature to lower value is due to the fact that these materials have larger proportion of atoms located on surface and enhancement in surface area that leads to increase in reactivity and faster decomposition.

To support this, the kinematic parameters of thermal decomposition in RDX with different particle size were evaluated from TGDSC data. In kinematic investigation, activation energy (E_a), pre-exponential factor (Z) and decomposition rate ($d\alpha/dT$) are the important parameters. Thermally stimulated decomposition process may be described [13] by Equation 4.1.

$$d\alpha/dt = k\,(T) \qquad\qquad\qquad \text{... 4.1}$$

where, α is degree of conversion, t is time and k is temperature dependant rate constant.

Temperature dependant rate constant k is assumed to obey Arrhenius equation [14]:

$$k\,(T) = Z\exp(-E_a/RT) \qquad\qquad \text{… 4.2}$$

where Z is the pre-exponential (Arrhenius) factor, E_a is activation energy in Joule, R is universal gas constant in J/K.mol and T is temperature in K.

From the exothermic peak temperature observed with various heating rates given in Table 4.2, the values of E_a are calculated by applying Kissinger's method [15].

$$-E_a/R = d\ln(\beta/T_p^2)/d(1/T_p) \qquad\qquad \text{… 4.3}$$

$$\ln(\beta/T_p^2) = \ln(ZR/T_p) - (E_a/RT_p) \qquad\qquad \text{… 4.4}$$

where β is the heating rate in K/min, T_p is the maximum temperature of DSC curve for that heating rate in K and Z is Arrhenius constant.
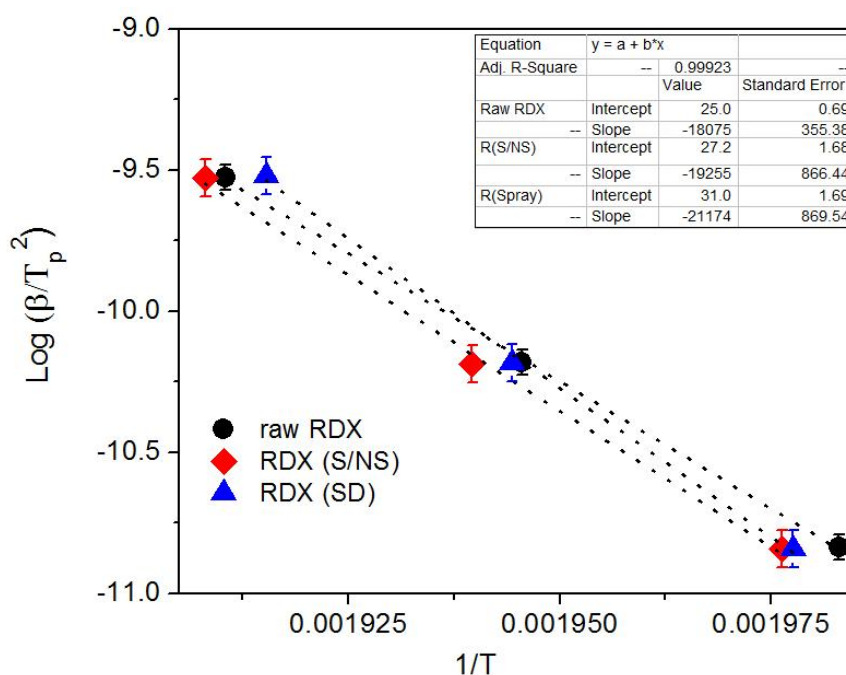
Fig. 4.12 Relationship between ln (β/T_p^2) and $1/T_p$ for RDX processed by different techniques.

Values of E_a are obtained from the slope of straight line in plot of ln (β/T_p^2) vs $1/T_p$ (Fig. 4.12) and the values are listed in Table 4.3

Table 4.3 Kinetics parameters for RDX derived from TG-DSC curves.

RDX material	Particle size [µm]	Kinetics parameters			
		E_a [kJ mol^{-1}]	$d\alpha/dtx10^{-2}$	Z [s^{-1}]	k x 10^{-2} [s^{-1}]
Raw	126 ± 45	149 ± 3	3.20 ± 0.10	4.7 x 10^{15}	69 ± 1
S/NS	4.37 ± 2	159 ± 7	3.21 ± 0.07	1.4 x 10^{16}	72 ± 1.5
SD	0.194 ± 0.063	176 ± 7	3.28 ± 0.12	6.5 x 10^{17}	81± 1.5

S/NS: solvent/ non-solvent crystallization; SD- spray dried

The calculated value of activation energy for raw RDX is 149 ± 3 kJ which is close to the reported value in literature [16]. Activation energy for RDX (S/NS) with particle size of 4.37 µm is 159 ± 7 kJ and for RDX (SD) with particle size of 194 nm, it is 176 ± 7 kJ. These values are higher than that of raw material with particle size of 126 µm. Heat buildup in energetic materials depends upon temperature as well as its thermal conductivity. With reduced particle size, surface losses and thermal conductivity is more as compared to heat generated in decomposition. Therefore, it requires higher temperature to trigger ignition (higher value of onset temperature in DSC curve) as indicated by high activation energy with reduced particle size.

From DSC curves, the reactivity and decomposition rate is estimated to improve with reduced particle size. The energy release rate has been calculated using Arrhenius equation given above where f (α) represents the extent of decomposition and is associated with reaction mechanism. Fig. 4.13 shows the plot of conversion (α) obtained from weight loss of RDX materials against corresponding temperature derived from TGDSC curves.

The chart contains an inset table:

Equation	Slope	Standard Error
y = a + b*x	value/100	--
Raw RDX	3.2	0.0010
Solvent precipitatio	3.21	0.0007
Sprya dried	3.28	0.0013
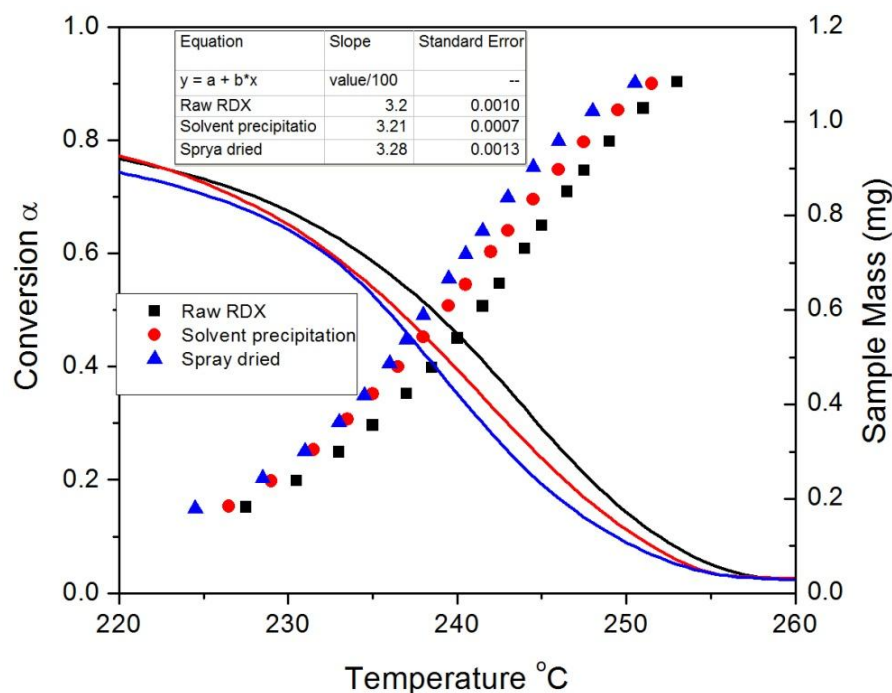
Fig. 4.13 Conversion (α) – Temperature (T) curve for RDX materials

Slope of α-T curve (dα/dt) in Fig. 4.13 is steeper for RDX with reduced particles size indicating faster decomposition rate in these materials. It is supported from the dα/dt values given in Table 4.3. The increase in dα/dt in these materials may be attributed to high surface energy associated with increase in specific surface area with reduction in particle size from 126 μm to 194 nm. It suggests a possible improvement in performance of these samples.

To explain it further Z and k are calculated using Equation (4.1) and (4.3) and are listed in Table 4.3. The Z and k values for RDX with reduced particles size are higher than that of relatively coarser materials. It may be attributed to more number of atoms undergoing decomposition simultaneously due to high proportion of surface atoms with reduced particle size [17]. These are in vicinity of large number of other particles which increase the collision frequency Z. The reaction rate constant (k)

values are also found to increases from 69 x 10^{-2} s^{-1} in raw RDX to 81 x 10^{-2} s^{-1} in RDX (SD) as seen in Table 4.3.

Similarly, the effect of reduced particle size on thermal decomposition of TNT is studied by TGDSC analysis. Fig. 4.14 shows typical TG-DSC curves observed for TNT materials with heating rate of 20 ^{o}C/min.
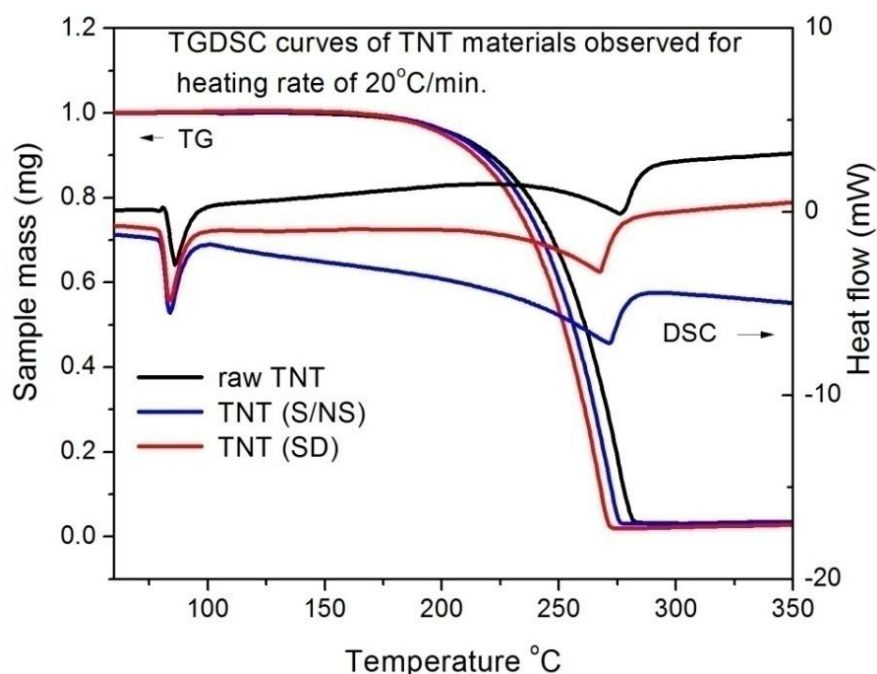
Fig. 4.14 TGDSC curves for TNT materials at heating rate of 20°C/min

In DSC curves of all samples, an endothermic peak at 80 ^{o}C is associated with melting of TNT. In all samples weight loss of about 99 % indicating TNT content in sample. The sudden weight loss in TG curves at around 225 to 275 ^{o}C is due to decomposition of TNT. It is accompanied with an endotherm followed by an exotherm observed in DSC curve. The decomposition peak is observed to be shifted to lower temperature with reduction in particle size of TNT materials. However, effect on sensitivity in these materials can be appreciably expressed in terms of change in activation energy. For kinematic investigations, TNT materials were heated from room temperature to 400 ^{o}C at heating rate of 10, 15 and 20 ^{o}C /min.
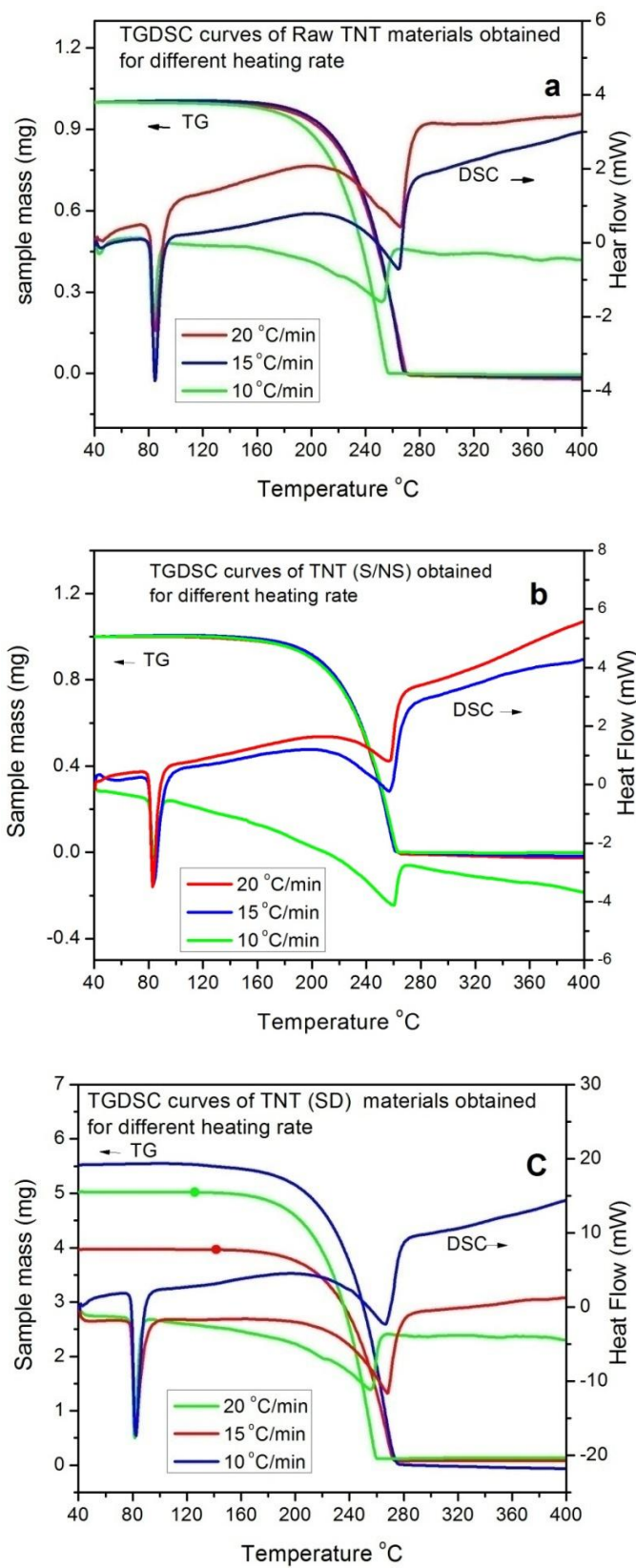
Fig. 4.15 TG DSC curves for a) raw TNT b) TNT (S/NS) and c) TNT (SD), recorded at heating rate of 10, 15 and 20 °C/min.

TG DSC curves for raw TNT, TNT processed by solvent /non solvent (S/NS) and spray drying (SD) at different heating rate of 10, 15 and 20 ^{o}C/min. are shown in Fig. 4.15. It can be seen from figure that the decomposition peak shifts towards higher temperature with increase in heating rate for raw TNT, TNT (S/NS) and TNT (SD) (average particle size of 350 µm, 5 µm and 500 nm, respectively). The values of decomposition peak temperature for TNT with different particle size are shown in Table 4.4.

Table 4.4. Decomposition peak temperature (Tp) for TNT materials with different particle size at varying heating rate

Heating rate in °C/min.	Decomposition peak temperature (Tp) for TNT with different particle size in ^{o}C		
	T (R) - 350 µm	T (S/NS) - 7 µm	T (SD) - 500 nm
10	255	254	252
15	264	262	256
20	276	272	267

By applying Kissinger's method [18], activation energies for TNT with different particle size are calculated from decomposition temperature peak and they are given in Table 4.4.

Table 4.5 Kinetics parameters for TNT material derived from TG-DSC curves

TNT	Particle size	Kinetics parameters		
		E_a (kJ mol^{-1})	Z (s^{-1})	k x 10^{-2} (s^{-1})
Raw	350 µm	78.7 ± 8%	2.09 x 10^7	63
TNT (S/NS)	7 µm	88.3± 10%	2.19 x 10^8	71
TNT (SD)	500 nm	103.4± 18%	8.64 x 10^9	85

Values of activation energy E_a, pre-exponential factor Z and reaction rate constant k are calculated and they are listed in Table 4.5. The calculated activation energy for raw TNT is in agreement with reported value in literature [19]. As shown in Table 4.5, the activation energy is more for TNT material with reduced particle size. However, shift in decomposition peak to lower temperature with reduced particle size indicate that ignition to detonation transition is rapid in these materials due to high surface energy associated with smaller size particles. Higher values of Z and k for TNT materials with reduced particle size may also be attributed to high proportion of surface atoms and hence a larger number of atoms decompose simultaneously.

The increase in activation energy in TNT and RDX materials with reduced particle size indicates a decrease in sensitivity to thermal initiation whereas increase in kinetic parameters like Z and k values with reduction in particle size observed for both these materials suggests a possible improvement in performance of these materials.

4.3.5 Impact Sensitivity:

Mostly the inadvertent initiation in energetic materials occurs due to impact. Drop weight impact test is an important and widely accepted technique to characterize sensitivity of energetic materials to ignition on impact. For the impact test, various weights are used to determine the drop height at which the energetic material samples react during some fraction of the number of impacts. This test is performed by dropping the weight from incremental heights and recording whether initiation occurs or not. In present work, measurements on impact sensitivity have been carried out with fall hammer impact test using Bruceton up-down method [20]. In this method, the drop height is increased or decreased based on preceding result. If initiation occurs in earlier attempt, drop height is reduced otherwise increased. Statistical average of

such 30 measurements is calculated the height with 50 % probability of initiation in sample. Energy required for initiation is calculated from drop weight and drop height. Results of impact sensitivity measurements for RDX materials with different particle size are shown in Table 4.6.

Table 4.6 Impact energy required for initiation in RDX materials with different particle size

Material	Particle size (μm)	Impact energy for 50 % probability of initiation in J Numbers in bracket indicate standard deviation.	
		Powder sample	Pelletized sample
Raw RDX	126 ± 45	6.14 (0.21)	13.2 (0.25)
RDX (S/NS)	4.37 ± 2	6.31 (0.21)	14.2 (0.28)
RDX (SD)	0.194 ± 0.063	7.45(0.25	15.4 (0.35)

From Table 4.6, it can be seen that impact sensitivity decreases with reduction in particle size (RDX (S/NS) and RDX (SD)) compared to that of raw RDX. The impact sensitivity for RDX (SD) with particle size of 194 nm is lowered by about 12 % as compared to raw material. It is due to reduced crystal defect and voids in materials with reduced particle size. Moreover, as seen from SEM in Fig. 4.9 a, raw RDX has more surface complexity in terms of irregular shape and sharp edges. It leads to plastic deformation and cause to increase in sensitivity on impact. RDX (S/NS) and RDX (SD) have smooth surface and near spherical geometry with reduction in particle size. Therefore, these materials are less sensitive to impact initiation.

Impact sensitivity for RDX materials with reduced particle size has also been studied for samples in pellet form. In pelletized samples, impact energy required for

initiation of these materials is higher by about 200 % as compared to that of powder samples. Ignition in energetic materials on impact is believed to occur at hot spots by localizing incident energy [21]. In powder samples, entrapped air leads to hot spot formation. In pelletized samples, porosity is less resulting in decrease in sensitivity of these samples. The effect of porosity is substantially demonstrated in following chapter dealing with energetic materials processed by sol-gel method. In pelletized samples also, sensitivity to impact initiation for RDX materials has been found to decrease by about 16 % with reduction in particle size. It may be explained from the morphology of these samples.
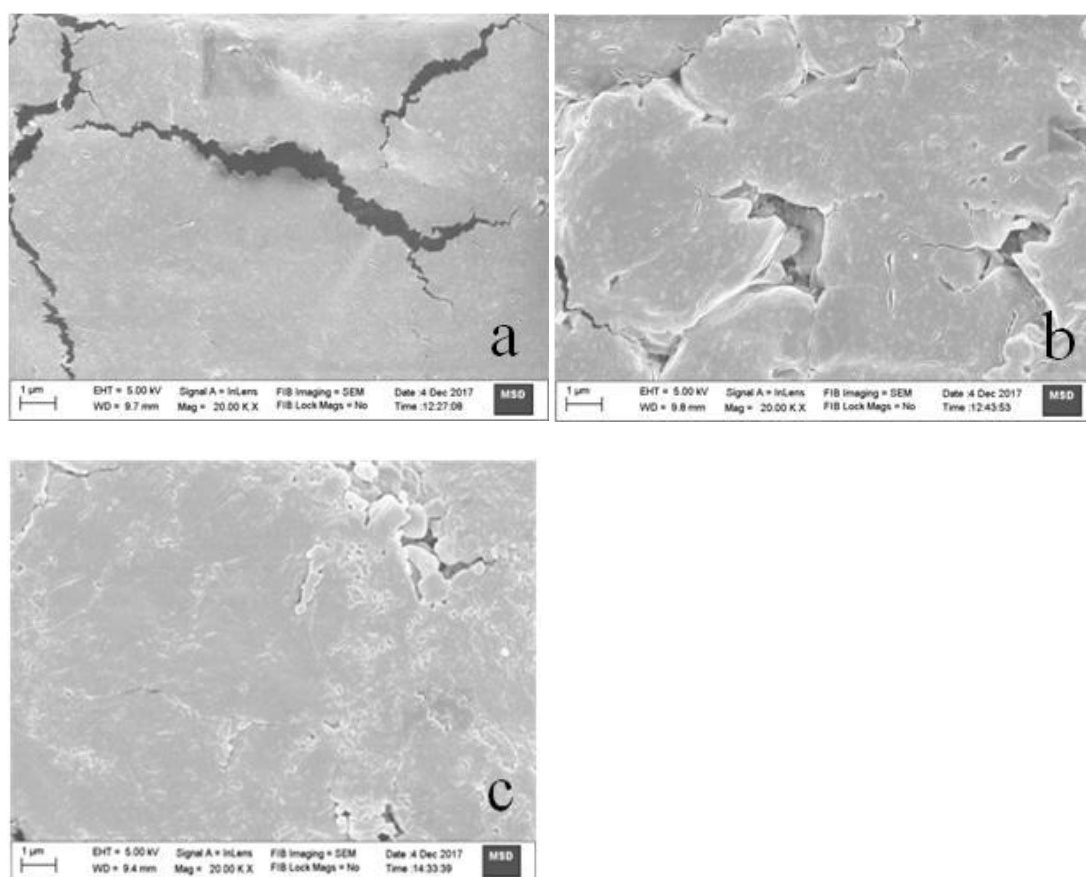
Fig. 4.16 FESEM images of pelletized samples of a) raw RDX, b) RDX (S/NS) and c) RDX (SD).

FESEM images for RDX pellets with different particle size are shown in Fig. 4.16. As shown in Fig. 4.16, the pellet of raw RDX has wide cracks in compaction due to irregular shape of particles. These can act as stress centers for concentrating the energy on impact for easy ignition. As seen in Fig. 4.9, RDX (S/NS) and RDX (SD) particles being more regular shaped have better packing density and more uniform morphology leading to decrease in sensitivity for impact initiation.

In measurements of impact sensitivity carried out with fall hammer impact test on TNT materials, impact height required to ignite these materials was found beyond the range of measurement of the equipment used in this study (> 50 J). Therefore, to measure impact energy required for initiation, a test configuration similar to Type 12 machine at LASL [22] was used. In this configuration, a sample material is placed on sandpaper. It increases sensitivity of material, but useful in relative measurements of sensitivity where required impact energy in normal test configuration is too high to measure with available experimental set up.
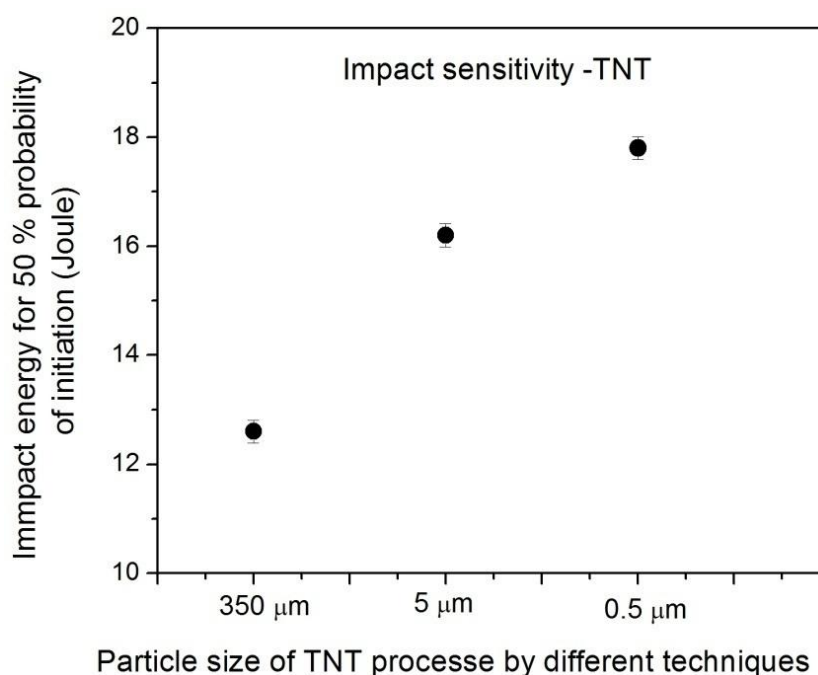
Fig. 4.17 Impact energy with 50 % ignition probability for TNT materials.

Fig. 4.17 shows impact energy required to initiate raw TNT, TNT (S/NS) and TNT (SD) with average particle size 350 µm, 7 µm and 500 nm, respectively, with 50% ignition probability. As shown in Fig. 4.17, impact energy required for ignition in TNT materials with average particle size of 350 µm, 7 µm and 500 nm is found to be 12.6 J, 15.8 J and 17.8 J, respectively. The impact energy required for ignition in TNT materials with particle size of 7 µm and 500 nm is 25 % and 40% more, respectively, as compared to that for raw materials with particle size of 350 µm. It indicates that sensitivity to impact initiation in TNT decreased with reduction in particle size. As mentioned earlier, reduced crystal defect and voids with reduction in particle size could be a reason for decrease in sensitivity.

PETN is considered as the most sensitive among the secondary energetic material. Therefore, impact energy required for ignition in PETN materials is expected to be less in comparison with TNT and RDX. This is also observed in this study. In PETN also, a similar trend of decrease in sensitivity with reduction in particle size has been observed. Impact energy required for ignition in PETN is found 3.7 J for raw PETN with particle size of 300 µm and 7.6 J in PETN (S/NS) with particle size of 5 µm. The impact sensitivity for PETN is lowered by about 200 % with reduction in particle size from 300 µm to 5 µm. It suggests that due to high surface losses in materials with reduced particle size, more energy is required for heat buildup to cause ignition in these materials. Impact energies required for initiation in pelletized samples of these materials are 10.02 J and 11.24 J, respectively. Higher value of impact energy in pelletized samples can be attributed to less porosity in the pellets.

It is an important aspect in energetic material handling that sensitivity to impact is considerably decreased in these materials with reduction in particle size.

4.3.6   Shock Sensitivity

Sensitivity of energetic materials to high pressure low duration impact is termed as shock sensitivity. This is useful property to evaluate response of such materials to accidental shock events like sympathetic detonation. It is also useful to design experimental assemblies for reliable detonation in energetic materials for specialized applications.
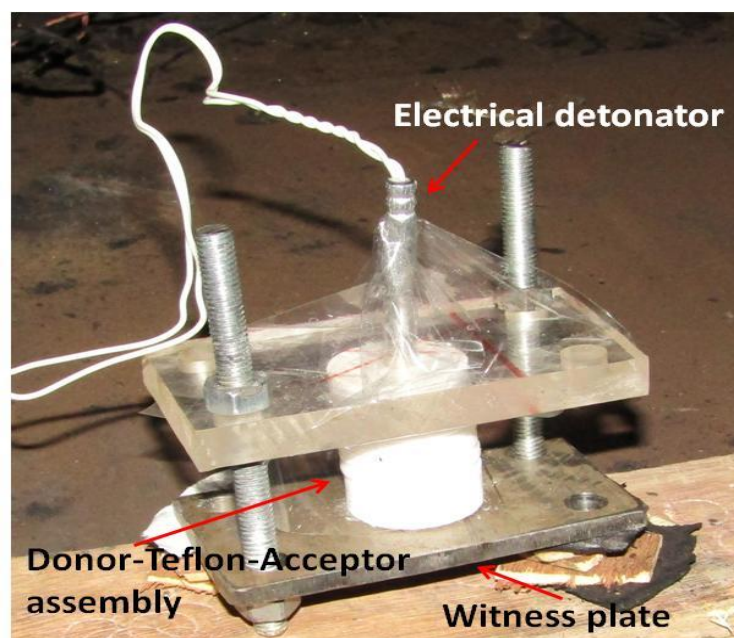
Fig. 4.18 Experimental assembly for shock sensitivity measurements

Shock sensitivity is measured using experimental configuration similar to gap test [23]. Test setup used in gap test experiment conducted to measure shock sensitivity is shown in Fig. 4.18. The acceptor charge, Teflon barrier and donor charge assembly is sandwiched between Perspex and steel plate. Acceptor charge was of TNT or RDX with dimensions of 30 mm diameter x 12 mm thickness, donor charge was of PETN with dimensions 30 mm diameter x 6 mm thick. Teflon disks of 30 mm diameter and 2 mm thickness were used in series between acceptor and donor charge for shock attenuation. A SS plate of 5 mm thickness and 75 mm x 100 mm (W X L)

size was used as witness plate. The gap thickness between acceptor and donor charge was varied using 2 mm thick Teflon disks. Donor charge was initiated using electrical detonator no. 33 and witness plate was checked to confirm whether the energetic materials charge has detonated or not. A clear-cut hole on the witness plate was considered as detonation of the energetic materials charge otherwise it was taken as no detonation. The increase or decrease of gap thickness on detonation or no detonation was followed to arrive at maximum gap thickness for ensured detonation. The effect on witness plate in case of detonation and no detonation is shown on Fig. 4.19.
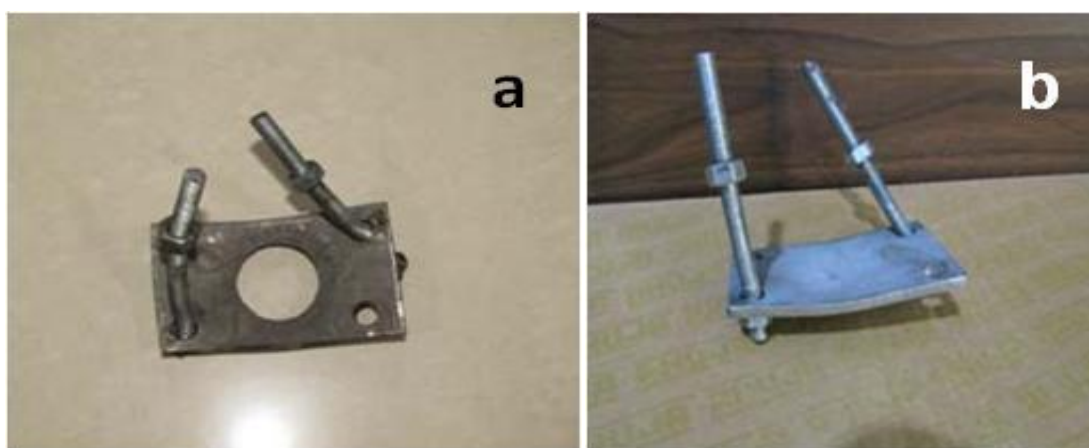
Fig. 4.19 Effect on witness plate a) Detonation   b) No Detonation

The barrier thickness for initiation in energetic materials with different particle size is shown in Table 4.7. The pore collapse and visco-plastic flow is dominant mechanism causing ignition in energetic materials with short duration high pressure shocks [24].When particle size is reduced, inter particle voids also becomes smaller. If the critical hotspot size for that pressure is greater than the mean heterogeneity in size, it is more difficult for hotspots to form and so the material will be less likely to ignite when shocked [25]. This results in decrease in sensitivity of energetic materials with reduced particle size. The trend of decrease in sensitivity with decrease in particle size could be observed from Table 4.7.

Table 4.7 Maximum gap thickness ensuring detonation in TNT and RDX

Material	Particle size (μm)	Teflon barrier thickness (mm)
Raw RDX	126	28
RDX (S/NS)	4.37	26
RDX (SD)	0.194	22
Raw TNT	350	16
TNT (S/NS)	7	14
TNT (SD)	0.5	12

4.3.7 Detonation velocity measurement:

Along with reduced sensitivity, performance is an important parameter for energetic material. The energetic material with higher velocity of detonation is more powerful. To study whether performance of energetic material can be improved by controlling particle size, detonation velocity measurements have been carried out.
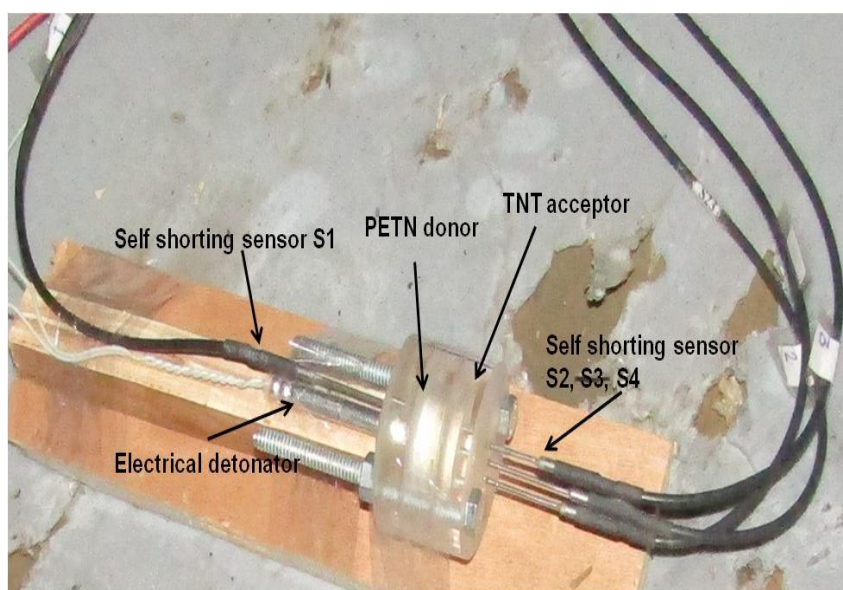
Fig. 4.20 Experimental assembly for detonation velocity measurement

Experimental assembly for these measurements consisting donor charge of PETN and acceptor charge of RDX along with sensors is shown in Figure 4.20. The donor charge is 5 mm thick and 20 mm diameter PETN pellet with density of 1.7 g/cc. The density of the acceptor charge (10 mm thick and 20 mm diameter) of RDX with different particle size was maintained at 1.55 g/cm^3. To detect the initiation of donor charge, a self-shoring sensor 'S1' is placed on the surface of the donor charge. To measure the detonation velocity of the acceptor charge, three self-shorting sensors 'S2', 'S3' and 'S4' separated by a distance of 3 mm are used. Sensor 'S4' is placed at rear surface of RDX charge, sensor 'S3' is 3 mm deep inside and sensor 'S2' is 6 mm deep inside from the rear surface of the same charge. Fig. 4.21 show typical signal profile recorded on oscilloscope for RDX (SD) with particle size of 194± 63 nm. Sensor output on the oscilloscope record indicates the arrival of detonation wave front at the sensor location. Detonation velocity is then, calculated by knowing the travel time of detonation front between two sensor location.
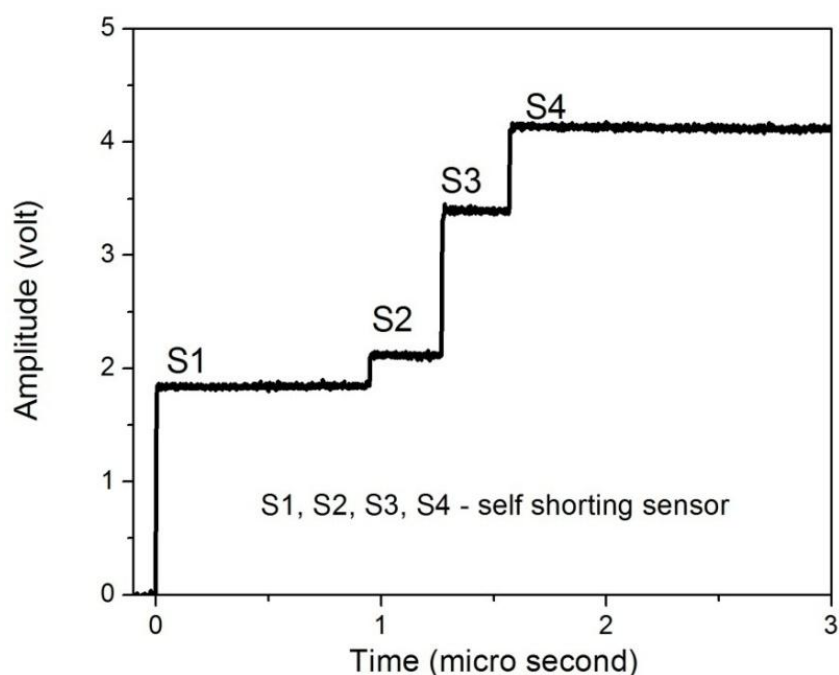
Fig. 4.21 Signal profile recorded for RDX with particle size 194± 63 nm

The signal profile recorded for detonation velocity measurement is shown in Fig. 4.21. In present case, output of four sensors ('S1', 'S2' 'S3'and 'S4') is shown in step signal form. The velocity of detonation is calculated from the known distance between the sensor pins and time measured between pin signals. Velocity measurement data for RDX is shown in Table 4.8.

Table 4.8 Detonation velocity for RDX with different particle size.

RDX material	Particle size [µm]	Detonation velocity [mm/µs]
Raw	126 ± 45	7.89 ± 0.2
Solvent precipitated	4.37 ± 2	8.26 ± 0.2
Spray dried	194 ± 63	8.89 ± 0.2

The results in Table 4.8 show that detonation velocity increased by about 12% with reduced particle size. The detonation velocity in RDX (4.37 µm) and RDX (194 nm) is higher than that of RDX (126 µm), and that indicates once ignited the spread of reaction leading to explosion occurs in these materials in a shorter time scale. As seen from thermal analysis, RDX materials with reduced particle size exhibit higher activation energy for ignition suggesting higher hot spot temperature that leads to faster rate of chemical decomposition. Faster transition to fully developed detonation may also result from a higher number density of hot spots as indicated by high value of pre-exponential factor Z [26]. The larger surface area of fine-grained materials also contributes to higher detonation velocity.

Experimental assembly used for detonation velocity measurement of TNT charges is similar to that used for RDX charge, and consist donor charge of PETN and acceptor charge of TNT along with four self-shorting sensors. Signal profile recorded for raw TNT, TNT (S/NS) and TNT (SD) is shown in Fig. 4.22.
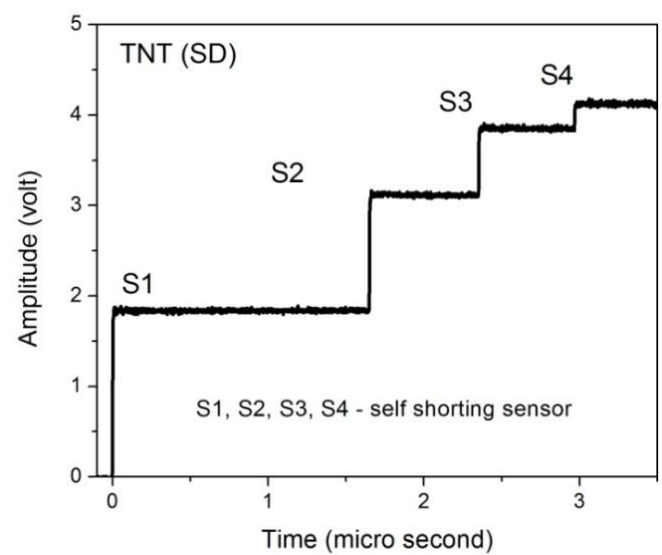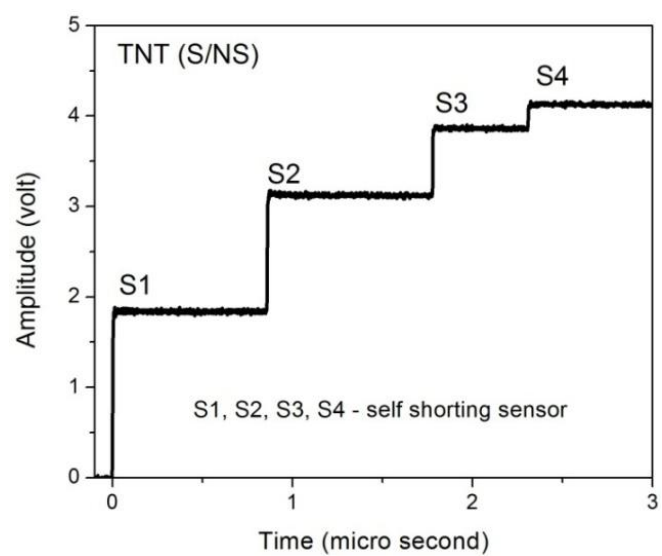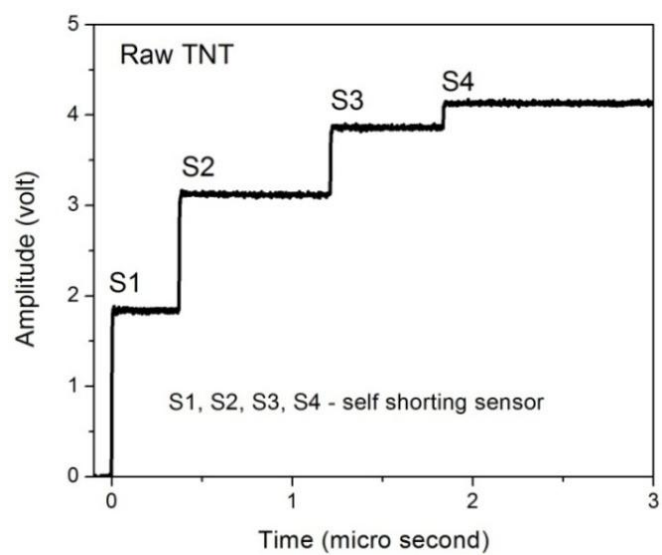
Fig. 4.22 Signal profile for TNT: particle size a) 350 μm b) 7 μm and c) 500 nm

To detect the initiation of donor charge, a self-shoring sensor 'S1' is placed on the surface of the donor charge. To measure the detonation velocity of the acceptor charge, three self-shorting sensors 'S2', 'S3' and 'S4' are used. Sensor 'S2' is placed at front surface of TNT charge, sensor 'S3' is 5 mm deep inside the acceptor charge from the rear surface and sensor 'S4' is placed on the rear surface of the same charge. Values of detonation velocity measured from the signals recorded for acceptor charges of TNT with different particle size are listed in Table 4.9.

Table 4.9 Detonation velocity for TNT material with different particle size

TNT processing method	Particle size	Detonation velocity
Raw	350 µm	6.39 ± 0.19 mm/µs
Solvent non solvent crystallization	7 µm	7.10 ± 0.21 mm/µs
Spray dried	500 nm	7.40 ± 0.22 mm/µs

The results in Table 4.9 show that detonation velocity in TNT (S/NS) is 7.1 mm/µs which is nearly 11% higher than that of raw TNT whereas detonation velocity in TNT (SD) with particle size of 500 nm increased by about 15 % as compared to that of raw material with particle size of 350 µm. Detonation velocity in TNT materials with particle size 7 µm and 500 nm is significantly higher than that of raw TNT. Similar to RDX, in TNT materials with reduced particle size, faster transition from ignition to detonation are observed that indicates once ignited the spread of reaction occurs in relatively short time scale. Larger specific surface area in these fine-grained materials and higher density of ignition centers with reduced particle size leading to more collision frequency as indicated by high value of pre-exponential factor Z could be reason for increase in detonation velocity. From the detonation

velocity measurements, it is observed that the performance of an energetic material can be greatly enhanced by reducing its particle size.

4.4   Conclusions:

Since the energetic materials are not as such available with the desired particle size, the processing methods viz. solvent precipitation and spray drying methods have been optimized to prepare TNT, RDX and PETN materials with typical particle size ranging from 350 micrometer down to 200 nanometers. It is revealed from the impact initiation studies that sensitivity to impact initiation decreased by about 15 % in RDX and by 40 % in TNT with reduction in particle size. Kinematic studies conducted for TNT and RDX materials show an increase in activation energy for thermal initiation with decrease in particle size. It also suggests improvement in energy release rate with smaller size particles which is further supported by detonation velocity measurements. The detonation velocity in these energetic materials with reduced particle has been found to be increasing up to 15 % as compared that for raw material.

REFERENCES:

[1]   Construction and Properties of Structure and Size-Controlled Micro/Nano Energetic Materials, B. Huang, M Cao, F Nie, H Huang, C Hu. *Def. Technol.* **9** (2013) 59–79.

[2]   Study on Preparation of Fine PETN for Initiating Devices, Shallu Gupta, Simran Kaur, D K Pal, T Raychaudhuri, *First National Symposium & Exhibition on Trends in Explosive Technology*, TBRL, Chandigarh, India (2008)

[3] Single Step Production and Formulation of HMX Nanocrystals, H. Qiu, V. Stepanov, T. Chou, A. Surapaneni, A R DiStasio, W Y Lee, *Powder Technol*. **226** (2012) 235-238

[4] Solubilities of Explosives. Dimethylformamide as General Solvent for Explosives, M E. Sitzmann, S C. Foti , *J. Chem. Engi. Data*, **20** (1975) 53- 55.

[5] Application of FT-IR Spectroscopy for Investigation of Pink Water Remediation by Pine Bark, M. Grube, O. Chusova, M. Gavare, K. Shvirksts, E. Nehrenheim, M. Odlare, *The Open Biotechnology Journal,* **9** *(*2015) 67-75

[6] Preparation and Characterization of Ultrafine RDX, A. Pant, A K Nandi, S P Newale, V P Gajbhiye, H. Prashanth, R K Pandey, *Central European J. Energ. Mater.* **10** (2013) 393-407

[7] Spectroscopic and Thermal Studies on Pentaerythritol Tetranitrate, P. Makashir, E. Kurian, *Propellants, Explos. Pyrotech.,* **24** (1999) 260-265

[8] Active Mode Remote Infrared Spectroscopy Detection of TNT and PETN on Aluminum Substrates, J R. Castro-Suarez, L C. Pacheco-Londoño, J Aparicio-Bolaño, S P. Hernández-Rivera, *Journal of Spectroscopy*, **2017**, (2017) Article ID 2730371, 11 pages

[9] Polymorphism in 2-4-6 Trinitrotoluene, R Vrcelj, J Sherwood, A Kennedy, H Gallagher, T Gelbrich, *Crystal Growth & Design*, **3** (2003) 1027-1032

[10] The Cystal Sructure of β-RDX - An Elusive Form of an Explosive Revealed, David Millar, Iain Oswald, Duncan. Francis, William Marshall, Colin Pulham, Adam Cumming, *Chemical Communications*, **5** (2009) 562- 564.

[11] Decomposition of Condensed Phase Energetic Materials: Interplay between Uni- and Bimolecular Mechanisms, D Furman, R Kosloff, F Dubnikova, S

Zybin, W Goddard, N Rom, B Hirshberg, Y Zeir, *J. Am. Chem. Soc.* **136** (2014) 4192-4200.

[12] Sol–Gel processing of Energetic Materials, T M Tillotson, L W Hrubesh, R L Simpson, R S Lee, R W Swansiger, L R Simpson, *J. Non-Cryst. Solids,* **225** (1998) 358-363.

[13] Kinetics and Mechanisms of the Thermal Dehydration of Dilithium Sulfate Monohydrate, N. Koga, H. Tanaka, *J. Phys. Chem.*, **93** (1989) 7793 - 7798

[14] Mechanism Investigation for Remarkable Decrease in Sensitivities from Micro to Nano Nitramine, Y. Wang, X. Song, D. Song, C. An, J. Wang, F. Li, *Nanomater. Nanotechnol.*, **6** (2016) 1–10

[15] Thermal Behavior and Decomposition Kinetics of RDX and RDX/HTPB Composition Using Various Techniques and Methods, M. Abd-Eeghany, A. Elbeih, S. Hassanein, *Cent. Eur. J. Energ. Mater.,* **13** (2016) 715-735

[16] A study on the Thermal Decomposition Behaviors of PETN, RDX, HNS and HMX, J. Lee, C. Hsu, C. Chang, Thermochim. Acta, **392** (2002)173–176

[17] Production and Sensitivity Evaluation of Nanocrystalline RDX Based Explosive Compositions, V. Stepanov, V. Anglade, H. Balas, A. Wendy, A. Bezmelnitsyn, L. Krasnoperov, *Propellants Explos. Pyrotechnic*. **36** (2011) 240-246

[18] Study on a Novel High Energetic and Insensitive Munitions Formulation: TKX-50 Based Melt Cast High Explosive, Y. Yu, S. Chen, T. Li, S. Jin, G. Zhang, M. Chenb, L. Li, *RSC Advances*, **7** (2017) 31485-31492

[19] The Kinetic of Mass Loss of Grades A And B of Melted TNT by Isothermal and Non-Isothermal Gravimetric Methods, H Pouretedal, S Damiri, P Nosrati, E Ghaemi, *Def. Technol.* **14** (2018) 126-131

[20] Modelling of Explosives Sensitivity Part 1: The Bruceton Method, R. Wild, E. Collani, *Economic Quality Control,* **17** (2002) 113-122

[21] A Mechanistic Model for Shock Initiation of Solid Explosives, J. Massoni, R. Saurel, G. Baudin and G. Demol, *Phys. Fluids*, **11** (1999), 710-736

[22] T Gibbs, A Popolato (Ed), *LASL Explosives Property Data*, University of California Press, (1980) p. 446

[23] On the Shock Sensitivity of Explosive Compounds with Small-Scale Gap Test, Bisheng Tan, Xinping Long, Rufang Peng, Hongbo Li, Bo Jin, Shijin Chu, *J. Phys. Chem. A* **115** (2011) 10610-10616

[24] Visco Plastic Collapse Mechanism of Hot-spot Formation in Porous TNT Explosives, Z. Y. Zhang, S. Huan, F. Y. Lu et al., *Energetic Mater.*, **2** (1994) 36–42

[25] Hot-spot Contributions in Shocked High Explosives from Mesoscale Ignition Models, G. Levesque, P. Vitello, and W. M. Howard, *J Applied Phys.* **113** (2013) 233513-9

[26] Developing of a Four-Channel Oscilloscope Multiplexer for Displaying Digital Sounds, V Ramachandran, *Phys. Educ*. **26** (1991) 392-394

[27] Particle Size on Sensitivity and Decomposition of Hexogen, S. V. Ingale, P. B. Wagh, Amit Rav, T. C. Kaushik, Studies on Effect of Science *and Technology of Energetic Materials* , **80** (2019) 222-228.

CHAPTER 5

PREPARATION OF ENERGETIC MATERIALS USING SOL-GEL METHOD
AND THEIR CHARACTERIZATION

It is known that ignition mechanism in energetic materials is affected by defects present in it. However, inducing the defects in controlled manner and to analyze effect of controlled defects on ignition mechanism is not explored in case of energetic materials. The feature of controlling porosity through sol-gel process is useful for understanding effect of the microstructure on the sensitivity and performance of energetic materials. Therefore, in the present work, the processing of energetic materials by sol-gel method was taken up.

Sol-gel processing is used to prepare nano-structured silica materials using alkoxy compounds, generally organo-metallic silicate, as precursors. Silica gels are widely studied nano structured materials [1]. To prepare silica gels, silicon alkoxide is dissolved in a suitable solvent. To this solution, water either as acidic or basic (depending on type of organo-metallic silicate precursor) is added. Hydrolysis of silicate results in nano sized silica particles suspended in solution, called as sol. These colloidal silica particles in sol cross link to form a three-dimensional network with solvent trapped in pores which is referred as gel. The solvent from the gel pores is extracted resulting in porous solid with nanosized pores. This porosity has been used for preparation of nanosized particles of other desired material.

In this work this method has been used to prepare nanostructured energetic materials with narrow size distribution. It is advantageous that the porosity and microstructure along with loading of the energetic materials in host matrix could be

controlled to study the effect of controlled defects on properties of these materials. To prepare energetic materials with reduced particle size, the material is dissolved in solvent which get entrapped in pores of gel. Evaporation of liquid from the gel at ambient conditions results in xerogel material with recrystallized energetic material in nano sized pores of silica. Various steps involved in sol-gel processing of energetic materials are shown in Fig. 5.1.
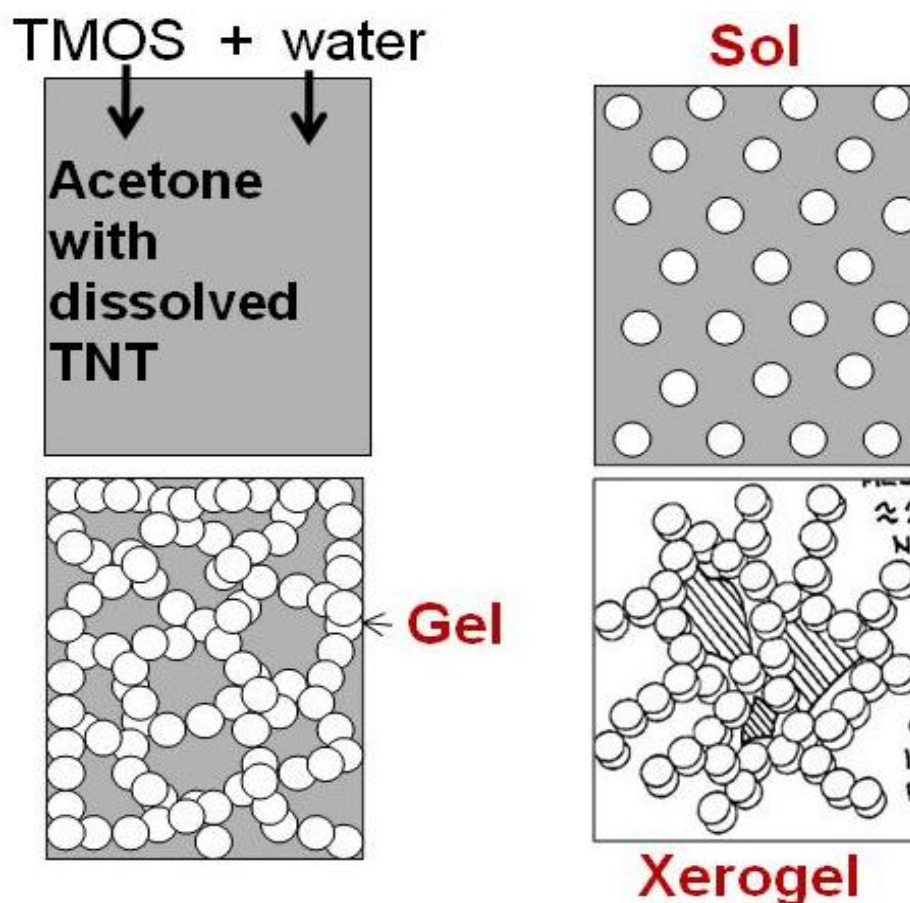
Fig. 5.1 Steps in sol-gel processing of energetic material

The sol-gel process has been optimized to obtain energetic materials with particle size of 20 to 80 nanometers in silica gel matrix by varying the process parameters such as molar ratio of precursor chemicals, the content of energetic material and catalyst concentration, etc. All chemicals used were of analytical grade from Merck.

5.1 Processing of RDX/ TNT/PETN material using sol-gel method:

For processing by sol-gel method, TNT was dissolved in acetone. To this solution, Tetramethoxysilane (TMOS) was added as a source of silica (SiO_2) and water in the form of catalyst required for hydrolysis of silica is used. Since the alkaline materials react with TNT and forms Meisenheimer complex [2]; acid catalysts were chosen to accelerate gelation. Various acidic catalysts viz. citric acid, oxalic acid, hydrochloric acid and hydrofluoric acid (HF) were used, and it was found that with HF catalyst, clear and transparent gels are obtained in less time. Faster gelation with HF acid catalyst may be due to the ability of fluoride ion to allow temporary expansion of the coordination number of silica from four to five or six that reduced the gel times [3]. The solution was constantly stirred for 15 minutes. TNT content in final xerogel was achieved by suitably choosing quantity of TNT while preparing TNT-acetone solution in first stage. Preparation of TNT/SiO_2 xerogels with higher content of TNT (90 %) requires higher acetone/TMOS ratio to dissolve TNT completely in acetone. But with higher acetone/TMOS ratio, gelation time increases and takes weeks for gelation of silica. After a series of trials, the molar ratio of precursors TMOS**:** Acetone**:** Water**:** 0.5 M HF was optimized at 1**:** 50**:** 6**:** 4 x10^{-3}, respectively, for preparation of TNT/silica xerogels with 90% TNT content. With this molar ratio, gelation occurs within reasonable time of 36 hours. Generally, in silica gels, the solvent is extracted by supercritical drying method in which the gel is heated to critical temperature of the solvent, preferably methanol (Critical temperature: 243 ^{o}C, critical pressure: 80 bars) [4]. Exchanging the solvent with liquid CO_2 and extraction of CO_2 at its supercritical conditions (Critical temperature: 31 ^{o}C, critical pressure: 70 bars) is another option for drying the gels [5]. However, TNT is a heat

sensitive material and may explode at temperature around 200 ˚C; therefore supercritical extraction of acetone from gel network has been prevented. The solubility of TNT in CO_2 supercritical fluid may affect the final composition of TNT/silica xerogels; therefore, CO_2 drying was also not opted. Instead the solvent from the pores of gel was evaporated at ambient conditions resulting in xerogels with TNT occupied in the pores of silica network. For comparison purpose, pure silica xerogel was also prepared using the same molar ratio mentioned above without adding TNT to the solution.

Similar to TNT-SiO_2 composites, silica xerogels incorporating RDX and PETN were prepared using sol gel process. For processing these materials by sol gel method using silica as host matrix, raw material was dissolved in acetone. The amount of RDX or PETN dissolved in acetone was chosen to obtain 90 % of energetic material in final xerogel. To this solution of energetic material dissolved in acetone, TMOS and dilute hydrofluoric (HF) acid (0.1M) were added. This solution transformed to gel, and the energetic material dissolved in acetone was trapped inside the gel pores. Ambient drying of gel to evaporate acetone resulted in silica xerogels with crystallized energetic material in pores. For RDX/SiO_2 xerogels, TMOS: Acetone: Water (0.1 M HF) molar ratio has been optimized at 1:90:5 whereas for PETN/SiO_2 xerogel, this ratio has been optimized to 1**:** 70**:** 4, respectively.

Also the processing of trinitrotoluene energetic material using sol-gel method was aimed to study the effect of induced defects in controlled manner on the sensitivity of energetic materials. TNT is the most suitable material for these studies because of its higher solubility in acetone. By controlling acetone to silica gel precursor molar ratio, the microstructure and porosity in the TNT-SiO_2 composite can

be controlled precisely over wide range to study these materials. To prepare the TNT-SiO$_2$ composites, a predetermined amount of TNT was dissolved in acetone. The molar ratio of TNT/Tetramethoxysilane (TMOS) was varied from 0.4 to 2.4 to obtain the TNT content in the gel ranging from 60 to 90 wt %. The molar ratio of H$_2$O/TMOS and Acetone/TMOS were kept constant at 16 and 50, respectively. It has helped to study the change in microstructure of silica xerogel getting more pores occupied by energetic materials with higher loading of TNT.

To vary the pore volume in gel matrix, the molar ratio of TMOS/Acetone in the samples containing 75 wt % TNT was varied from 50 to 20 by maintaining molar ratio of TNT/TMOS as 0.8 and H$_2$O/TMOS as 16. After formation of the gel, the solvent from gel pores was evaporated at ambient conditions to obtain nanosized TNT retained in the pores of gel. The samples containing 60 wt %, 75 wt % and 90 wt % of TNT and Acetone/TMOS ratio as 50 have been designated as T60, T75 and T90, respectively. The sample containing 75 wt % of TNT has been further designated as T75-I, T 75-II and T75-III with Acetone/TMOS ratio as 50, 35 and 20, respectively.

5.2   Characterization of Energetic Materials:

5.2.1   Fourier Transform Infra-Red (FTIR) spectroscopy:

It was important to know that whether energetic material retained in the final xerogel after sol-gel processing. Therefore, energetic materials processed by sol-gel method were characterized by FTIR spectroscopy. The presence of RDX/TNT/PETN materials in corresponding silica xerogel is confirmed from these studies. FTIR spectra of the raw materials and composites of sol-gel processed energetic materials were recorded in wave number range 400 to 4000 cm^{-1}.

Fig. 5.2 shows FTIR spectra for a) silica xerogel b) TNT and c) TNT processed by sol-gel method.
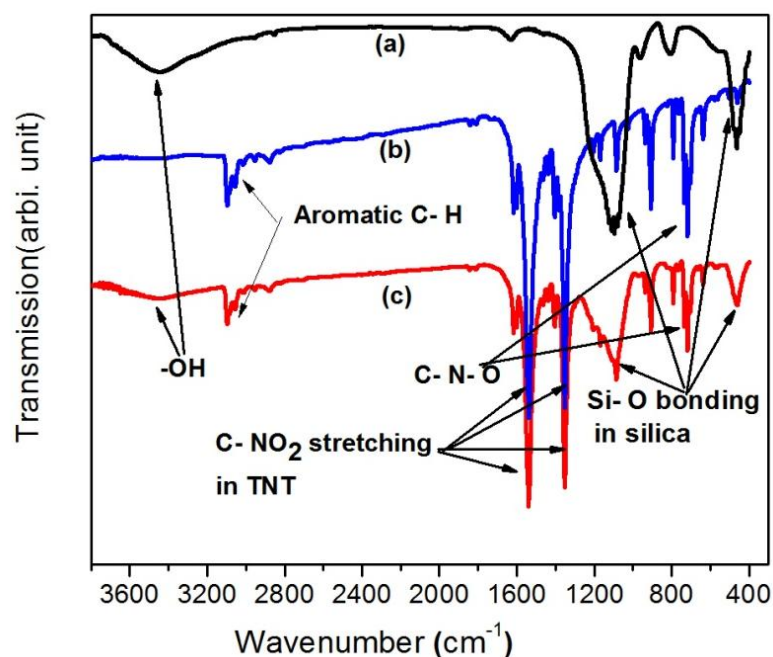
Fig. 5.2 FTIR spectra of (a) silica xerogel, (b) TNT and (c) TNT/silica xerogel

In FTIR spectrum of silica xerogel (Fig. 5.2 a), the band observed at wave number 450 and 1100 cm^{-1} is assigned to Si-O bonding in silica [6]. In FTIR spectra of TNT (Fig. 5.2 b) the bands observed at 3100 and 750 cm^{-1} assigned to C-H stretch vibrations of aromatic ring and bands at 900 and 1085 cm^{-1} correspond to C-N stretching and C-N-O bend. The peaks at 1355 cm^{-1} and 1540 cm^{-1} correspond to the characteristics C-NO$_2$ symmetric and asymmetric stretching vibrations of TNT, respectively [7]. The FTIR spectra of TNT/silica xerogels (Fig. 5.2 c), indicates bands at 1350 and 1550 cm^{-1} corresponding to C-NO$_2$ stretching from TNT and the bands observed at 1100 cm^{-1} and 450 cm^{-1} are assigned to Si-O vibration in Si-O-Si from silica and band at 3550 cm^{-1} which corresponds to vibration of structural -OH group indicating presence of silanol groups on surface of xerogel [8]. The presence of both

the silica and TNT in the resulting xerogel sample is marked with the characteristic peaks observed for both.

Fig. 5.3 shows the FTIR spectra of (a) pure SiO_2 xerogel, (b) RDX and (c) RDX/SiO_2 xerogel.
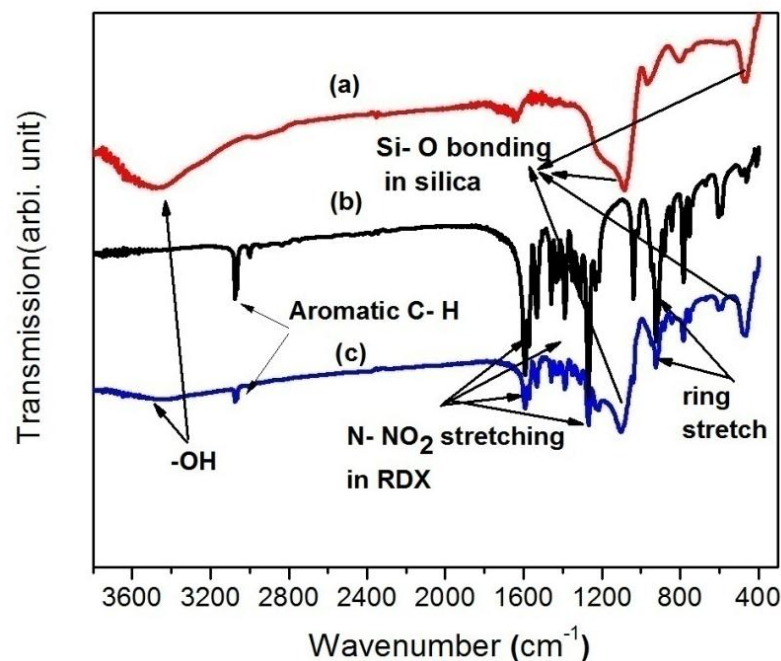
Fig. 5.3 FTIR spectra of (a) SiO$_2$ xerogel (b) RDX) and (c) RDX /SiO$_2$ xerogel

The peak at 1100 and 450 cm^{-1} in the spectra of SiO_2 xerogel (Fig. 5.3 a) is due to Si-O bond the and band at 3550 cm^{-1} corresponds to adsorbed water. The peaks at 1593 , 1573 , 1533 , 1395 and 1268 cm^{-1} in the IR spectra of the RDX (Fig. 5.3 b) are due to stretching of NO_2; the peak at 1456 cm^{-1} is assigned to CH_2 wagging; the peak at 1047 cm^{-1} is attributed to ring stretching whereas the peaks at 924 cm^{-1}, 782 cm^{-1} are assigned to ring stretching and non-planer stretching of N-NO$_2$ group in RDX [9]. The presence of peaks for both the RDX and silica materials in RDX /SiO_2 composite xerogel (Fig. 5.3 c) conforms that RDX is retained in silica gel after sol-gel processing.
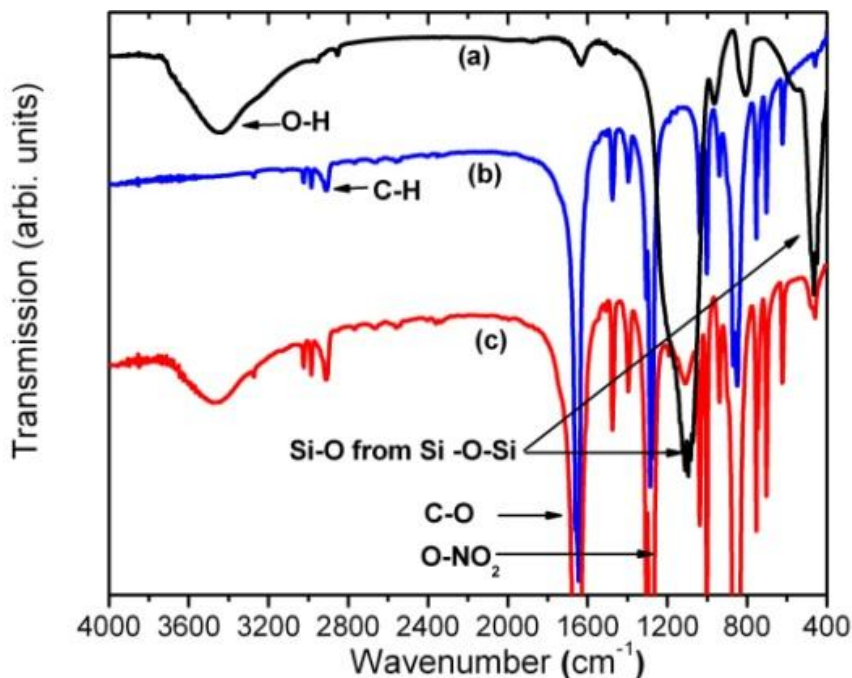
Fig. 5.4 FTIR spectra of (a) silica xerogel, (b) PETN and (c) PETN/silica xerogel

Fig. 5.4 shows FTIR spectra for silica xerogel (a), raw PETN (b) and PETN-SiO$_2$ xerogel with 90 % PETN content (c). FTIR spectra of PETN (Fig. 5.4 b) shows bands 2900 and 1400 cm^{-1} (C-H stretch vibrations of aliphatic compounds), 753 cm^{-1} (-ONO$_2$ umbrella),869 cm^{-1} (-ON stretching), 1038 and 1306 cm^{-1} (-NO$_2$ rocking). The absorbance band at 1285 cm^{-1} corresponds to NO$_2$ symmetric stretching vibration of O-NO$_2$ band, characteristic of nitrate ester like PETN [10]. The peak observed at 1700 cm^{-1} is due to CO from the formaldehyde structural group. FTIR spectra of silica xerogel shows bands at 1100 and 450 cm^{-1} from Si-O vibration from silica and band at 3550 cm^{-1} indicate presence of silanol group. FTIR spectra of PETN-SiO$_2$ xerogel (Fig. 5.4 c) show peaks from both the spectra of PETN and silica indicating that resulted xerogel contains both PETN and silica [11].

FTIR characterizations of energetic materials processed by sol-gel method conformed formation of energetic materials and silica composites.

5.2.2 XRD:

To ascertain that whether there is any change in crystal structure of energetic materials after processing by sol-gel method, these materials were characterized by X-ray diffraction. X-rays diffraction data for the sol-gel processed samples were recorded in step scan mode between 2θ of $10°$ to $80°$ using CuKα X-rays (1.54 Å).
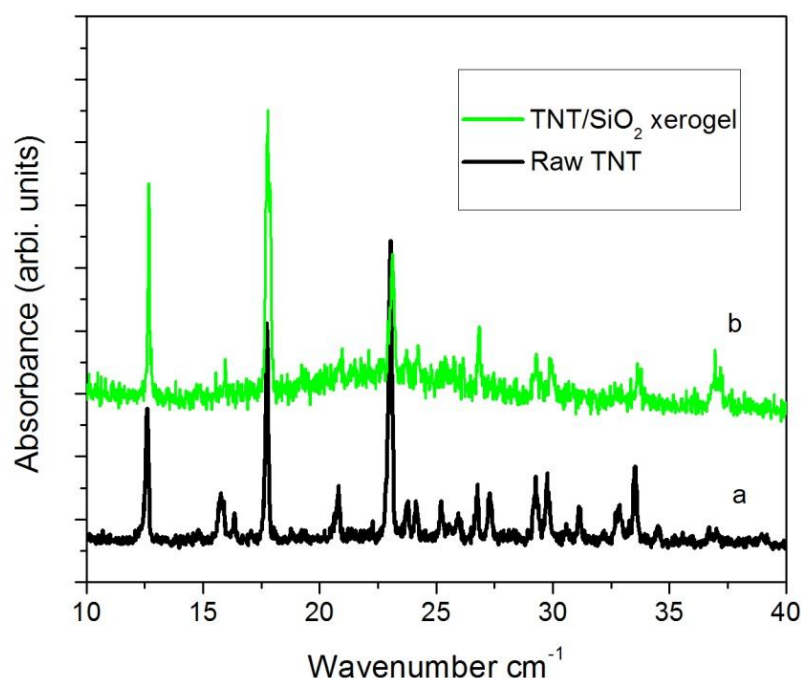
Fig. 5.5 XRD patterns for a) raw TNT and b) TNT /SiO$_2$ xerogel

Fig. 5.5 shows the XRD patterns for raw TNT (5.5 a) and TNT/SiO$_2$ composite processed by sol-gel method (5.5 b). XRD results of TNT processed by sol-gel method (Fig. 5.5 b) shows that the specimen contains a mixture of crystalline and amorphous phase. The diffraction peaks of crystalline phase from XRD pattern observed at 13.3, 16.1, 18.1, 20.9, 23.8, 25.3, 26.5, 28.5, 29.9, 32.9 and 33.5 degree could be assigned to monoclinic phase of TNT [12]. The presence of amorphous silica matrix appeared in XRD pattern as a large hump at around 20-30° [13]. This confirmed the presence of TNT in the composite. The mean crystallite grain size of

90

TNT derived from XRD pattern using Scherrer formula [14] considering full-width-at-half maximum (FWHM) for the most intense diffraction line is around 41 nm. The XRD analysis suggests that nano crystallites of TNT are formed in the gel matrix.
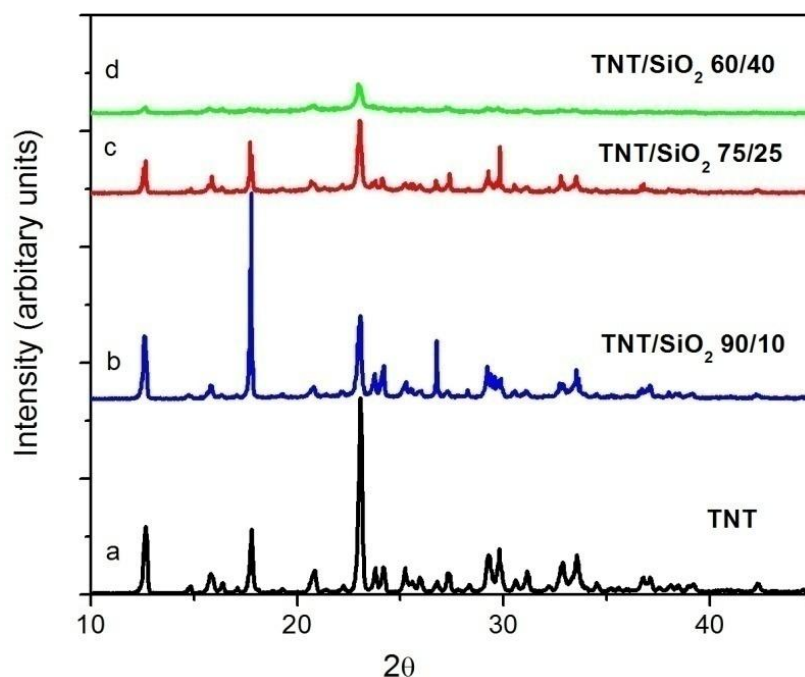
Fig. 5.6 XRD patterns for raw TNT and the sol-gel processed TNT-SiO$_2$ composites containing 90, 75 and 60 wt % TNT

Fig. 5.6 shows the XRD patterns for raw TNT and the sol-gel processed TNT-SiO$_2$ composites containing 90, 75 and 60 wt % TNT. It indicates the presence of TNT in the TNT/SiO$_2$ composites. As the silica content in the composite samples increases from 10 to 40 %, the visibility of crystalline nature of TNT is less prominent due to amorphous nature of silica gel. As TNT recrystallizes in the pores of silica gel, there is some variation in the peak intensity of scattering planes.

In Fig. 5.7 showing XRD for raw RDX and RDX/SiO$_2$ composite prepared by sol-gel method, diffraction peaks at 13.0, 15.4, 16.5, 17.3, 17.8, 20.3, 22.0, 25.3, 26.9, 29.3, 32.3 and 35.1, recorded for both materials, are assigned to the orthorhombic crystal structure of RDX (PCPDF 46-1606) [15]. It indicates the presence of RDX in

sol-gel processed composites. As seen from XRD patterns in Fig. 5.7, the crystal structure for RDX processed by sol-gel techniques is same as that of raw material.
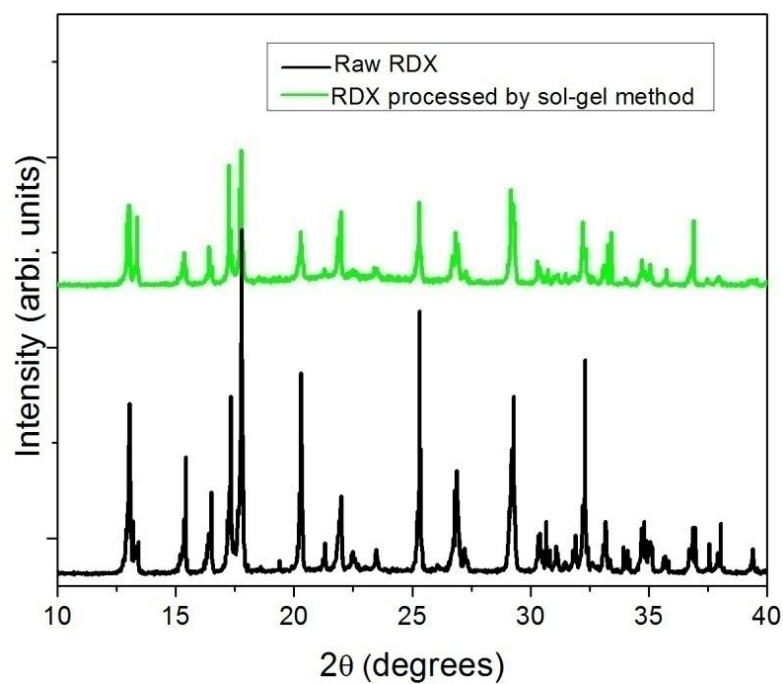
Fig. 5.7 XRD patterns for raw RDX and RDX/SiO$_2$ xerogel
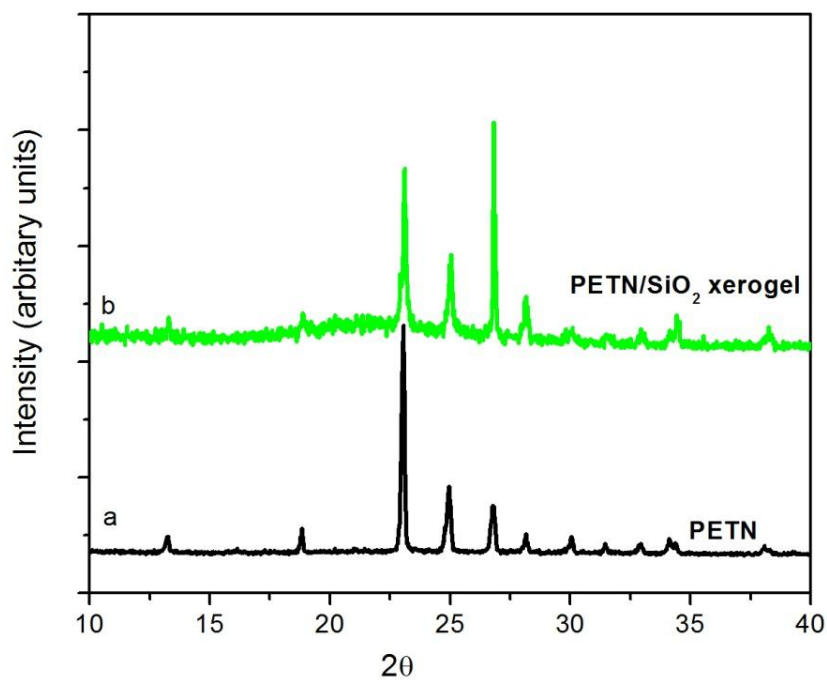
Fig. 5.8 XRD patterns for a) PETN and b) PETN processed by sol-gel technique

Similar to RDX and TNT, XRD patterns for raw PETN and PETN/SiO$_2$ xerogel (Fig. 5.8) indicate presence of PETN in xerogel. XRD peaks at 13.3, 18.9, 23.1, 25.0, 26.8, 30.1 and 34.4 degrees (PCPDF 44-1623) confirmed the crystal structure for PETN processed by sol-gel techniques is tetragonal [16] same as that of raw material.

5.2.3 Morphology Studies:

Morphology of energetic materials processed by sol-gel method was studied using FESEM and TEM techniques. The SiO$_2$ xerogels are porous networks of interconnected silica particles. In sol-gel processing, energetic materials are made to crystallize in the pores of silica gel network hence constrained in the particle sizes to about few nanometers. Fig. 5.9 shows TEM image of SiO$_2$ xerogel.
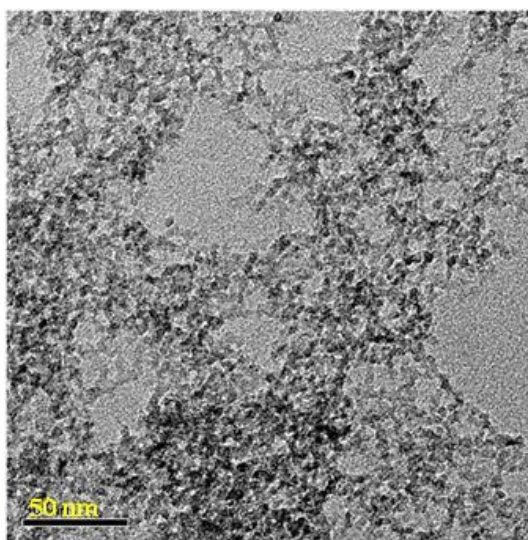
Fig. 5.9 TEM image of SiO$_2$ xerogel

The pores of the silica network are around 50 to 100 nm size and the sizes of primary silica particles forming the clusters are about 5 to 10 nm. This porous structure is utilized to load energetic materials in the gel. Particle size of the materials loaded in gel is restricted by pore dimensions and hence energetic materials with particle size restricted to less than 100 nm could be prepared using this method.

5.2.3.1 FESEM:

Fig. 5.10 shows FESEM for raw TNT and TNT processed by sol-gel method.
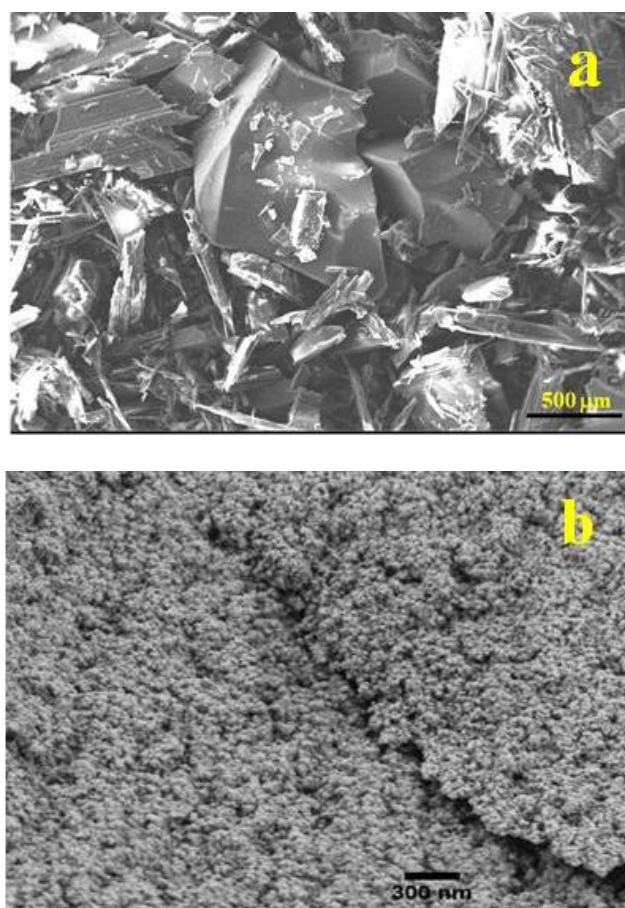
Fig. 5.10 FESEM of a) raw TNT and b) TNT processed by sol-gel method

Particles of raw TNT (Fig. 5.10 a) have irregular shapes with sharp edges. Particle size of raw TNT is of the order of 500 μm. In FESEM of TNT/SiO_2 xerogel (Fig. 5.10 b), it can be seen that the size of all particles are within the range of 30 to 80 nm. The average size of these particles is 50 nm with standard deviation of 15 nm. Porous microstructure of TNT/SiO_2 xerogel with closely spaced pores and particles with rough surface morphology is observed.

The microstructure of TNT/SiO_2 composites containing TNT in range of 60 to 90 % was studied and FESEM images of TNT/SiO_2 composites are shown in Fig. 5.11[17].
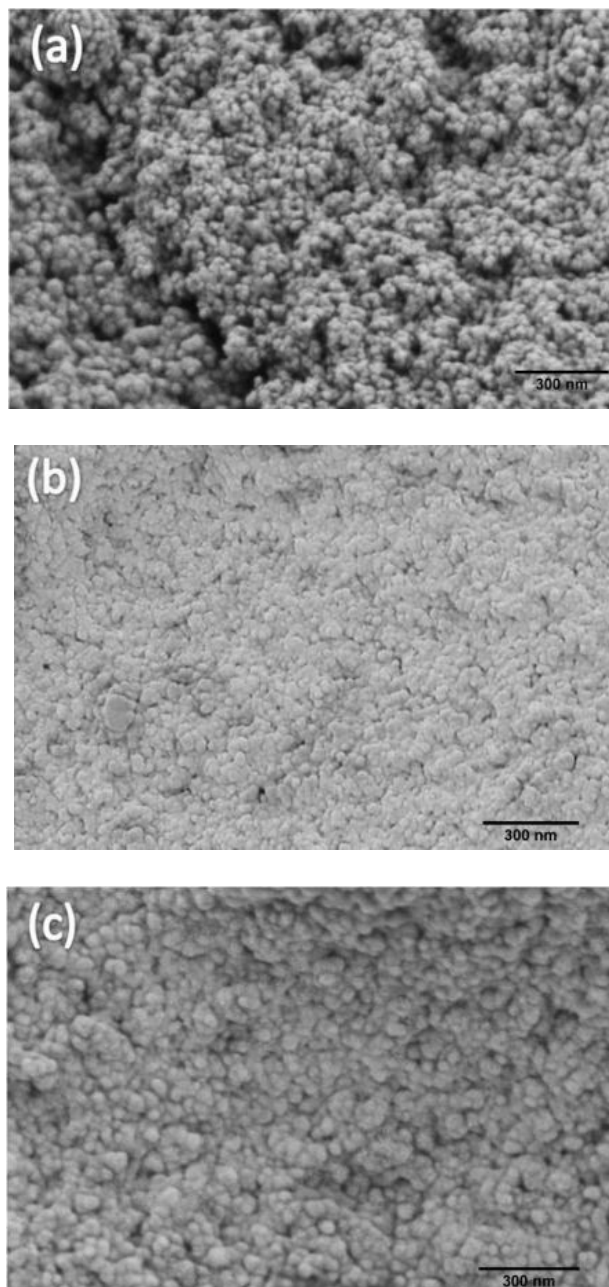
Fig. 5.11 FESEM images of TNT-SiO$_2$ xerogels: a) T75-I b) T75-III c) T90 [17]

Figs. 5.11 (a) and (b) show FESEM images of TNT-SiO$_2$ xerogels containing 75 wt% TNT processed with Acetone/TMOS ratio as 50 and 20, respectively. As mentioned earlier, these samples are designated at T75-I and T75-III, respectively. Fig. 5.11(c) shows FESEM image of TNT-SiO$_2$ xerogels with 90 wt % TNT prepared with Acetone/TMOS ratio of 50 and this material is designated as T90.

It is observed from FESEM that the sample T75-I (Fig. 5.11 a) is more porous as compared to T75-III (Fig. 5.11 b). As the molar ratio of Acetone/TMOS for the T75-I is 50 which is more than that for T75-III samples (20), the pores in T75-I are more widespread and larger pore volume. The pores and particles are in mesoporous range. In the T75-III sample, the particles are closely spaced due to low acetone/TMOS ratio and the microstructure is more compact that indicates a significant decrease in porosity. Fig. 5.11 c shows SEM image of T90 sample. The Acetone/TMOS ratio for both T 75-I and T 90 is 50. Compared to T75-I sample, the particles in T90 sample are well grown and has larger particle size. Due to higher loading of TNT, more number of pores are occupied with TNT. Since the particles are well grown and larger in size, the microstructure of T90 sample becomes less porous compared to T75-I. As compared to T75-III sample, the microstructure in T90 sample is less compact that is due to higher Acetone/TMOS ratio. These observations suggest that by varying the process parameters like solvent to TMOS ratio and TNT content in the composite, the microstructure can be suitably controlled [17].

Fig. 5.12 (a) and (b) shows FESEM image of raw RDX and RDX/SiO_2 xerogel, respectively. FESEM image of raw RDX (Fig. 5.12 a) indicates the RDX particles with irregular shape and horny edges with particle size in range of 200 µm. In FESEM images of RDX/SiO_2 xerogel (5.12 b) which is prepared by processing RDX using sol-gel method, though RDX and SiO_2 phases cannot be resolved from one another, the overall small particles sizes indicate that distribution of both the constituents is in nanometer range. In RDX/SiO_2 xeogel, particles are spherical in shape with sizes in the range of 55 ± 25 nm. These particles are well connected to form aggregates, resulting in porous microstructure of interconnected clusters.
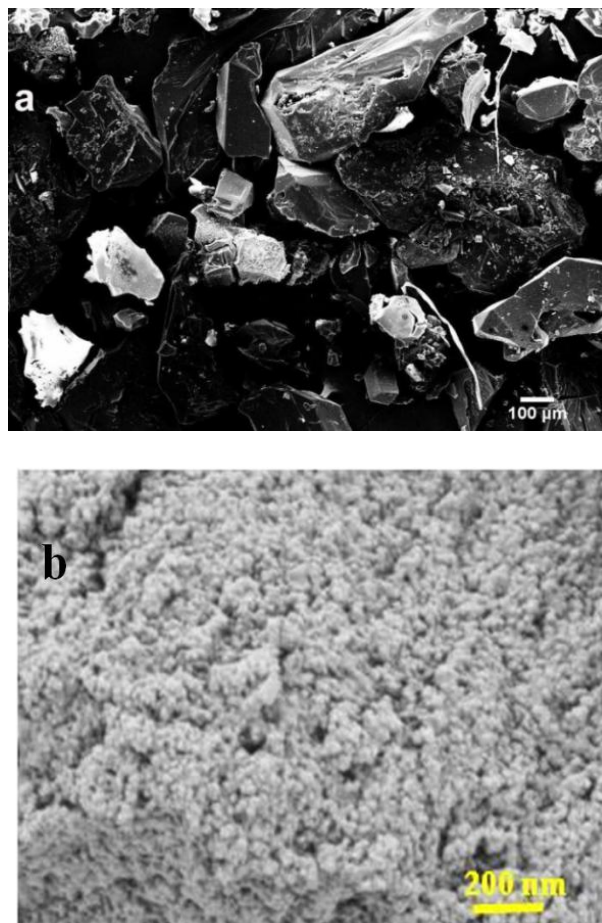
Fig. 5.12 FESEM of a) raw RDX and b) RDX processed by sol-gel method

Fig. 5.13 shows FESEM images of PETN processed by sol-gel method. The PETN/SiO$_2$ xerogel have particles with size in the range of 20-50 nm.
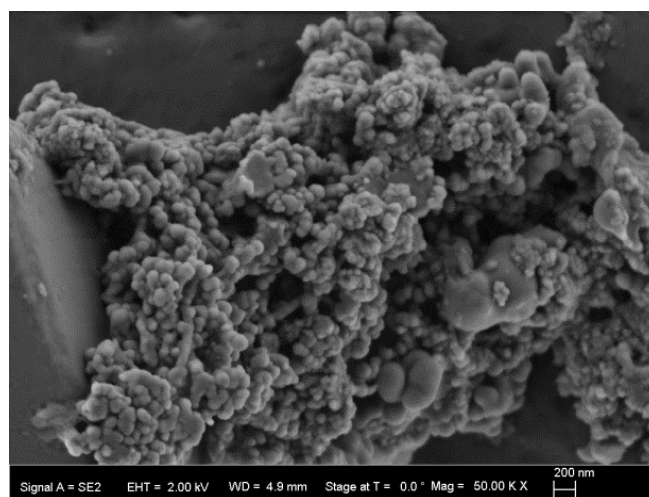
Fig. 5.13 SEM image of PETN/SiO$_2$ xerogel

5.2.3.2 Transmission Electron Microscopy (TEM):

To ascertain retention of energetic materials in porous silica gel network, these samples were further characterized by Transmission Electron Microscopy (TEM) along with Selected Area Electron Diffraction (SAED). For TEM analysis, the powdered sample suspended in methanol was dispersed on a carbon coated copper grid and the micrographs were recorded on negative films which have been subsequently scanned to obtain digital images.
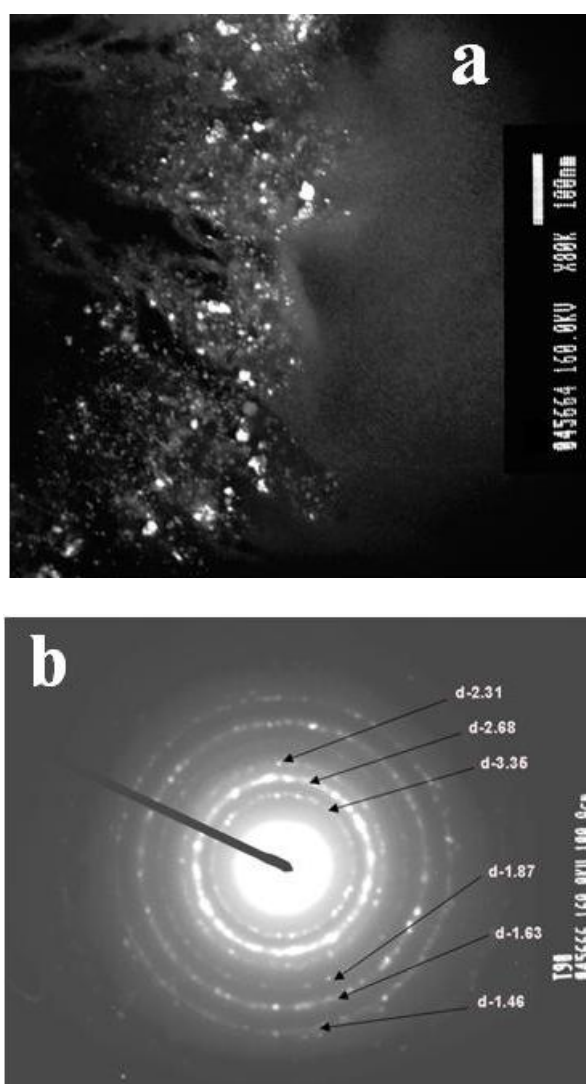
Fig. 5.14 a) TEM image of TNT nanoparticles embedded in silica xerogel matrix b) SAED pattern of TNT nanoparticles (numbers indicate d spacing in A^0)

Fig. 5.14(a) shows transmission electron micrographs for TNT/silica xerogel with 90 % TNT content and the corresponding selected area electron diffraction (SAED) pattern is shown in Fig. 5.14 (b). TEM image of the xerogel sample indicate that TNT particles are dispersed in the xerogel matrix. Presence of TNT particle is confirmed by electron diffraction recorded over selected area. The concentric rings with strong diffraction spots from electron diffraction pattern (Fig. 5.14 b) indicate polycrystalline nature of TNT. The radius of the concentric rings is converted to d- spacing [18]:

$$Dd = \lambda L \qquad \qquad \dots 5.1$$

where, λ – electron wavelength (0.03 A°); L - distance from target to screen (1000 mm); and D – radius of diffraction pattern ring

The d-spacing values derived from the diffraction pattern matches with the reported values for monoclinic TNT [19].

From the TEM micrograph, particle size distribution has been evaluated and the characteristic size histogram is displayed in Fig. 5.15.
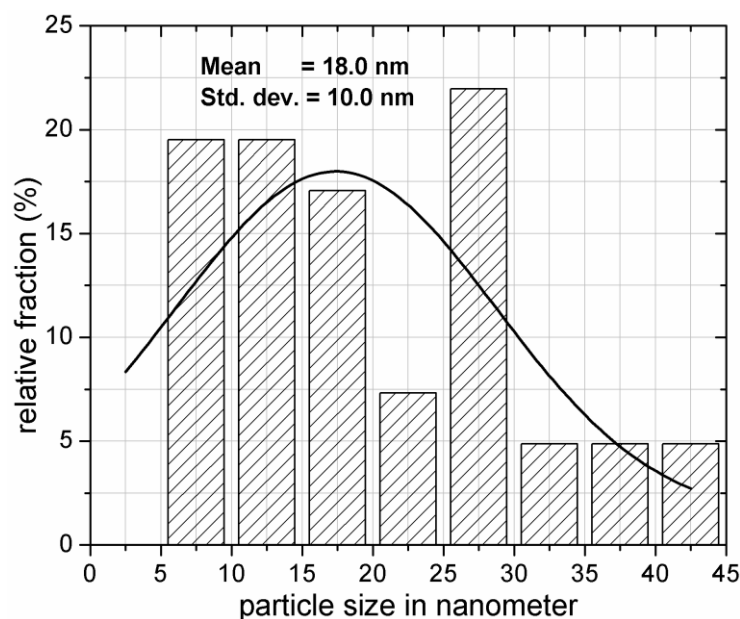
Fig. 5.15 Histogram showing size distribution of TNT in silica xerogel matrix

As shown in Fig. 5.15, particle size of TNT in the xerogels is found in the range of 10 nm to 50 nm, and the majority of particles with size around 20 to 30 nm. Average diameter of TNT particles is 18 nm (standard deviation 10 nm). The average crystallite size derived from XRD data is comparable with this value.

Fig. 5.16 shows the high resolution TEM micrograph and the selected area electron diffraction (SAED) pattern for RDX processed by sol-gel method.
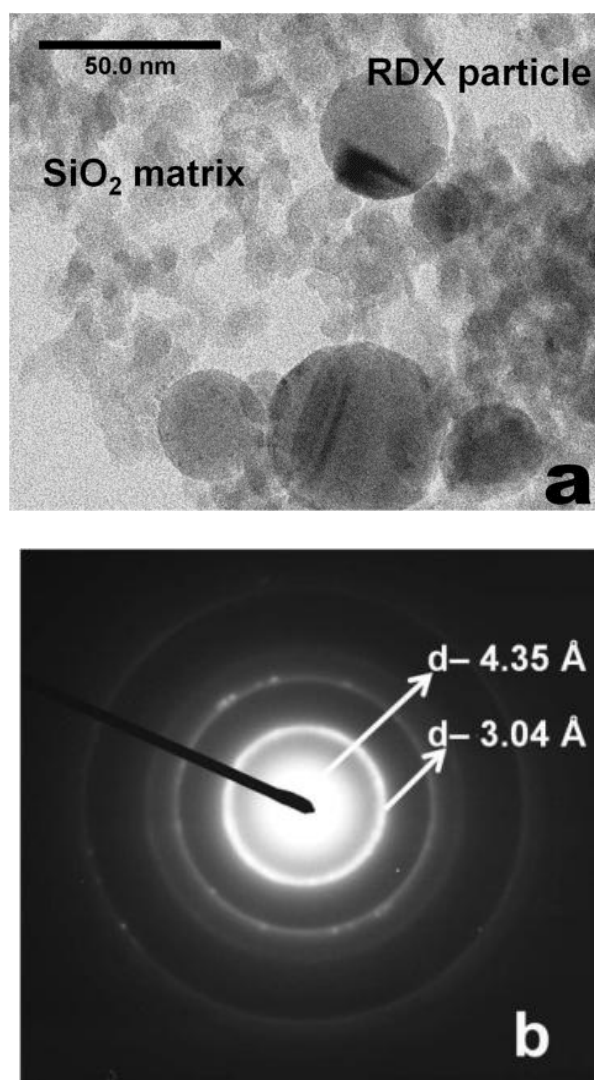
Fig.5.16 (a) HRTEM image, (b) SAED of RDX processed by sol-gel method

The High Resolution TEM (HRTEM) image of RDX/SiO$_2$ xerogel (Fig. 5.16 a) suggests that RDX nano particles of size ranging from 20-50 nm are

dispersed in silica matrix. The strong diffraction spots on the concentric rings (Fig. 5.16 b) indicate crystalline nature of RDX. In the SAED, the radii of the concentric rings are attributed to inter planer spacing of RDX [15].

The TEM image of PETN-SiO$_2$ xerogels and particle size distribution of PETN in gel matrix is shown in Fig. 5.17. TEM pictures of PETN-SiO$_2$ xerogel (Fig. 5.17 a) shows that PETN particles are dispersed in the xerogel matrix, and the typical particle size of PETN particles is estimated to be around 10-50 nm.
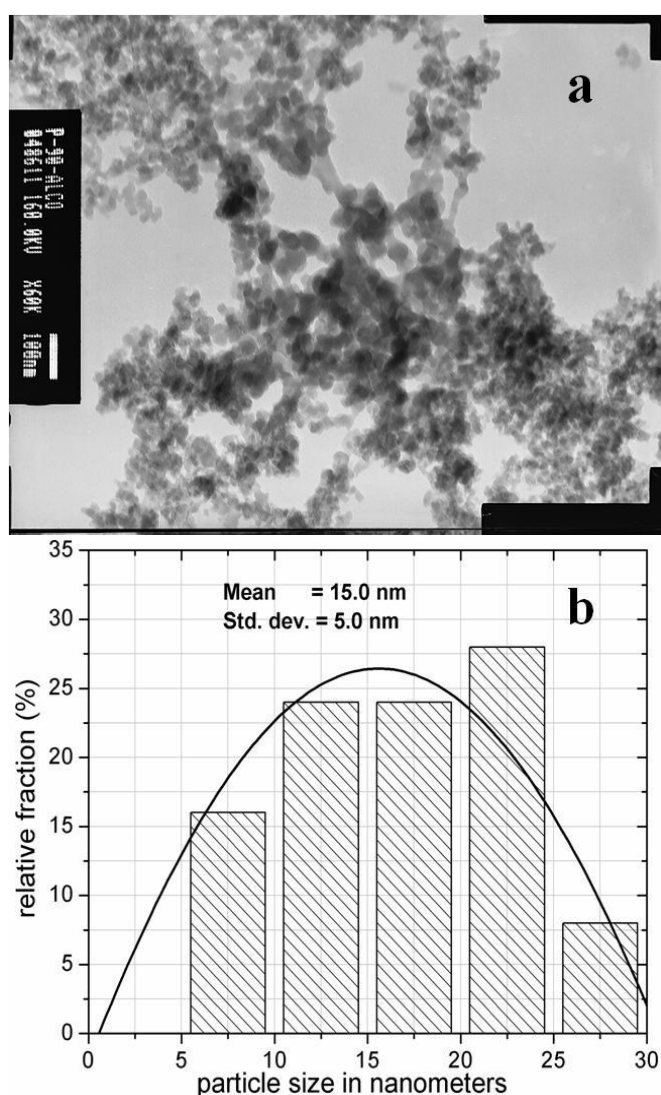
Fig.5.17 (a) TEM image and (b) particle size distribution of PETN-SiO$_2$ xerogel

5.2.4 Small Angle X-ray Scattering (SAXS)

Considering the fact that pores in silica network gets occupied by energetic materials in sol-gel processing, SAXS is promising technique to study the microstructure of these composites. The study of pore particle interface at boundary of gel pores is useful to understand the response of energetic materials to initiation by heat or impact energy. Therefore, to understand the effect of processing parameters on the microstructure of these sol-gel processed energetic materials more clearly, these samples have been further characterized by SAXS.
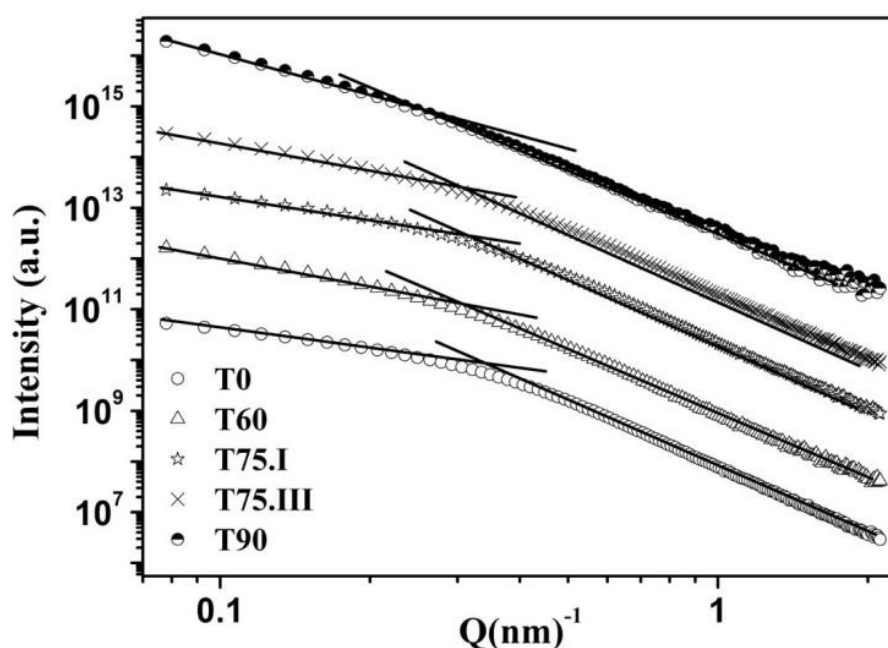
Fig. 5.18 Small angle X-ray scattering of silica xerogel with TNT (T). Symbols are observed data and lines are fits of the data.

The SAXS profiles obtained for SiO_2 xerogels and TNT-SiO_2 xerogels are showed in Fig 5.18. T0 is the sample of silica xeogel without any TNT content. T60, T75 and T90 indicate TNT-SiO_2 xerogels samples containing 60, 75 and 90 wt % TNT by weight. T75.I and T75.III represent TNT-SiO_2 xerogel samples containing 75 wt% TNT and processed with Acetone/TMOS ratio as 50 and 20, respectively

Here Q is the scattering vector equal to $4\pi \sin(\theta)/\lambda$, λ is the wavelength of incident (CuK$_\alpha$) X-rays. Scattered intensity I (Q) is recorded using a scintillation counter by varying the scattering angle 2θ. The SAXS profiles for pure SiO$_2$ and composites of SiO$_2$ and energetic materials processed by sol-gel method have been analyzed based on the data available in literature for the other porous composite samples consisting of pores in the gel solid matrix [20-22]. In the silica xerogel, the scattering at low-Q (Q < Q$_1$) region occurs from larger, sub-micron size particles and the inter-particle voids. Whereas in the region Q2 < Q < Q1, the scattered intensity arises due to surfaces of the smaller particles or pores within the aggregates. The scattering profiles plotted on log-log scale are straight lines over wider Q-range with change of slope at low-Q regions as marked in the Fig 5.18. The linear behavior of the profiles indicates that the SAXS profiles follow a power-law: I (Q) ~ Q$^{-\alpha}$. The value of α would be 4.0 for smooth surface of the scattering object. Whereas a non-integer value for α indicates the fractal structure. For mass fractals with dimension D$_m$, α = D$_m \leq 3$ whereas for surface fractals with dimension D$_s$, α = (6-D$_s$) > 3.0 and $2 \leq D_s \leq 3$. Thus, the slope of the scattering curve on log-log scale indicates the type of the fractal. The SAXS profiles of TNT/SiO$_2$ xerogels are fitted to the function

$$I(Q) = I(0)/[1+(\xi Q)^2]^{-\alpha/2} \qquad\qquad \dots 5.2$$

Where ξ is the correlation length [23]. For nearly spherical scattering object, ξ represents average radius (R).

SAXS profile of SiO$_2$ without any energetic materials follows a linear behavior with a change of slope at a Q. Below this crossover point, I(Q) varies as Q$^{-\alpha}$ with a value of 1.1 for α. This suggests that the silica particles are in the form of mass fractal aggregates with fractal dimension 1.1. From the crossover point, the average

size (D) of the basic particles within the aggregates is found to be about 18.5 nm. In the high-Q region, the slope of the linear profile is steeper than 4.0 suggesting a fuzzy or diffuse boundary [24] between particles and pores. For silica xerogels with TNT, the SAXS profiles are in the same shape as for pure sample but the mass fractal dimension has increased with highest value of 2.26 for 90 % TNT (T90). Thus, the matrix became compact with the presence of TNT. The size of the basic particles increased marginally to about 20 nm for T60 and T75-I samples. It is increased to 22.5 nm for T75-III sample and further rise to 30.4 nm for 90 wt % TNT sample. The typical size of the particles is concurrent in order of magnitude with TEM analysis.

The profiles obtained for SAXS measurements on silica xerogels and PETN-SiO$_2$ xerogels containing 70 and 90 weight % PETN are presented in Fig. 5.19. SAXS profiles follow a power-law I (Q) ~ Q$^{-\alpha}$ with α = 3.98, 4.0 and 4.1 for SiO$_2$ xerogel, PETN-SiO$_2$ (70:30) xerogel and PETN-SiO$_2$ (90:10) xerogel, respectively.
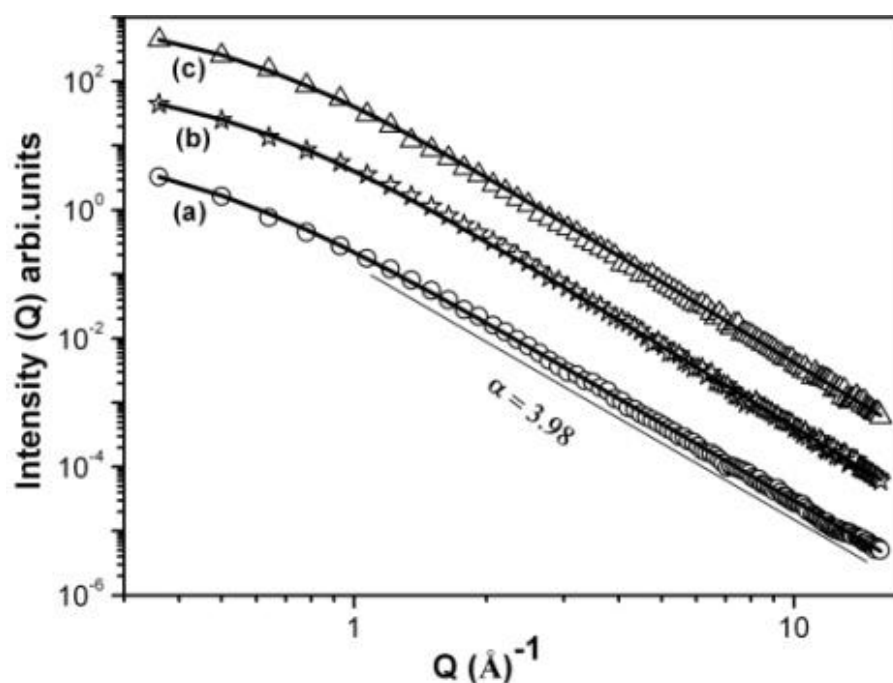
Fig. 5.19 SAXS profiles for a) silica xerogel (b) PETN-SiO$_2$ xerogel with 70% PETN and (c) PETN-SiO$_2$ xerogel with 90% PETN content.

The average pore size reduced considerably to a minimum of 19.9 nm in PETN-SiO$_2$ xerogel with 90 % PETN content from the value of 24.7 nm obtained for pure silica xerogel. This suggests that the PETN particles have entered into the pores, thus reducing the average pore size of the original matrix. The surface morphology of the pores is marginally affected. The value 4.1 of the exponent for the xerogel sample with PETN content indicates a slightly diffuse interface between the pores and the matrix [25]. This suggests that, at least some parts of PETN remains at the interface between the pore and the matrix causing a change in the surface morphology.

Fig. 5.20 shows slit-corrected SAXS profiles for RDX/SiO$_2$ xerogels. Intensities are shown in arbitrary units and are shifted vertically for clarity.
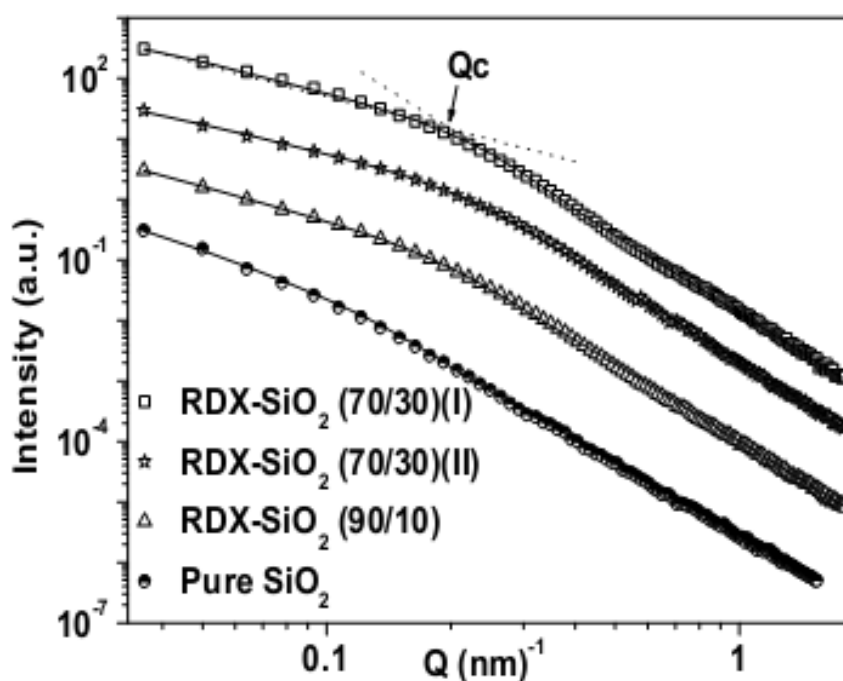
Fig. 5.20 Small Angle X-ray scattering of RDX-SiO$_2$ composite xerogels. Symbols are experimental points and lines are fits to the data.

In Fig. 5.20, the samples containing 70 wt % and 90 wt % of RDX and Acetone/TMOS ratio as 100 have been designated as RDX/SiO$_2$ (70/30) and RDX/SiO$_2$ (90/10), respectively. The samples containing 70 wt % of RDX have been

designated as RDX/SiO$_2$ (70/30)I and RDX/SiO$_2$ (70/30)II with Acetone/TMOS ratio as 100 and 50, respectively. In Fig. 5.20, slope (x) of the line profiles changes at Qc, with a value < 3.0 for Q < Qc and ≥ 4 beyond Qc. The samples consist of mass fractal aggregates of radius of gyration Rg made of primary particles (unit blocks of fractal aggregates) of radius Rs. SAXS data has been fitted to the expression (Equation 5.3) based on the unified theory for scattering from systems with multiple levels of structural features [26].

$$I(Q) = G_1.\exp(-Q^2.R_g^2/3) + B_1.\exp(-Q^2.R_s^2/3).\{[erf(Q.R_g/6^{1/2})]^3/Q\}^{P1} +$$

$$G_2.\exp(-Q^2.R_s^2/3) + B_2.\{[erf(Q.R_s/6^{1/2})]^3/Q\}^{P2} \qquad \qquad \dots 5.3$$

Here, the constant coefficients include scattering density contrast between mass consisting silica, RDX and pores. For spherical entities, the radius of gyration is equal to √3/5 x r where r is the radius of the sphere. The parameters obtained from fitting of SAXS data are listed in Table 5.1 in which R$_P$ is the average radii of pores.

Table 5.1 Parameters obtained from fitting of SAXS data of RDX-SiO$_2$ xerogel

	Radius (nm)	Power-law exponent	
Sample	R$_P$	P$_1$	P$_2$
R0	18.0	2.30	3.98
R70(I)	14.3	1.95	4.25
R70(II)	12.4	1.80	4.30
R90	12.1	1.73	4.30

Table 5.1 list parameters obtained from fitting of SAXS data of RDX-SiO$_2$ composites. The exponent P$_1$ (Eq. 5.3), which is equal to mass fractal dimension Dm, varies between 2.3 and 1.7 whereas P$_2$ is 4.0 for pure silica indicating smooth surface

for the particles. With presence of RDX, P_2 becomes greater than 4.0, suggesting diffuse inter-face between particles and the pores [27].

Thus, the porous structure of pure silica xerogel and silica xerogels incorporated with energetic materials has been analyzed by means of SAXS. The average pore size in the SiO_2 xerogel reduces after incorporating energetic materials suggesting that energetic materials particles have entered the pores of gel matrix. From the values of the exponent α which is 4 for pure silica xerogel, it is inferred that the surface of the pores was nearly smooth in the pure xerogel. However, the value of exponent α measured for xerogels incorporated with energetic materials deviates from the value of 4 suggesting that the surface becomes rough with surface fractal structure. This indicates that with increasing loading amount of energetic material in the xerogel, all this material did not confined in the pores but at least some parts of it remain at the interface between the pore and the matrix causing a change in the surface morphology resulting in the rough pore/surface interaction.

5.2.5   Surface area measurements:

The results observed from SAXS measurement about the occupancy of energetic materials in pores have been further supported by surface area measurements. Specific surface area of energetic materials processed by sol-gel technique has been measured by nitrogen physisorption method [28]. The specific surface area has been calculated using the Brunauer-Emmett-Teller (BET) method from the amount of N_2 gas adsorbed at 77 K at various partial pressures (eleven points; $0.05 < p/p_0 < 0.3$). The pore volume measurements have been carried out at a partial pressure of $P/P_0 = 0.99$ and the pore size distributions (PSD) has been determined by Horvath- Kawazoe (H-K) method [29].

For TNT materials processed by sol-gel method, prior to surface area measurements, the samples were first degassed at 40 ^{o}C under vacuum for 6 hours. The results of surface area and pore volume measurements for silica xerogel and typical TNT-SiO$_2$ composites are shown in Table 5.2.

Table 5.2: Textural properties of SiO$_2$ xerogel and TNT-SiO$_2$ composites

Sample	Weight %		Molar ratio TMOS: Acetone: HF(0.1M):TNT	Pore volume (cm^3/g)	Specific surface area (m^2/g)
	TNT	SiO$_2$			
T90	90	10	1:50:16:2.4	0.053	74
T75 I	75	25	1:50:16:0.8	0.136	189
T75 III	75	25	1:20:16:0.8	0.011	18
SiO$_2$	0	100	1:50:16:0.0	0.87	483

As shown in Table 5.2, pore volume and surface area values measured for TNT-SiO$_2$ composite are lower than that of SiO$_2$ xerogel. The decrease in pore volume of TNT-SiO$_2$ composites indicates that pores of the gel have been occupied by TNT. For samples T75-I and T90 which were prepared with Acetone/TMOS ratio as 50, the surface area has been found to be decreased from 189 to 74 m^2/g and the pore volume has been found to be decreased from 0.136 to 0.053 cm^3/g, respectively. This is due to more occupancy of TNT particles in the pores at higher TNT content. In the T75-I sample, some of the pores may also be non-occupied which might have resulted in high pore volume and surface area. For T75-I and T75-III samples, the surface area has been found to be drastically decreased from 189 to 18 m^2/g. The Acetone/TMOS

ratios for T75-I and T75-III samples are 50 and 20, respectively. The decrease in solvent/precursor ratio has resulted in much compact network leading to decrease in porosity. The pore volume has been found to be decreased from 0.136 to 0.011 cm^3/g for T75-I and T75-III samples, respectively. The results show that porosity in TNT-SiO_2 composites can be suitably controlled by controlling the process parameters like TNT content or solvent/precursor ratio.

The specific surface area (SA), pore volume and pore diameter of RDX/SiO_2 samples obtained by N_2 adsorption technique are listed in Table 5.3.

Table 5.3. Textural properties of SiO_2 xerogel and RDX-SiO_2 composites

Sample	BET specific surface area in m^2/g	Pore volume in cm^3/g (at $P/P_0 = 0.99$)	Pore diameter in nm
R0	339	1.40	21
R70 (I)	179	0.94	14
R70 (II)	132	0.30	10
R90	108	1.07	13

As noted earlier, samples containing 70 wt % and 90 wt % of RDX and Acetone/TMOS ratio as 100 have been designated as RDX/SiO_2 (70/30) and RDX/SiO_2 (90/10), respectively. The samples containing 70 wt % of RDX have been designated as RDX/SiO_2 (70/30)I and RDX/SiO_2 (70/30) II with Acetone/TMOS ratio as 100 and 50, respectively. From the data in Table 5.3, it is found that the surface area of RDX-SiO_2 xerogel is much higher compared to that of raw RDX (~ 2 m^2/g). Moreover, it decreases systematically with increase in RDX content.
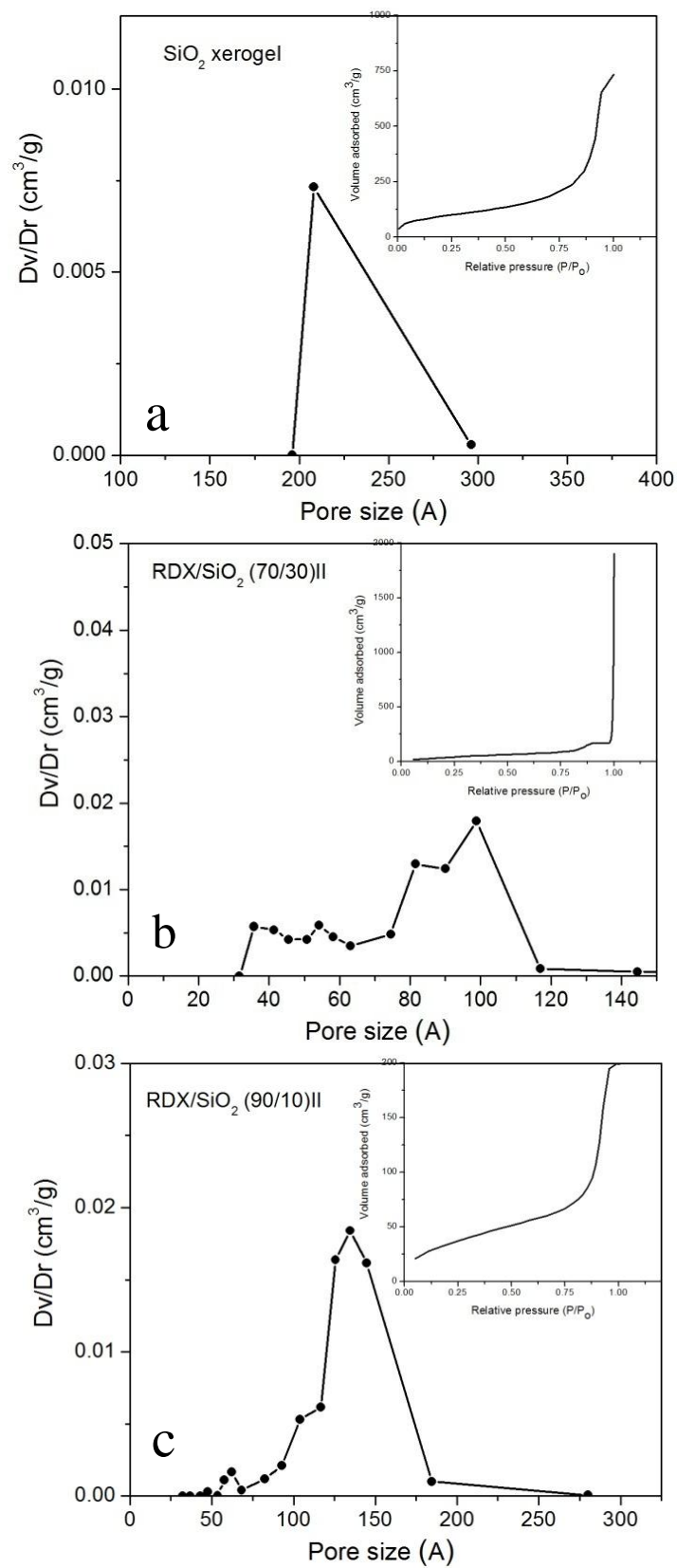
Fig. 5.21 PSD: a) SiO₂, b) RDX/SiO₂ (90/10), c) RDX/SiO₂ (70/30)II xerogels

The pore size distribution profile for SiO_2, RDX/SiO_2 (90/10) and RDX/SiO_2 (70/30) II xerogels is shown in Fig. 5.21. It can be noticed from Fig. 5.21 that pore size for RDX/SiO_2 xerogels (100 A^o) is smaller than that of SiO_2 xerogel (210 A^o). The average pore radius measured from pore size distribution is noted in Table 5.3. It can also be seen from Table 5.3 that the pore volumes and pore sizes are significantly reduced after incorporating RDX. Pore volume for SiO_2 xerogel is 1.4 cm^3/g which is reduced to 0.3 cm^3/g after incorporating RDX in xerogels. This may be attributed to occupation smaller particles of RDX in pores of silica matrix. The lower pore volume for R70 (II) as compared to that in R70 (I) is due to reduced Acetone: TMOS ratio.

Similarly, specific surface area of $PETN-SiO_2$ xerogel is found to be 75 m^2/g, whereas the same for pure silica xerogel is 512 m^2/g. The reduced surface area for $PETN-SiO_2$ xerogel is due to occupation of silica gel pores by PETN.

The observed trend in surface area and pore volume measurements for $TNT-SiO_2$, $RDX-SiO_2$ and $PETN-SiO_2$ xerogels is in consistence with the results observed from SAXS studies.

5.2.6 Impact sensitivity:

Initiation of energetic materials is believed to result from localization of incident energy generating hot spots within these materials. Therefore, porous gel matrix is an ideal host to study in a controlled fashion how defect can affect the ignition mechanism in such materials by providing the voids as initiation centers. Impact initiation of the sol-gel processed energetic materials has been carried out to study the effect of porosity on sensitivity of these materials. Impact sensitivity studies has been carried out by Fall Hammer Impact Test. Powder sample of about 30 - 40 mg was placed on anvil and the height of drop weight was varied to arrive at a height

where 50 % probability of initiation is found. The data for sensitivity to impact of nano-sized TNT processed by sol-gel method is shown in Fig. 5.22.
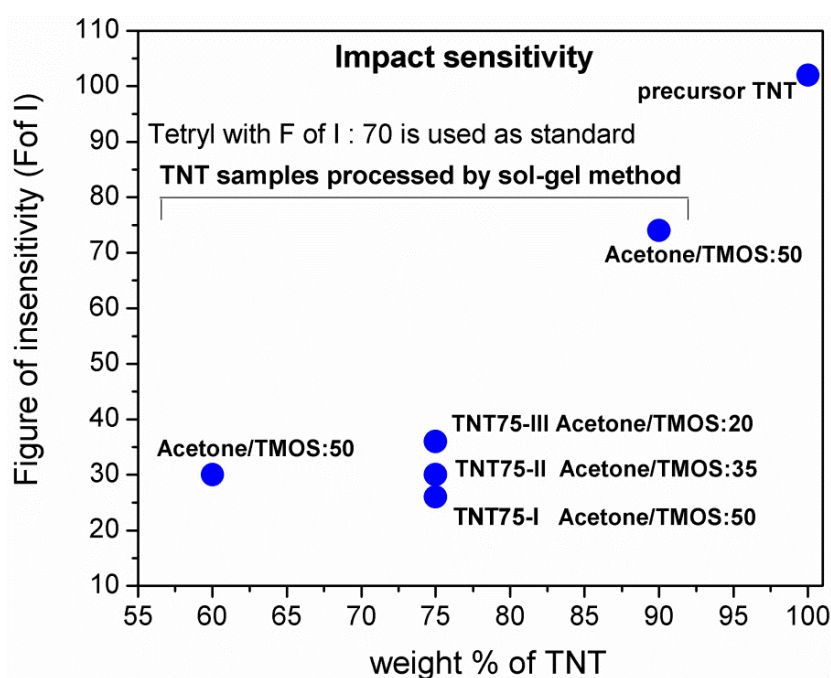
Fig. 5.22 Impact sensitivity data for raw TNT and TNT-SiO$_2$ composites

As seen in Fig. 5.22, the figure of insensitivity for TNT materials processed by sol-gel technique is lower than that of raw TNT. Unlike TNT materials with reduced particle size obtained by solution crystallization and spray drying method, here, the sensitivity to impact of the TNT-SiO$_2$ composite material increases even though the particle size is less than 100 nanometers. This indicates that porosity affect the ignition mechanism of the energetic materials. The sensitivity to impact for TNT-SiO$_2$ composites has also been found to be increased with a decrease in TNT content in the composite from 90 to 75 wt. %. In samples with lesser TNT content, the number of non-occupied pores will be more which has also been observed from fractal dimensions in SAXS studies. It results in higher defect density like pores/voids. It may lead to adiabatic compression of interstitial gases and act as centers for initiation

112

of chemical decomposition resulting in an increase in sensitivity of these materials. When the TNT content in gel was kept constant at 75 wt. % and the Acetone/TMOS ratio was decreased from 50 to 20, the sensitivity of the TNT decreased. This is due to decrease in porosity as revealed from pore volume measurements.

Fig. 5.23 shows data on impact sensitivity measurements for nanosized RDX. Tetryl with figure of insensitivity (F of I) 70 is considered as standard for sensitivity test. A decrease in FoI indicates an increase in sensitivity of the material.
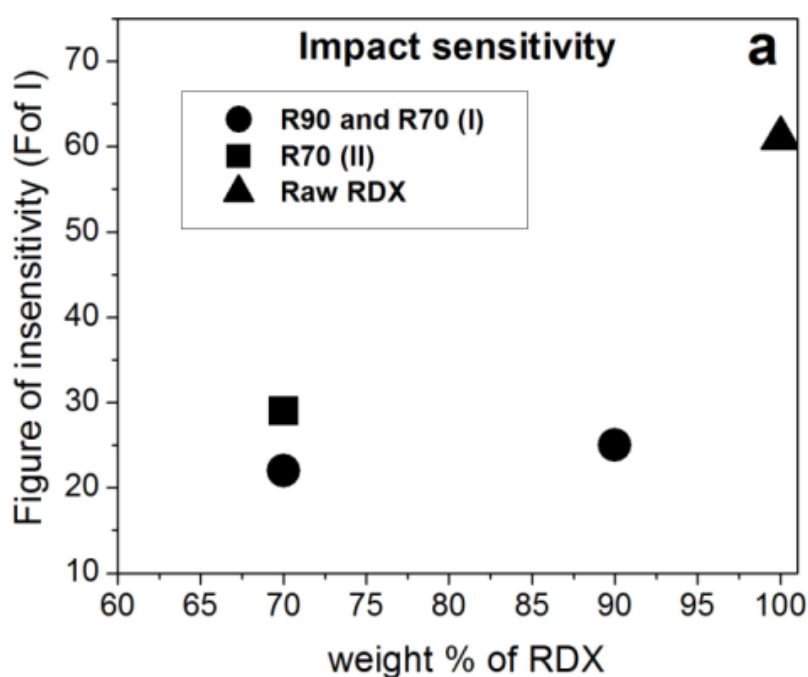
Fig. 5.23 Impact sensitivity data for RDX/SiO$_2$ xerogels and raw RDX.

As seen in Fig. 5.23, RDX materials processed with sol-gel method require less impact energy for initiation than that of raw material implying that these samples are more sensitive. The porosity in these samples leads to hot spots raising local temperature to ignition and plays vital role in impact initiation [30]. The sensitivity of the R70 (II) is significantly lower than that of R70 (I), which may be due to the less porosity in the R70 (II). For friction sensitivity measurements also, a similar trend of

increase in sensitivity for RDX/SiO$_2$ xerogels as compared to that of raw RDX has been observed.

Results on impact sensitivity of TNT, RDX and PETN xerogels materials in powder and pelletized samples are compiled in Table 5.4.

Table 5.4 Impact sensitivity data for powder and pellet sample of TNT, RDX and PETN xerogels materials

sample	Impact energy (J) with 50 % probability of initiation
Raw RDX	6.14
RDX/ SiO$_2$ (90/10)	5.87
TNT	Not initiated
TNT/ SiO$_2$ (90/10)	7.01
TNT/ SiO$_2$ (75/25)	3.45
TNT/SiO$_2$ (60/40)	4.46
PETN	3.79
PETN/SiO$_2$ (90/10)	3.66
PETN/SiO$_2$ (75/25)	4.99

Impact sensitivity in all xerogels increased as compared to raw materials indicating ignition mechanism in energetic materials is controlled by defect density. It is an important observation that the sensitivity to initiation by impact can be tuned as per requirement by controlling in the sol-gel processed energetic materials.

5.2.7 TG-DSC

DTA and TGA measurements on the xerogels within the temperature range from room temperature to 400°C were carried out in an inert gas atmosphere to prevent combustion of these materials with air.

Fig. 5.24 shows TGA and DTA curves for silica xerogel and TNT/silica xerogel with 90% TNT content.
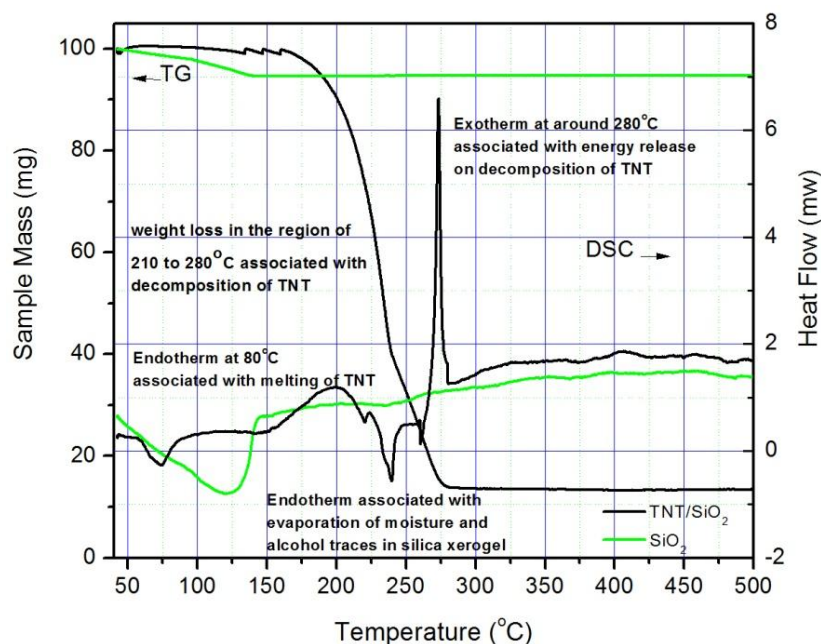
Fig. 5.24 TGDSC curves for SiO$_2$ xerogel (——) & TNT/SiO$_2$ (90/10) xerogel (——)

In Fig. 5.24, TGA curve for TNT/ SiO$_2$ xerogel shows sudden weight loss of more than 85 % within a temperature range from 210 ^{o}C to 280 ^{o}C. This weight loss is attributed to decomposition of TNT resulting in gaseous products. TNT decomposes above 200 ^{o}C forming gaseous compounds like CO, CO$_2$, H$_2$, N$_2$ etc. with a little residue left over as shown in TGA curve. The remaining weight is attributed to silica. These results are in good agreement with precursor composition. The weight loss of around 5 to 6% noticed at around 100 ^{o}C in TG curve silica xerogel sample is due to loss of adsorbed moisture and residual acetone in the sample.

In Fig. 5.24, an endothermic peak in DSC curve of TNT/SiO$_2$ xerogel may be noticed at around 80 ^{o}C which could be attributed to melting of TNT. An exothermic peak is observed at around 280 ^{o}C preceded by an endotherm in the DTA curve. This exothermic peak indicates the decomposition in TNT. These observations are in good

agreement with reported data for TNT [31] and indicate the presence of TNT in xerogel. An endotherm observed at around 100 °C in the DTA curve for pure silica xerogels is attributed to evaporation of moisture and solvent traces.

Fig. 5.25 shows typical TG-DSC curves for a) R70 (I) and b) R90.
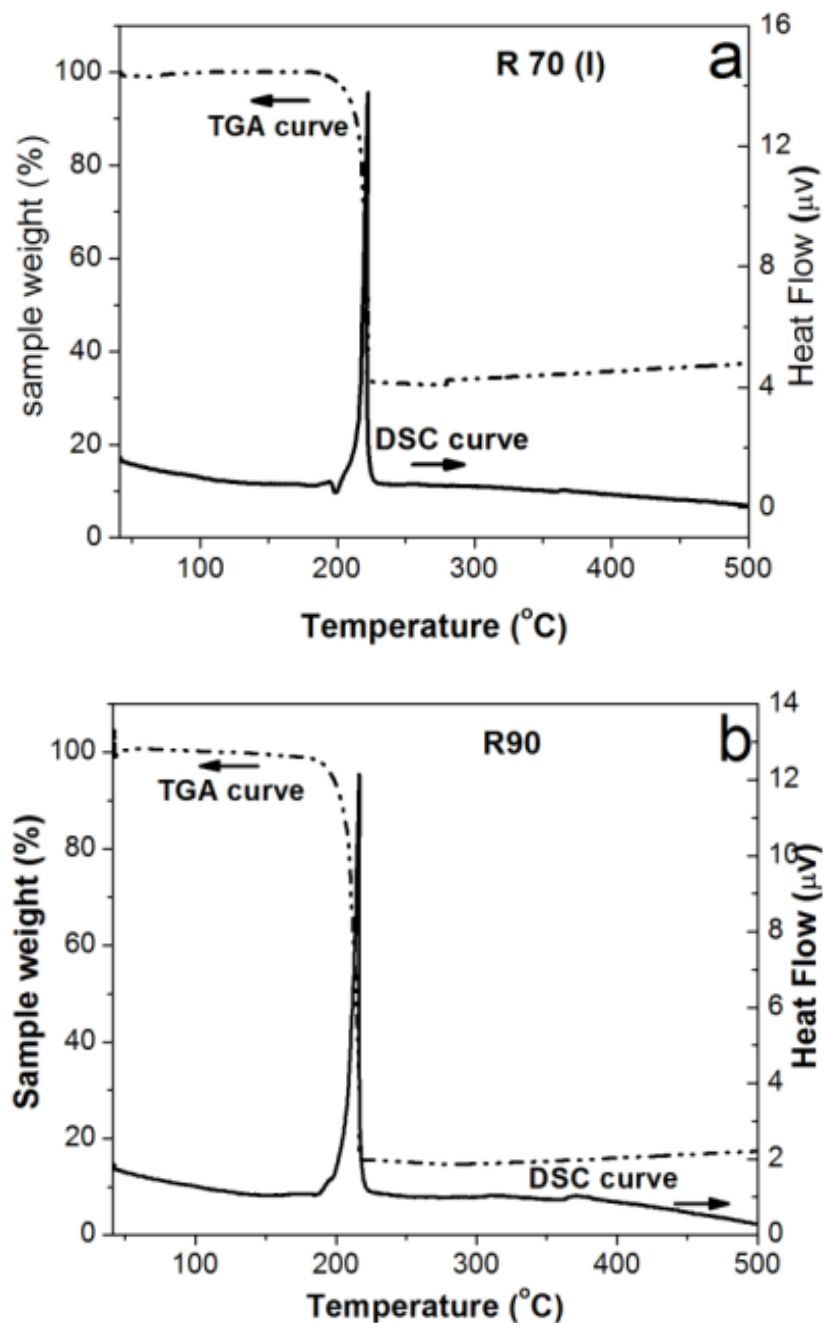
Fig. 5.25   **TG (–·–·–) and DSC (——) curves for a) R70 (I) and b) R90.**

In Fig. 5.25, the weight loss indicated in TG curve of both the samples is due to decomposition of RDX and is in concurrence with the initial weight content of RDX in the composites. The DSC curves of RDX/SiO$_2$ xerogels in both samples show an exothermic peak at around 210 ˚C due to decomposition of RDX. An endothermic peak at 205 ^{o}C is associated with RDX melting [32].

Fig. 5.26 shows results of TGA and DSC analysis for SiO$_2$ xerogel and PETN-SiO$_2$ xerogel with 90% PETN content.
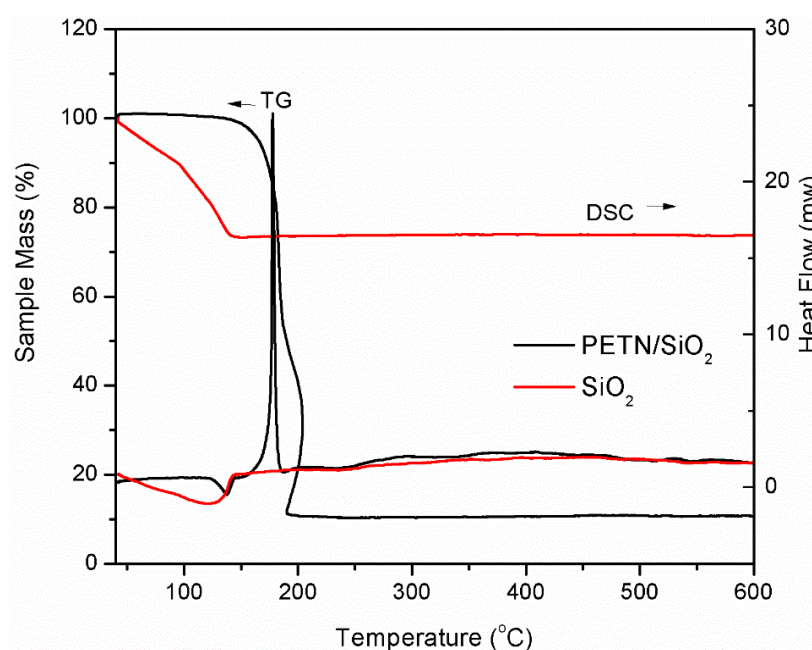
Fig. 5.26 TGA and DSC curve for SiO$_2$ xerogel (---) and PETN-SiO$_2$ xerogel (---) with 90% PETN content

In TG curves of Fig. 5.26, a major weight loss of around 85 % in PETN-SiO$_2$ xerogel is seen within a temperature range from 150 to 200 ^{o}C. This weight loss is attributed to the decomposition of PETN. The confirmation of PETN content in the xerogels could be verified from the TG curve as the mass loss has occurred mainly due to decomposition of PETN. The weight loss in silica xerogel at around 100 ^{o}C is attributed to loss of moisture adsorbed on the silica due to surface –OH groups [33].

In case of PETN-SiO$_2$ xerogel the silica content is much less and PETN has the hydrophobic nature, and therefore in PETN-Silica xerogel loss due to water is much less as compared to pure silica.

In DSC curve of Fig. 5.26, a sharp endothermic peak at temperature around 140 ^{o}C and a broad exothermic peak at temperature around 185 ^{o}C is noticed in the DTA curve recorded for the PETN- SiO$_2$ xerogel. It agrees well to the characteristic peaks reported for pure PETN [34]. An endothermic peak at around 140 ^{o}C is attributed to the melting of PETN whereas the exothermic peak next to the endotherm noticed at around 185 ^{o}C is attributed to the decomposition of PETN and formation of gaseous products. The results from TG-DSC analysis confirmed survival of PETN through sol-gel processing and its presence in the resulted xerogel matrix.

5.2.7.1 Thermal Initiation and Kinetic Parameters Study Using Thermal Analysis Data

Thermal ignition mechanism in energetic materials on inclusion of voids can be appreciated with study of kinetic parameters. Therefore, decomposition of energetic materials is studied as a function of temperature for RDX and TNT materials processed by sol-gel method at different heating rates. Fig. 5.27 shows the TGDSC curves for raw RDX and RDX processed by sol-gel method from room temperature to 300 ^{o}C at heating rate of 5 ^{o}C/min (a), 10 ^{o}C/min (b) and 20 ^{o}C/min (c).
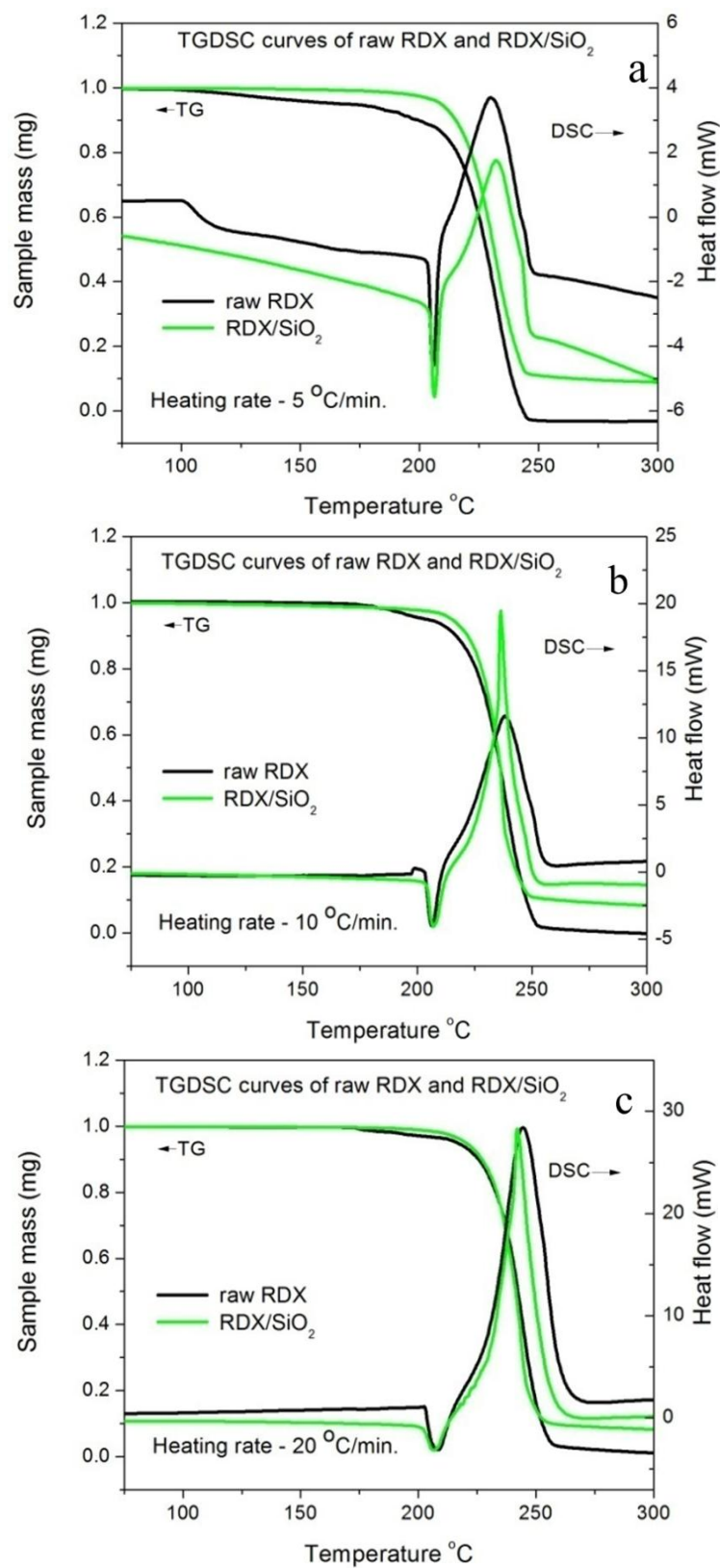
**Fig. 5.27   TGDSC curves for raw RDX and RDX processed by sol-gel method
with heating rate of a) 5 ^{0}C/min. b) 10 ^{0}C/min. and c) 20 ^{0}C/min.**

It can be noticed in the TG curves (Fig. 5.27) that raw RDX shows mass loss of 99 % accompanied with an exothermic peak. This is attributed to thermal decomposition of RDX. However, RDX/SiO$_2$ composite shows a mass loss of 88 % indicating that major content is RDX with remaining residue as silica and agreeing well to our precursor composition.

In DSC curves (Fig. 5.27), the endothermic peak at about 205 ^{o}C is associated with melting of RDX. As it can be seen in Fig. 5.27, at higher heating rate, exothermic peak is shifted towards higher temperature in both the samples. In RDX/SiO$_2$ xerogel, width of exothermic peak becomes narrower at higher heating rate. It may be because at higher heating rate, the heat deposition in samples is faster than it can dissipate, and it may cause overlapping of thermo kinetic events like visco-plastic flow at particle - pore interface and adiabatic air compression resulting in high heat of reaction. The exothermic peak temperature for RDX and RDX/SiO$_2$ xerogel noted from DSC curve is shown in Table 5.5.

Table 5.5 Exothermic peak temperature (T_p) and Onset Temperature (T_o) for RDX materials (value in brackets indicates particle size) at different heating rate.

Heating rate β [°C/min.]	Exothermic peak temperature (T_p) and Onset Temperature (T_o) for RDX and RDX /SiO$_2$ [^{o}C]			
	RDX (126 µm)		RDX /SiO$_2$ (0.055 µm)	
	T_p	T_o	T_p	T_o
5	233	212	231.1	220
10	242.5	215	240.2	225
20	251.1	220	246.5	233

Though the exothermic peak temperature shifted to lower value, it can be noticed from Fig. 5.28 that the onset (T_o) of exothermic peak is found to be shifted at relatively higher temperature in RDX /SiO_2 materials as compared to raw RDX. The higher values of onset temperature in sol-gel processed materials may be related to higher activation energy. The value of activation energy (E_a) is evaluated from exothermic peak temperature obtained with various heating rates as shown in Table 5.5 and applying Kissinger's method [35].

Temperature dependent rate constant k is assumed to obey Arrhenius equation:

$$k (T) = Z \exp (-E_a/RT) \qquad\qquad … 5.4$$

$$\ln (\beta /T_p^2) = \ln(ZR/E_a) – (E_a/RT_p) \qquad\qquad …5.5$$

Where β is the heating rate in K/min and T_p is the maximum temperature of DSC curve for that heating rate in K, E_a is activation energy in J, Z is Pre exponential factor (s^{-1}) and R is gas constant in J/K.mol

The values of E_a obtained from the slope of the straight line of plot ln (β/T_p^2) against $1/T_p$ are listed in Table 5.6.

Table 5.6 Kinetics parameters for RDX (derived from TG-DSC curves)

Samples	Particle size	Kinetics		
		E_a (kJ mol^{-1})	Z (s^{-1})	k x 10^{-2} (s^{-1})
Raw RDX	126 $\pm$ 45 μm	149 $\pm$ 3 kJ	4.7 x 10^{15}	69 $\pm$ 1
Sol-gel processed RDX	55 $\pm$ 25 nm	215 $\pm$ 9 kJ	8.0 x 10^{21}	98 $\pm$ 2.1

In RDX-SiO_2 composite, RDX is surrounded by silica because of which higher temperature is required to heat and ignite RDX in these materials. It is supported by significantly higher value of activation energy of 215 $\pm$ 9 kJ in this material than that

of raw material of 149 ± 3 kJ as shown in Table 5.6. RDX material processed by sol-gel method is reported to be more sensitive to impact initiation than raw RDX due to increased density of defect like high porosity. However, this phenomenon is mainly seen in shock or impact sensitivity of these materials. In thermally stimulated decomposition under present studies, porosity is not seen to increase the sensitivity of the material. As seen from Table 5.6, the frequency of collisions (Z) and reaction rate constant (k) values for RDX/SiO$_2$ are higher than that of raw material. It may be attributed to high surface area which contributes to faster decomposition due to high proportion of surface atoms. Moreover, in RDX/SiO$_2$ materials, due to high onset temperature, decomposition reaction favors more NO$_2$ and CO$_2$ contributing to more energy release accelerating the reaction rate [36]. Increase in Z and k values suggests a possible improvement in detonation velocity of RDX with reduced particle size.

Fig. 5.28 shows typical TG-DSC curves observed with heating rate of 20, 15 and 10 ^{o}C/min for TNT processed by sol gel method. In Fig. 5.28, the sudden weight loss in TG curves at around 225 to 275 ^{o}C is due to decomposition of TNT. In sol-gel processed material, the weight loss is 90 % with 10% residue for silica. It indicates that TNT content in this material matches well with precursor composition. In DSC curves of the two samples, an endothermic peak at 80 ^{o}C is associated with melting of TNT. The decomposition peak is observed to be shifted to lower temperature for TNT/SiO$_2$ xerogels indicating decomposition at higher reaction rate.
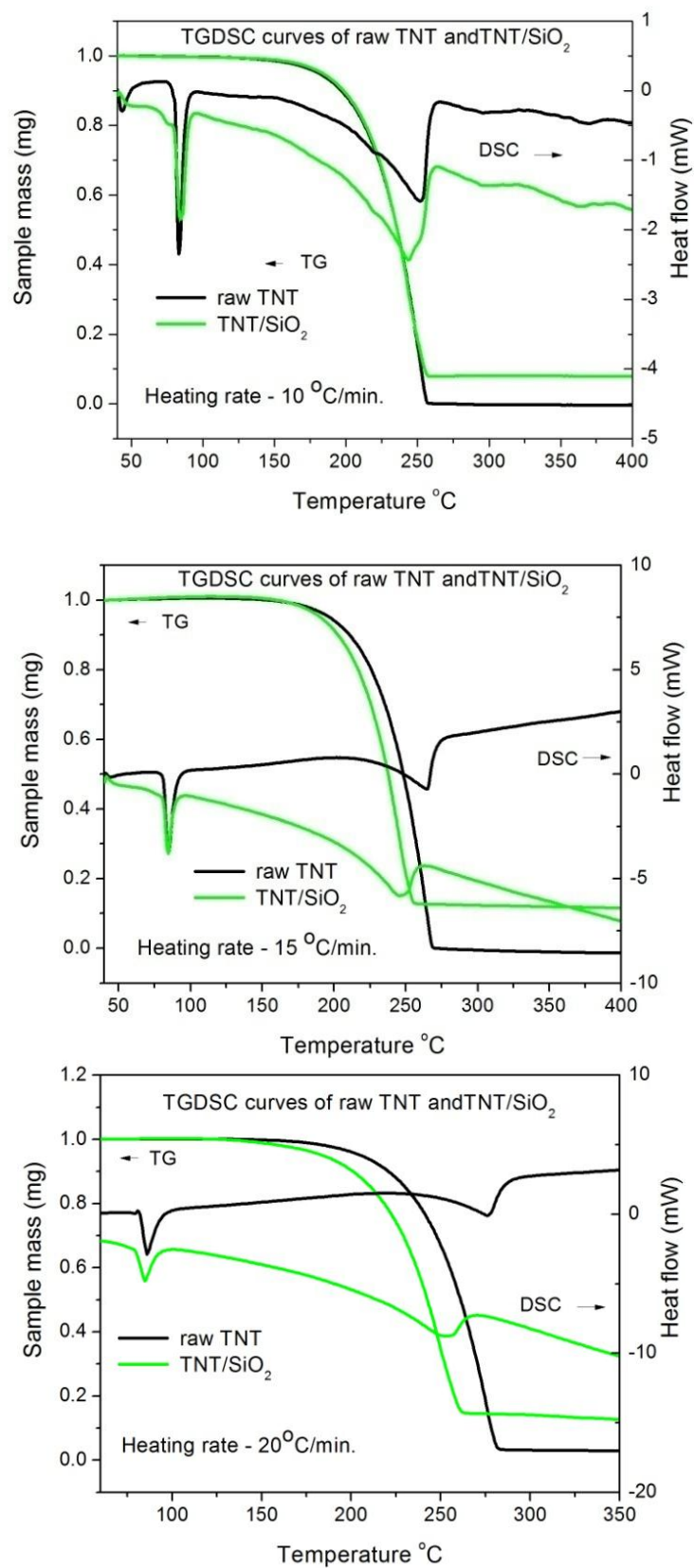
Fig. 5.28 TGDSC curves: raw TNT & TNT/SiO$_2$ xerogel at different heating rate.

To understand effect on sensitivity in these materials in terms of change in activation energy, kinematic parameters have been calculated from TGDSC curves obtained at heating rate of 10, 15 and 20 °C /min. Similar to RDX materials, shift in decomposition peak towards higher temperature is observed with increase in heating rate. Values of decomposition peak temperature are shown in Table 5.7.

Table 5.7 Decomposition peak temperature (T_p) for TNT materials at different heating rate

	Decomposition peak temperature (T_p) for TNT	
Heating rate	Average particle size of TNT	
	350 μm	50 nm
10 K/min.	255 °C	243 °C
15 K/min.	264 °C	246 °C
20 K/min.	276 °C	255 °C

Activation energy of TNT is calculated from decomposition temperature peak for various heating rates as shown in Table 5.7 and calculated values of activation energy E_a and pre-exponential factor Z are shown in Table 5.8.

Table 5.8. Kinetics parameters for TNT (derived from TG-DSC curves)

TNT processed by	Average particle size	Kinetics parameters		
		E_a (kJ mol^{-1})	Z (s^{-1})	k (s^{-1})
Raw	350 μm	78.7 ± 8 %	2.09 x 10^7	0.63
Sol-gel method	50 nm	144.4± 20 %	2.70 x 10^{14}	1.25

The value of activation energy for raw TNT agrees with reported value in literature for TNT. As shown in Table 5.8, activation energy of 144 kJ for TNT

materials processed by sol-gel method is much higher compared to that of raw TNT. It indicates that as TNT particles are confined in silica gel network, it requires more heat for ignition. However, shift in decomposition peak to lower temperature indicates that ignition to detonation transition is rapid in these materials. High surface energy may contribute to faster decomposition in these materials. Higher values of Z and k for TNT materials may be attributed to a greater number of atoms undergoing decomposition simultaneously due to high proportion of surface atoms. In sol-gel processed material, with high activation energy decomposition reaction triggers at higher temperature that favours reaction products liberating more energy and accelerating reaction rate.

5.2.8 Velocity of Detonation (VoD) measurements:

Thermal analysis of energetic materials processed by sol-gel method indicated high reaction rate constant that suggest improvement in energy release rate. To assess the performance in terms of energy release rate, velocity of detonation was measured for these materials.

The experimental assembly to measure detonation velocity is shown earlier (Fig. 4.20). To measure detonation velocity, three pins 'S2', 'S3' and 'S4' were inserted in acceptor charge. Distance between 'S2' - 'S3' and 'S3' - 'S4' was 5 ± 0.1mm. Fig. 5.29 show typical signal profile recorded on oscilloscope for TNT-SiO_2 xerogel.
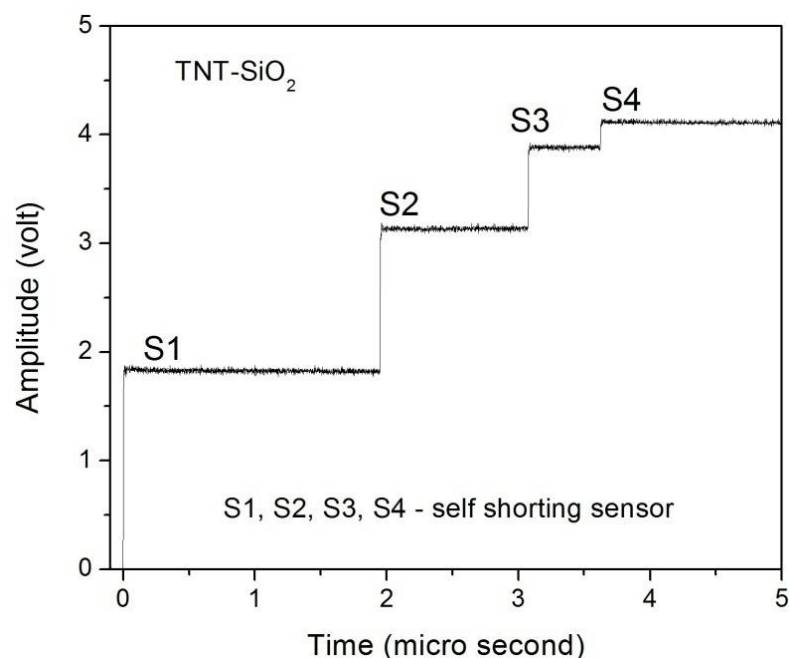
Fig. 5.29 Signal profile recorded for TNT-SiO$_2$ xerogel

From the signal profile in Fig. 5.29, it is observed that initially the velocity is less; however, in second region it accelerates fast. These results support kinematic data that initially buildup of reaction takes time but high surface area and high defect density (as indicated by high value of pre-exponential factor *Z)* in xerogel materials favor propagation of ignition transition in very small length scale. Sensor output on the oscilloscope record indicates the arrival of detonation wave front at the sensor location. Detonation velocity is then, calculated by knowing the travel time of detonation front between two sensor location.

Table 5.9 Data on VoD for TNT, RDX and PETN processed by sol-gel method

Energetic material	Detonation velocity (mm/µs)		
	TNT	RDX	PETN
Raw	6.39 ± 0.19	7.89 ± 0.2	7.71 ± 0.2
Processed by sol-gel method	6.66 ± 0.20	8.12 ± 0.2	8.05 ± 0.2

The data on velocity measurement for TNT, RDX and PETN is listed in Table 5.9. Detonation velocity in energetic materials and silica composites is 5 % higher than that of raw materials. It indicates improvement in energy release rate as ignition to explosion transition is fast due to higher defect density and high surface area of nanosized particles. However, detonation velocity in silica composites is lower than that of these materials with reduced particle size processed by solution crystallization and spray drying method as noted in Chapter 4. It may be due to lower content of energetic materials (90 %) in these materials resulting in lowering the energy density.

5.3   Conclusions:

As voids also contribute to the initiation of energetic compounds but introducing the voids in controlled manner and analyzing its effect on sensitivity of energetic materials has not been studied. Therefore, sol gel process has been utilized for preparation of energetic materials in silica gel matrix with induced defects like porosity and studied its effect on sensitivity and performance of these materials. The sol-gel method has proved promising technique for preparation of energetic materials with particle size less than 100 nanometers and with controlled porosity. The sol gel process has been optimized to obtain energetic materials with particle size in range of 20 to 80 nanometers in silica gel host. Impact test studies on these sol-gel processed samples showed increase in sensitivity even though the particle size is reduced. This indicates that decomposition mechanism in these samples is affected by the defects like porosity. With the energetic materials composites with silica having different material loading and varying pore volume, it is also demonstrated that microstructure of the sol-gel processed material can be tailor made and effectively used to control their sensitivity and energy release rate.

REFERENCES:

[1] Micro structural Investigations of Titania-Silica Nano Composite Aerogels, S. V. Ingale, P. U. Sastry, P. B. Wagh, A. K. Tripathi, R. Rao, R. Tewari, P. T. Rao, R. P. Patel, A. K. Tyagi, Satish C Gupta, *Materials Chemistry and Physics*, **135** (2012) 497-502

[2] Meisenheimer Complex Between 2,4,6-Trinitrotoluene and 3-Aminopropyltriethoxysilane and Its Use for a Paper-Based Sensor, S. Hughes**,** S. S.R. Dasary**,** S. Begum**,** N. Williams**,** H. Yu**,** *Sensing and Bio-Sensing Research*, **5** (2015) 37-41

[3] Nanocrystalline Trinitrotoluene (TNT) Using Sol–Gel Process, S.V. Ingale, P.B. Wagh, R. Tewari, Satish C. Gupta, Journal of Non-Crystalline Solids **356** (2010) 2162–2167

[4] Synthesis of Silica Aerogel by Supercritical Drying Method, T Błaszczyński, A Ślosarczyk, M Morawski, *Procedia Engineering,* **57** (2013) 200 – 206

[5] Drying of Silica Aerogels by Liquid and Supercritical CO_2 , G. Rogacki, P. Wawrzyniak, Z. Bartczak, *Drying Technology*, **14** (1996) 259-270

[6] Effect of MTMS as a Co-precursor on the Optical Properties of Silica Aerogels, A.V. Rao, G.M. Pajonk, *J. Non-Cryst. Solids,* **285** (2001) 202-209

[7] Application of FT-IR Spectroscopy for Investigation of Pink Water Remediation by Pine Bark, M Grube , O Chusova , M Gavare, K Shvirksts, E Nehrenheim, M Odlare, *The Open Biotechnology Journal*, **9** (2015) 67-75

[8] Comparison of Some Physico- Chemical Properties of Hydrophilic and Hydrophobic Silica Aerogels, P. B. Wagh, S. V. Ingale, *Ceram. Int. 28 (2002) 43-50.*

[9] Comparison of the Molecular Structure of Hexahydro-1,3,5-trinitro-s-triazine in Vapor, Solution and Solid Phases, R. J. Karpowicz, T. B. Brill; *J. Phys. Chem.* **88** (1984) 3480.

[10] Spectroscopic and Thermal Studies on Pentaerythritol Tetranitrate, P. Makashir, E. Kurian, *Propellants, Explos. Pyrotech*. **24** (1999) 260-265.

[11] Micro structural Investigations on TNT and PETN Incorporated Silica Xerogels, S V Ingale, P U Sastry, A K Patra R Tewari, P B Wagh, S C Gupta. *J Sol-Gel Sci Technol.* **54** (2010) 238- 42.

[12] The High-Pressure Phase Stability of 2,4,6-Trinitrotoluene (TNT), P. R. Bowden, R. S. Chellappa, D. M. Dattelbaum, V. W. Manner, N. H. Mack, Z. Liu, *Journal of Physics: Conference Series*, **500** (2014) 052006

[13] Ambient-Dried Silica Aerogel Doped with TiO_2 Powder for Thermal Insulation Y. G. Kwon, Y. S. Choi, *J Mater. Sci.* **35** (2000) 6075-6079

[14] The Scherrer Formula for X-Ray Particle Size Determination, A. L. Patterson, *Phys. Rev*. **56** (1939) 978-981

[15] Crystallization and Characterization of RDX, HMX, and CL-20, Antoine E. D. M. van der Heijden, Richard H. B. Bouma, *Crystal Growth & Design* , **4** (2004) 999-1007

[16] D R Lide, *CRC Handbook of Chemistry and Physics*, 88th Edition 2007-2008. CRC Press, Taylor & Francis, Boca Raton, (2007)

[17] Studies on Impact Sensitivity of Nanosized Trinitrotoulene (TNT) Confined in Silica Processed by Sol-Gel Method, S. V. Ingale, P. B. Wagh, P. U. Sastry, C. B. Basak, D. Bandyopadhyay, S. B. Phapale, Satish C Gupta, *Defence Technology*, **12** (2016) 46-51

[18] Transmission Electron Microscopy as Best Technique for Characterization in Nanotechnology, M A Asadabad, M J Eskandari, *Synthesis and Reactivity in Inorganic, Metal-Organic, and Nano-Metal Chemistry*. **45** (2015) 323–326

[19] X ray Powder Diffraction Data of Some Molecular Complexes of TNT, L. A. Burkardt, *Anal. Chem.* **28**, 8 (1956) 1271-1272

[20] Small angle scattering and the structure of aerogels, A. Emmerling, J. Fricke, *J Non-Cryst Solids.* **145** (1992) 113-20

[21] Synthesis and Characterization of Ammonium Molybdophosphate–Silica Nano-Composite (AMP–SiO2) as a Prospective Sorbent for the Separation of ^{137}Cs from Nuclear Waste, S. V. Ingale, Ramu Ram, P. U. Sastry, P. B. Wagh, Ratanesh Kumar, Ram Niranjan, S. B. Phapale, R. Tewari, A. Dash, S. C. Gupta, *J Radioanal Nucl Chem,* **301** (2014) 409-415

[22] SAXS investigations of the fractal character of additive silica xerogels, H. Fei, H. Xiaodong, M. Li, S. Zhang, *J Ceramic Proc Res.* **9** (2008) 389-392

[23] Scattering by an Inhomogeneous Solid. II. The Correlation Function and Its Application, P. Debye, H R Anderson Jr, H Brumberger, *J Appl Phys.* **28** (1957) 679–683

[24] Characterization of Anisotropic Poly(vinyl alcohol) Hydrogel by Small and Ultra- small Angle Neutron Scattering, S Hudson, J Hutter, M Nieh, J Pencer, L Million, W. Wan, *J Chem Phys.* **130** (2009) 34903

[25] Nanocrystalline Pentaerythritoltetranitrate (PETN) using Sol-Gel Process, S. V. Ingale, P. B. Wagh, P. U. Sastry, A. K. Patra, R. Tewari, I. K. Singh, S. B. Phapale, R.D. Wasnik, A. Subhananda Rao, Satish C. Gupta, *Defence Science Journal*, **61** (2011) 87-94.

[26] Approximations Leading to a Unified Exponential/Power-Law Approach to Small-Angle Scattering, G. Beaucage, *J. Appl. Crystallogr.* **28** (1995) 717-728

[27] Small Angle X-ray Scattering from the Surfaces of Reversed Phase Silica: Power law Scattering Exponents Greater than Four, P. Schmidt, D. Anvir, D. Levy, A. Hohr, M. Steiner, A. Röll, *J. Chem. Phys.* **94** (1991)1474-1479

[28] Determination of Specific Surface Area of Natural Clay by Comparative Methods, M. S. El-Geundi, E. A. Ashour, R. M. A. Abobeah, N. Shehata , *Int. J. of Sci. Engineering and Technol. Research,* **3** (2014) 2100-2104

[29] Method for the Calculation of Effective Pore Size Distribution in Molecular Sieve Carbon, G. Horvath, K. Kawazoe, *J. Chem. Eng. Jpn.* **16** (1983) 470-475

[30] Crystal Size Dependence for Impact Initiation of Cyclotrimethylenetrinitramine Explosive, R. W. Armstrong, C. S. Coffey, V. F. DeVost, W. L. Elban, *J. Appl. Phys.* **68** (1990) 979-984

[31] Autocatalytic Thermal Decomposition Kinetics of TNT, G. T. Long, B. A. Brems, C. A. Wight, Thermochimica Acta, **388** (2002) 175-181

[32] Numerical Analysis of Thermal Decomposition for RDX, TNT, and Composition B, S H Kim, B W. Nyande, H S Kim, J S Park, W J Lee, M Oh, *J. of Hazardous Mater.* **308** (2016) 120–130

[33] Physico-Chemical Properties of Silica Aerogels Prepared from TMOS/MTMS Mixtures, S V Ingale, P B Wagh, A K Tripathi, V S Kamble, Ratanesh Kumar, S C Gupta, *J. Porous Mater.*, **18** (2011) 567-572

[34] Sol–Gel processing of Energetic Materials, T M Tillotson, L W Hrubesh, R L Simpson, R S Lee, R W Swansiger, L R Simpson, *J. Non-Cryst. Solids,* **225** (1998) 358-363

[35]   Study on a Novel High Energetic and Insensitive Munitions Formulation: TKX-50 Based Melt Cast High Explosive, Y. Yu, S. Chen, T. Li, S. Jin, G. Zhang, M. Chenb, L. Li *RSC Advances*, **7** (2017) 31485-31492

[36]   Critical Conditions for Impact- and Shock-Induced Hot Spots in Solid Explosives, C. Tarver, S. Chidester, A. Nichols, *J. Phys. Chem,* **100** (1996) 5794- 5799

CHAPTER 6

PREPARATION OF RESORCINOL - AMMONIUM NITRATE NANO COMPOSITE USING SOL-GEL METHOD AND ITS CHARACTERIZATION

An energetic material requires combination of fuel and oxidizer that release energy through oxidation. Energetic materials like TNT, RDX and PETN etc., contain fuel and oxidizer species within one molecule and therefore they are very powerful. These materials have high brisance that could be a demerit in civil applications like coal mining, road blasting or metal welding, and also pose safety issues due to their sensitive nature. Therefore, composite explosives in which fuel and oxidizers are separate entities and mixed together are being explored to obtain a wide range of energetic materials suitable for various civil applications [1]. Gun powder which is mixture of charcoal, nitrate salt and sulfur, is the oldest known and commonly used composite energetic material. Ammonium Nitrate / Fuel Oil (ANFO) and Ammonium per chlorate base materials used for rocket propellants etc. are some of the recent examples of energetic composites in which fuel and oxidizers are physically mixed. As fuel and oxidizer are physically mixed in these composites, they have weak performance in terms of energy release rate and another major issue with uncertainty in reliable ignition. The performance of these composites is governed by the particle size of components and homogeneity of resultant mixture [2].

Nanostructured energetic composites could be a solution for this. The energetic composites with reduced particle size of component materials to nanometer scale can have better homogeneity in mixture of a fuel and an oxidizer and therefore can offer high energy density with higher rate of energy release comparable with

monomolecular energetic materials [3]. Therefore, focus in present work is mainly on reducing the particle size of constituents to nanometer scale to have better energy density of the energetic composites. Sol-gel method is a promising technology to achieve the particle size in nanometer range and have better homogeneity and proximity of the components [4]. The gel material consisting of a three-dimensional porous network could be ideal pathway to prepare energetic nano composites utilizing the porous network as host fuel to load oxidizer as disperse phase. In nano structured TNT and RDX composites with silica, there is no contribution from the oxide network in the detonation energy and the sensitivity of the energetic materials found to be more as compared to that of raw materials. Therefore, for developing energetic composites, organic gel is better option to work as fuel network with oxidizers as dispersed phase.

Resorcinol is one of commonly used precursor in organic gels which has chemical structure similar to styphnate and is suitable for forming three-dimensional network through cross linking using formaldehyde. Ammonium nitrate is generally used in ANFO type energetic materials for its positive oxygen balance. Therefore, to prepare energetic composites using suitable composition, we developed a method to prepare nanostructure composite consisting of Resorcinol (R) organic gel and ammonium nitrate (AN) as an oxidizer using sol-gel method. One of the difficulties in the development of such energetic composites is to prepare a uniform organic/inorganic composite with high oxidizer content which is imperative for good energy output due to highly oxygen deficient organic gel structure [5]. The efficient organic-inorganic nano composites should have nearly stoichiometric oxygen balance for high energy output and sensitivity suitable for safe handling and reliable performance. To have nearly stoichiometric oxygen balance, quantity of ammonium

129

nitrate in the composite was estimated to 85 % and the preparative parameters were accordingly optimized.

6.1 Preparation of Resorcinol-Ammonium Nitrate (R-AN) composite:

R-AN nanocomposite has been prepared using sol-gel method [6]. All the chemicals used in the present work viz. Resorcinol, Formaldehyde (F), Ammonium nitrate, acetone, hydrochloric acid (HCl) are of analytical grade and Merck make. To prepare R-AN composite, resorcinol and formaldehyde, in molar ratio 1:2, were added to the acetone. To this solution, ammonium nitrate was added in suitable proportion to achieve desired composition of R and AN in final xerogel. Concentrated hydrochloric acid (HCl) has been used as catalyst to accelerate the gelation. The molar ratio of precursor chemicals R: F: Acetone: HCl was optimized to 1:2:35:0.25. The solution turned into gel within half an hour. The solvent from the gel pores was extracted under vacuum at 40 ^{o}C. This resulted in RF gel with gel pores occupied by ammonium nitrate. This composite containing 85 % AN is designated as R-AN (15/85).

6.2 XRD characterization of R-AN composite:

The presence of AN in the gel has been confirmed by the X-ray diffraction (XRD) characterization. The XRD data for the resultant R-AN composite had been obtained using CuKα (1.54 Å). The diffracted X-rays were collected by scanning between 10.01 to 79.99° in a scan step size of 0.02. The X-ray diffraction data recorded for Resorcinol gel, ammonium nitrate and RF-AN composite are shown in Fig. 6.1.
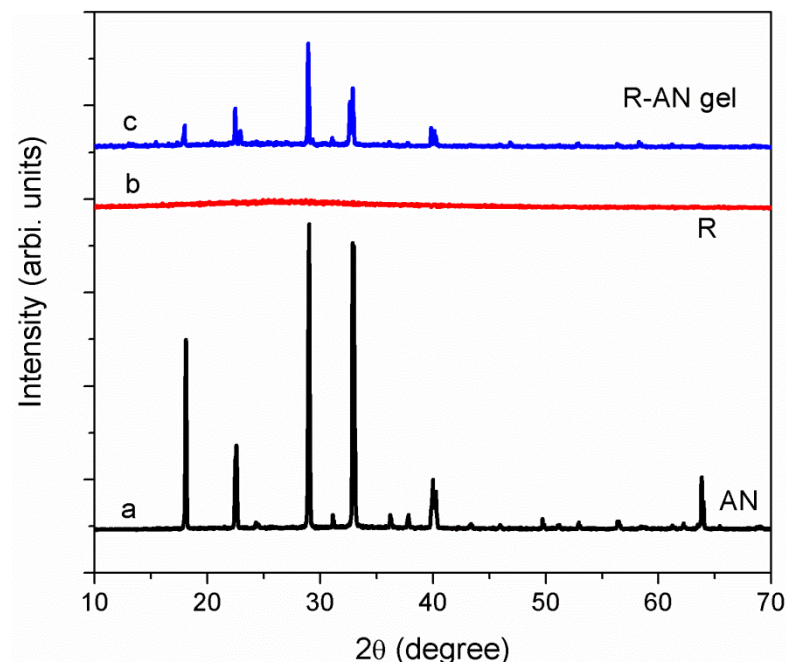
Fig. 6.1 XRD patterns of Resorcinol (R), Ammonium Nitrate (AN) and R-AN gel

The diffraction peaks from the XRD pattern of R-AN composite in Fig. 6.1 are assigned to ammonium nitrate. Solid ammonium nitrate (NH_4NO_3) exists in five stable polymorphic forms (designated as phases I, II, III, IV, and V) below its melting point at around 170 $^{\circ}$C. The diffraction peaks observed at observed at 17.9 $^{\circ}$, 22.4 $^{\circ}$, 29.0 $^{\circ}$, 33.0 $^{\circ}$ and 40.0° show that the NH_4NO_3 powder sample is in phase IV [7]. XRD studies of the composite materials revealed that the ammonium nitrate survives the sol gel processing and retained in the gel structure.

6.3   FTIR characterization of R-AN composite:

The presence of AN in the gel has also been confirmed by FTIR characterization. FTIR spectra for AN and R-AN composite prepared by sol-gel method are shown in Fig. 6.2.

131
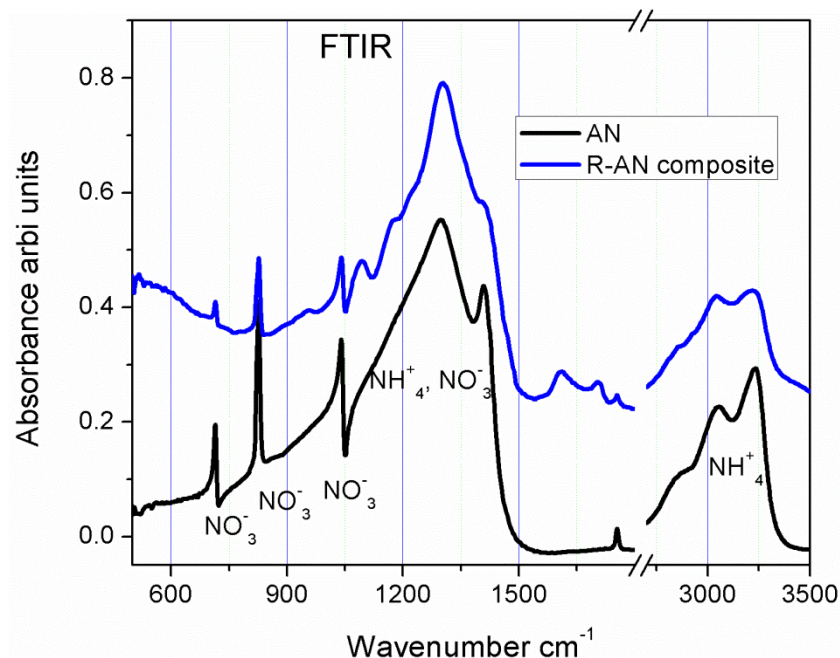
Fig. 6.2 FTIR spectra for AN and R-AN composite prepared by sol-gel method

In Fig. 6.2, the band observed at 3100 to 3300 cm^{-1} corresponds to asymmetrical stretching of NH_4^+ [8]. The region near 1300 -1400 cm^{-1} is complex consisting overlapping of bands for triply degenerate deformation vibration, of NH_4^+ and doubly degenerate stretching vibration of NO_3^-. The bands at around 1050, 830, 720 cm^{-1} are attributed to three distinct absorption peaks of NO_3^-. These characteristics peaks for NH_4NO_3 are also present in R-AN gel indicating that AN is present in R-AN gel.

6.4   Morphology study of R-AN composite:

The microstructure of the composites has been observed in a high resolution field emission scanning electron microscope (FESEM). For FESEM, the R-AN composite powder was dispersed on carbon substrate and it was subsequently coated with gold to get rid of charging effect.
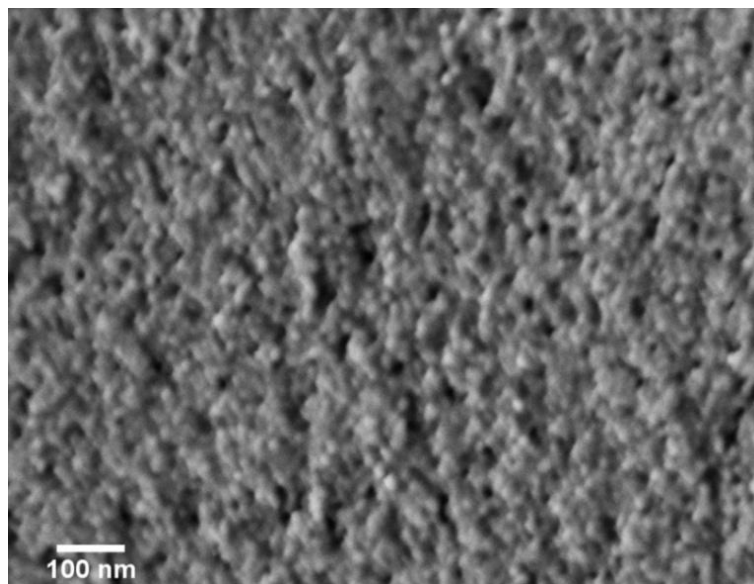
Fig. 6.3 FESEM of R-AN (15/85) composite processed by sol gel method

A homogeneous microstructure of RF-AN composite can be seen in the SEM micrograph (Fig. 6.3). Pores of nanometer range have been found present all over the samples. The AN recrystllizes in the pores of RF gel confining particle size of AN in the range of nanometers. In R-AN composite, though the organic and inorganic phases cannot be resolved from one another, the small particle size indicates that the distribution of both the constituents is in the nanometer range. The particles are connected to form aggregates resulting in a structure of interconnected clusters. The resorcinol xerogel has porous microstructure and the porosity in the gel has been exploited to load the inorganic component of the composite.

Specific surface area measurement is an important technique to characterize the sol gel process derived materials. The specific surface area, specific pore volume and pore size distribution of R-AN composite have been measured by nitrogen physi-sorption method. Prior to measurement, the samples were degassed at 100 $^\circ$C. The specific surface area has been calculated using Brunauer-Emmett- Teller (BET) method from the amount of N_2 gas adsorbed at 77 K at various partial pressures

(eleven points; $0.05 < p/p_0 < 0.3$). The BET specific surface area as determined from the adsorption isotherms for R xerogel is 136 m^2/g whereas the specific surface area of R-AN composite is 28 m^2/g. The BET specific surface area has been found to be decreased from 136 to 28 m^2/g for RF-AN composites. It indicates that pores of R gel have been occupied by AN in the composite.

6.5   Thermal analysis of R-AN composite:

Thermo-gravimetric (TG) and differential scanning calorimetric (DSC) analysis on R/AN composites has been carried out in inert atmosphere by heating the weighed samples (2-5 mg) in the temperature range 40- 500 ˚C. Alumina sample holders were used as sample and reference carriers during this measurement.

The TG-DSC curves for AN and R-AN (15/85) composite gel at the heating rate of 10 ˚C/min have been shown in Fig. 6.4. For comparison purpose, TG-DSC curve obtained for physically mixed Resorcinol and Ammonium nitrate composition in same proportion to that of R-AN gel are also shown. In Fig. 6.4, DSC curve of Ammonium nitrate shows endothermic peaks within range from 50 to 130 ˚C.
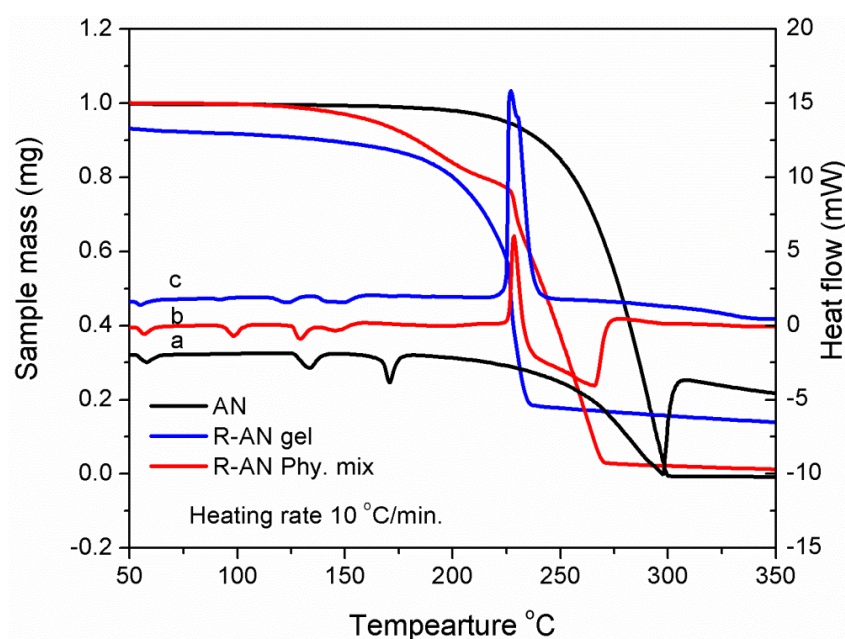
**Fig. 6.4 TG-DSC curves for AN and R-AN (15/85) composite gel and R-AN (15/85) physical mixture**

These are associated with solid-solid phase transitions in AN [9]. Endothermic peak at 170 ^{o}C indicates melting of AN. TG curve of AN shows mass loss within temperature range from 200 to 300 ^{o}C. It is attributable to decomposition of AN in this range [10]. Decomposition of AN is accompanied with endothermic peak that indicates formation of NO. DSC curve recorded for physically mixed R-AN mixture and R-AN composite gel are different from that of recorded for Ammonium nitrate by an exothermic peak suggesting oxidation of carbon from resorcinol by Ammonium nitrate. The DSC curve for physically mixed R-AN mixture also shows endothermic peaks associated with AN phase transition. For this composition, the mass loss of about 25 % is seen to be gradual within the temperature range of 150 to 220 ^{o}C and is accompanied with an exothermic peak. It indicates a partial oxidation of resorcinol at slower rate. The exothermic peak is followed by distinct endothermic peak with steep mass loss. The endothermic decomposition of AN indicates that it decomposes afterwards. It suggests that R and AN behave as separate entities and needs more intimacy between these constituents for reaction. R-AN composite gel processed by sol-gel method shows strong exothermic peak at 230 ^{o}C accompanied with weight loss in TG curve. This exothermic peak with large amount of heat release associated with formation of oxidized species indicates oxidation of carbon and hydrogen of resorcinol fuel by AN [11]. It shows a weight loss at lower temperature compared to physical mixture. This indicates an early decomposition of R-AN composite gel. It is due to nano sized particles of fuel and oxidizer with close proximity. Endothermic peak is minimized in this composition that indicates AN has been used for oxidation

135

of fuel. These results are supported by evolved gas analysis (Fig. 6.5) which is in consistence with these observations.

At 1051 sec. / 199 °C

H_2O, CO_2

At 1383 sec. / 265 °C

H_2O, CO_2
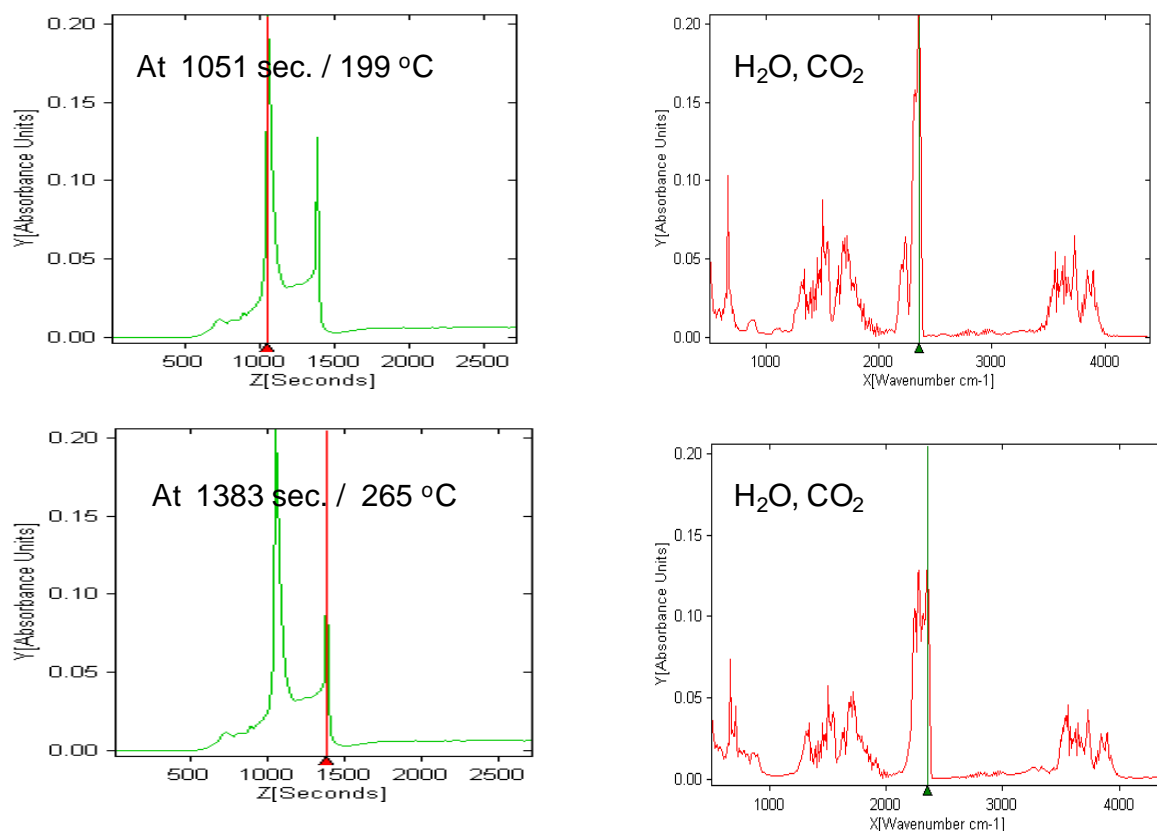
Fig. 6.5 Evolved gas data during R-AN (15/85) gel thermal analysis

Fig. 6.5 shows that gas monitored during decomposition of R-AN composite gel associated with exothermic peak in thermal analysis consists of H_2O and CO_2. It indicates improvement in decomposition characteristics in R-AN composite gel. Nano structured composite has certainly modified the reaction kinetics of this composite that suggests it as promising candidate in the class of energetic materials [12].
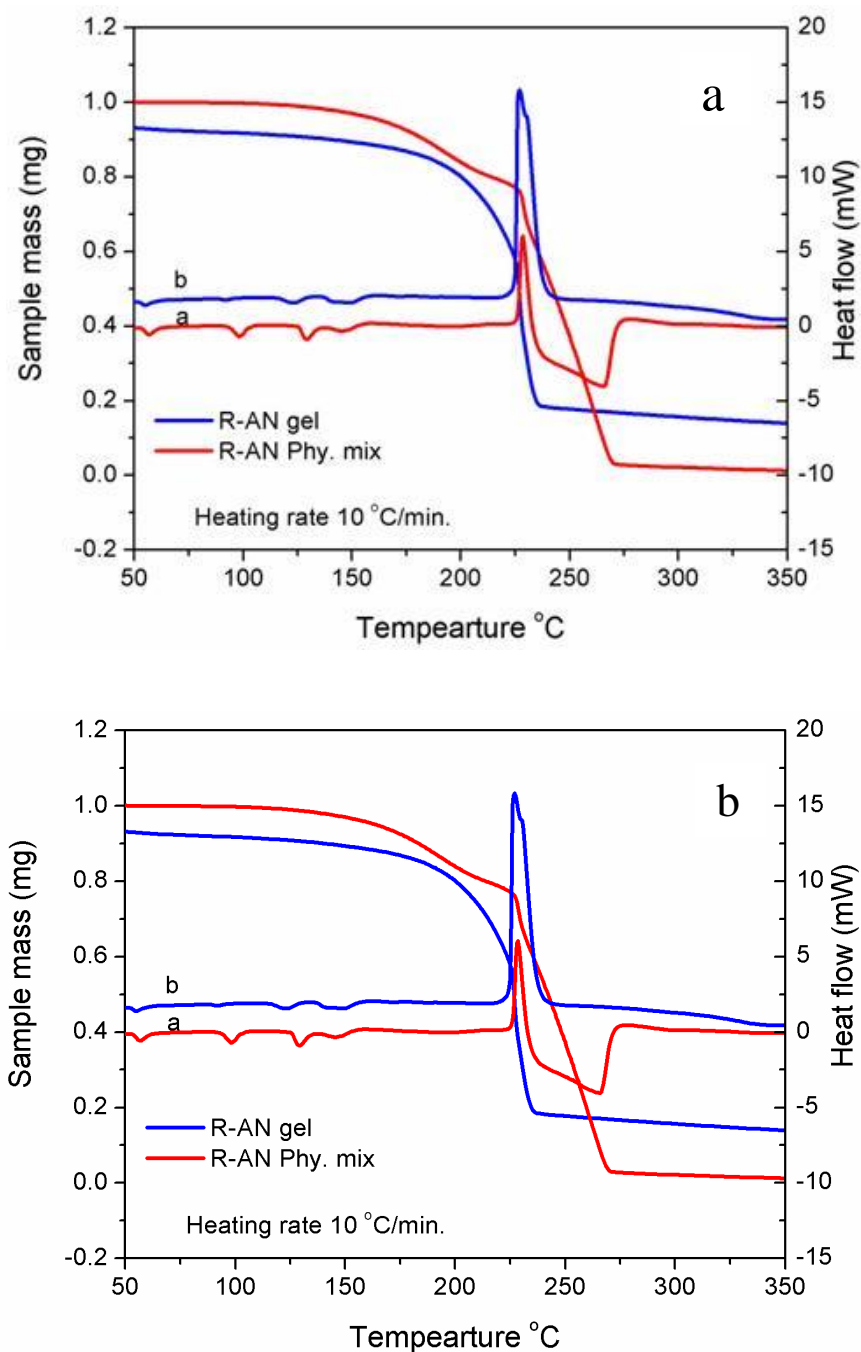
Fig. 6.6 TG-DSC curves for physically mixed R-AN (15/85) composition and R/AN composite gel processed by sol-gel method with heating rate a) 10 ^{o}C/min and b) 20 ^{o}C/min.

Kinetics of R-AN decomposition has been studied by thermal analysis by heating this material at different heating rate. Fig. 6.6 shows TG-DSC curves for physically mixed R-AN (15/85) composition and R/AN composite gel processed by

sol-gel method. Kinetic parameters calculated from exothermic peak temperature of DSC curves using Kissinger method are listed in Table 6.1.

Table 6.1 Kinetic parameters calculate for R-AN (15/85) composite gel and physically mixed Resorcinol an ammonium nitrate (15/85 wt ratio)

	Activation energy	Z (s^{-1})	K (s^{-1})
R-AN physically mixed	116 kJ/mole	6.06×10^{11}	1.05
R-AN composite gel	261 kJ/mole	1.98×10^{27}	2.44

In table 6.1, activation energy in R-AN composite gel is found to be higher in comparison with that of physically mixed RF-AN formulation. However, values for collision frequency 'Z' and reaction rate constant 'k' both are very high for R-AN composite gel. This is due to the nano sized particles and close intimacy of fuel and oxidizer particles in homogeneous gel. This suggests high energy release rate in the R-AN composite gel material. With these kinetic parameters, it can be inferred that these composites are better performing energetic materials. With control on constituent proportion, these can be tailor made over wide range of energy.

6.6   Impact sensitivity measurements of R-AN composite:

The comparative data on impact sensitivity for R/AN composite gel along with monomolecular energetic materials is shown in Fig. 6.7. Impact sensitivity studies have been carried out using Fall Hammer Impact Test apparatus with 2 kg weight. For impact sensitivity test, powder sample of about   30 - 40 mg was placed on anvil and the height of impact for 2 kg hammer was varied to arrive at a height where 50 % probability of initiation.
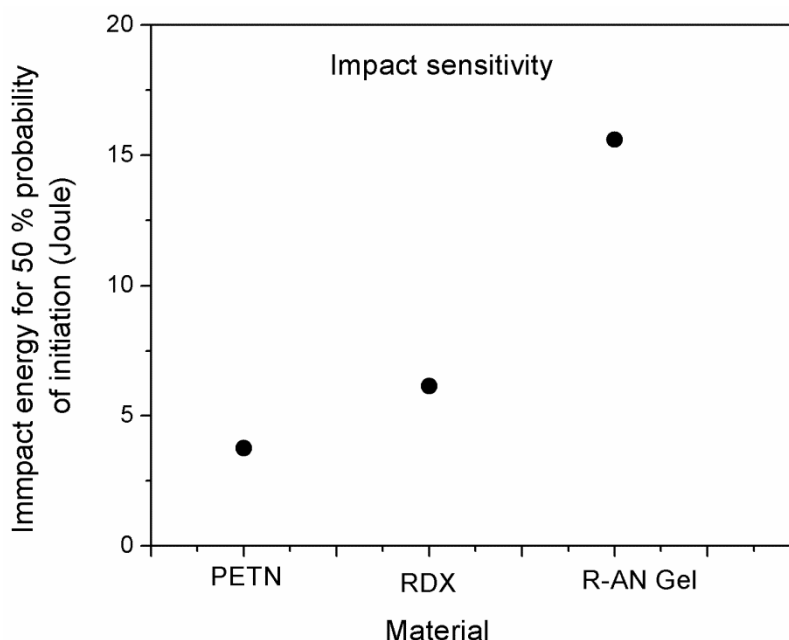
Fig. 6.7 Impact sensitivity data for PETN, RDX and R/AN (15/85) gel

As shown in Fig. 6.7, energy required for initiating the R-AN composite with 50 % initiation probability is 15.6 J whereas the initiation energies for RDX and PETN materials are 6.4 and 3.9 J, respectively. The increase in initiation energy indicates the decrease in sensitivity of the material. The R/AN gel is found to be more insensitive as compared to PETN and RDX. It enhances safety in handling and processing of these materials. However, the sensitivity is in the range where it can be initiated reliably using proper initiating source. Thus, the R-AN nanocomposite is found to be suitable as a safe and reliable energetic composite. The decomposition of composite on impact was found to be complete with little traces of undetonated material which indicated that oxygen balance is achieved. The oxygen balance in the fuel (resorcinol) and oxidizer (ammonium nitrate) which is distributed homogeneously offer the energy output comparable with traditional energetic materials.

6.7   Conclusions:

In conclusion, the nanostructure composite of R-AN processed by sol – gel method containing 85% ammonium nitrate provide desired oxygen balance so as to harness maximum energy from this fuel-oxidizer composite. This R-AN composite is more insensitive than monomolecular energetic materials like RDX and PETN. The impact sensitivity of R/AN gel is lowered by about 200 % as compared to that of RDX. However, the impact initiation sensitivity is in the range such that it could be initiated reliably with proper initiation source. Thermal analyses of the composite indicated improvement in decomposition characteristics of the R-AN (15/85) composite with better energy output as compared to physically mixed formulation with same composition. The nanosized particles and homogeneity of mixture at nanometer scale in R-AN gel composites has contributed to improve the energy release rate in this material which is comparable to monomolecular conventional energetic materials.

REFERENCES:

[1]   Towards New Directions in Oxidizers/Energetic Fillers for Composite Propellants: an Overview, A. Dey, A. K. Sikder, M. B. Talawar, S. Chottopadhyay, *Central European J of Energetic Mater.*, **12** (2015) 377-399.

[2]   Size and Shape of Ammonium Perchlorate and Their Influence on Properties of Composite Propellant, S. Jain, Mehilal, S. Nandagopal, P.P. Singh, K.K. Radhakrishnan, and B. Bhattacharya, *Def. Sci. J*, **59** (2009), 294-299.

[3]   Formulation and Performance of Novel Energetic Nanocomposites and Gas Generators Prepared by Sol-Gel Methods, B. J. Clapsaddle, L. Zhao, D.

Prentice, M. L. Pantoya, A. E. Gash, J. H. Satcher Jr., K. J. Shea, R. L. Simpson, *36th Annual Conference of ICT,* Karlsruhe, Germany, (2005)

[4] Nanoscale Homogeneity of Silica -Poly(Vinyl Alcohol) Membranes by Controlled Cross-linking via Sol–Gel Reaction in Acidified and Hydrated Ethanol, S. G. Chaudhri, B. H. Rajai and P. S. Singh , *RSC Advances,* **5** (2015) 65862-65869.

[5] Preparation and Characterization of Energetic Nanocomposites of Organic Gel – Inorganic Oxidizers, S. Cudziło and W. Kicioski, *Propellants Explos. Pyrotech.*, **34** (2009) 155 – 160.

[6] Preparation of Nano-Structured RDX in a Silica Xerogel Matrix, S. V. Ingale, P. U. Sastry, P. B. Wagh, A. K. Tripathi, R. Tewari, V. B. Jayakrishnan, S. B. Phapale, P. T. Rao, R. D. Wasnik, B, Bhattacharya, S. C. Gupta, *Propellants Explos. Pyrotech.*, **38** (2013) 515-519

[7] FTIR Characterization of Polymorphic Transformation of Ammonium Nitrate, H. Wu, M. N. Chan, C. K. Chan, *Aerosol Science and Technology*, **41** (2007) 581–588

[8] Spectra and Crystalline Phase Transitions of Ammonium Nitrate, A. Theoret, C. Sandorfy, Infrared *Canadian Journal of Chemistry,* **42** (1961) 57-62

[9] Review on Thermal Decomposition of Ammonium Nitrate, S. Chaturvedi, P. N. Dave , *J of Energetic Mater.*, **31** (2013) 1–26.

[10] Mellor, J. W. *A Comprehensive Treatise on Inorganic and Theoretical Chemistry*. Vol. 2. London: Longmans Green (1992)

[11] Review on Thermal Decomposition of Ammonium Nitrate, Shalini Chaturvedi, P. N. Dave, *Journal of Energetic Materials*, **31** (2013) 1–26

[12] Resorcinol-Formaldehyde Ammonium Nitrate Energetic Nanocomposites Processed by Sol-Gel Method, S. V. Ingale , P. B. Wagh, N. H. Raje, A. Ghosh, R. Shukla, T. C. Kaushik, S. C. Gupta, *Int. J. of Multidisciplinary and Current Research,* **3** (2015) 961-965.

CHAPTER 7

SUMMARY AND FUTURE PROSPECTS

7.1   Summary

Energetic materials are combination of a fuel and an oxidizer which produces energy by a process called oxidation. For energy release, fuel and oxidizer can be physically mixed to allow them to react or can be present in the same molecule as is the case with most of efficient energetic materials. The intimacy of fuel (mostly carbon and hydrogen atoms) and oxidizers (oxygen atoms) is the main reason for violent energy release through rapid decomposition process causing explosion in these materials. In an explosion, stored chemical energy in energetic materials is suddenly released, and that generates hot gas and very high pressures. The sudden release of energy makes these materials different from other fuels and makes them suitable for specialized applications. Energetic materials are widely used in civil applications like road blasting, metal welding, for warheads in military applications, and as a tool for generating high pressure for basic research purpose.

The choice of energetic materials for practical applications is limited by several factors like thermal stability, chemical compatibility, handling sensitivity and energy output. Therefore, the properties of available materials need to be modified to improve their performance and usability. Sensitivity to initiation is an important parameter which needs to be controlled. It is because unless the accidental release of the stored chemical energy is controlled, the material is unsafe and hence has limitations in use. Therefore in the development of energetic materials, a major objective is to have desired control on sensitivity to initiation and energy release rate.

From the studies conducted in this area, it is revealed that the energetic properties of the material depend upon microstructure, particle size, particle size distribution, internal voids and defects. Among these, one of the parameters that can be effectively used to modify the properties of the energetic materials is particle size. Several researchers have attempted to study effect of particle size on sensitivity of the energetic materials, but the results are still inadequate to lead to some conclusion. Thus, it is still of great interest to investigate the effect of particle size on the sensitivity of energetic materials to initiation.

The focus of the present research work is to study the effect of particle size and to infer whether decrease in sensitivity and improvement in performance can be achieved by reducing particle size of the commonly used energetic materials like TNT, RDX, PETN and fuel-oxidizer composite like mixture of Resorcinol and Ammonium nitrate. Moreover, effect of introducing voids in controlled manner on ignition mechanism in energetic materials and their sensitivity has also been studied. To analyze effect of particle size on initiation sensitivity of energetic materials, a wide range of particle size has been studied. Since the energetic materials are not as such available with the desired particle size, appropriate processes have been developed for producing energetic materials with desired particle size. On basis of simplicity in processing, infrastructure required, safety and desired particle size, solution crystallization method, spray drying method and sol-gel method have been chosen to process the raw materials. The sol- gel method is useful to prepare the materials in nanometer size and with narrow size distribution. Also the porosity and solid loading of the energetic materials can be controlled in this process which is suitable to study the effect of controlled defects on sensitivity of these materials.

Scope of present work include developing methods like solvent/non solvent precipitation, spray drying and sol-gel process to obtain the energetic materials with particle size ranging from 350 micrometer down to 50 nanometers and study energetic properties of these materials. For preparation of energetic materials with controlled defects like porosity, the sol gel process has been utilized to obtain these materials with particle size in the range of 20 to 80 nanometers within silica gel matrix. Sol-gel method has also been used to prepare resorcinol-ammonium nitrate nano-composites.

The processed materials have been characterized by Fourier Transform Infra-Red (FTIR) spectroscopy and X-ray Diffraction (XRD) to confirm that chemical and crystal structures of these materials are same as those of raw materials. Thermo-gravimetric and differential scanning calorimetric (TG-DSC) studies have been performed for qualitative and quantitative analyses of the energetic materials in samples under study. Electron microscopy and small angle X-ray scattering measurement techniques were used to analyze the microstructure while particle sizes were measured using SEM and TEM micrographs.

The inadvertent initiation of energetic materials can basically occur due to energy received from impact or heat stimuli. Therefore, measurements with respect to initiation of energetic materials due to thermal or impact energy have been carried out. The studies conducted on processed energetic materials using fall hammer impact apparatus showed that sensitivity to impact initiation decreased by about 15 % in RDX and 40 % in TNT with reduction in particle size. Impact sensitivity in RDX material increased by about 5 to 7 % with inclusion of porosity. The impact sensitivity in TNT could be tuned in range of 25 % to 65 % by varying the process parameters of sol-gel method. The kinematics parameters calculated from thermal

analyses to understand decomposition mechanism in energetic materials showed an increase in activation energy with decrease in particle size. It also suggests improvement in energy release rate due to high surface energy associated with smaller size particles. More number of atoms undergoing decomposition simultaneously due to high proportion of surface atoms contributes to faster decomposition in materials with reduced particle size.

In sol-gel processed materials, effect of inclusion of voids on ignition mechanism has been studied. The activation energy has been found to increase in sol - gel processed samples. The silica environment around energetic particles and reduced particle size has led to increase in activation energy. However, impact test showed increase in sensitivity of these materials even though the particle size is reduced. In the composites of silica with TNT, RDX and PETN having different energetic material loading and varying pore volume, it is also demonstrated that microstructure of the sol-gel processed material can be tailored to control their sensitivity and energy release rate. In sol-gel processed materials also, the energy release rate is enhanced as compared to that of raw materials. This suggests that high defect density leads to increased number of ignition centers with increase in collision frequency that leads to faster ignition to detonation transition.

The improvement in energy release rate as predicted by thermal analysis is further substantiated by detonation velocity (VoD) measurements. The detonation velocity in energetic materials with reduced particle was found to increase by about 15 % as compared that for raw material.

The effect of particle size is prominently demonstrated in Resorcinol and Ammonium Nitrate (AN) composites containing more than 85 % AN with

stoichiometric oxygen balance. The nanostructure composites processed by sol-gel method with reduced particle size showed increase in energy release rate as compared to that from physical mixture of Resorcinol and Ammonium Nitrate. These composites are safer than traditional energetic materials like RDX and PETN due to less sensitivity and hence can be useful in various civilian applications.

7.2   Conclusions:

(i) Energetic materials like TNT, RDX and PETN have been prepared with particles size over wide range and with variation in particle size studied its effect on the ignition sensitivity and performance of energetic materials.

(ii) Ignition mechanism is affected by defects present in charge. However, inducing the defects in controlled manner to analyze its effect on ignition mechanism is the less studied aspect. The feature of controlling particle and pore size through sol-gel process has been utilized to process energetic materials with 60 to 90 % loading of energetic materials in porous silica and the role of microstructure and defects on sensitivity of energetic materials has been investigated

(iii)A detailed study on initiation of energetic materials by thermal and impact energy has helped to understand the ignition process in energetic materials. Sensitivity of energetic materials to initiation by impact or heat energy is found to decrease with reduction in particle size. However, the sensitivity to impact initiation in these materials is found to be affected by the defects like porosity that control ignition mechanism.

(iv)Detonation velocity and hence the performance of the energetic materials is improved with the reduction in particle size.

(v) Decrease in ignition sensitivity enable safe handling and improvement in detonation velocity with reduction in particle size of energetic materials is inferred and it is demonstrated that microstructure of these materials can be tailored using sol-gel process for controlling their sensitivity and energy release rate.

7.3   Future Prospects:

The experimental data obtained from present studies is good input to improve the models developed to study ignition and transition from ignition to detonation in energetic materials. Sol-gel processed energetic materials have provided data to develop models to predict effect of defect density and role of microstructure in ignition of energetic materials. Properties of composite energetic materials strongly depend on particle size of its components and homogeneity in mixing and in this regard, our data on Resorcinol-Ammonium Nitrate nano composite are encouraging. It needs more understanding through exploration over a large variety of compositions so as to offer formulations over wide range of energy and sensitivity useful in civil applications. Processing of nano materials is difficult due to their increased tendency to agglomerate. This especially creates difficulty in processing of composite propellants using nano aluminium. Sol-gel processing using a porous network as host for these nano particles can minimize this problem by preventing agglomeration of these trapped particles. Some more study needs to be conducted on the processing of such composites to optimize it to suit for various civil applications in near future.